Sudden Stratospheric Warmings and Their Impact on Northern Hemisphere Winter Climate

Jessica Oehrlein

Submitted in partial fulfillment of the
requirements for the degree of
Doctor of Philosophy
under the Executive Committee
of the Graduate School of Arts and Sciences

COLUMBIA UNIVERSITY

2021

ABSTRACT

Sudden Stratospheric Warmings and Their Impact on Northern Hemisphere Winter Climate

Jessica Oehrlein

Sudden stratospheric warmings (SSWs) are a key driver of winter climate variability in the Northern Hemisphere. SSWs are a disruption of the strong stratospheric westerlies over the winter pole in which the winds in the upper to middle stratosphere, from about 30 to 50 km above the surface, weaken and reverse and the polar cap temperatures increase by up to 50 K in only a few days. These events affect tropospheric conditions for the two months following, on average shifting the North Atlantic storm track equatorward and resulting in a negative Northern Annular Mode and North Atlantic Oscillation at the surface. These changes are associated with colder and drier than average conditions in Northern Europe and Eurasia and warmer and wetter than average conditions across Southern Europe, as well as high temperatures across North Africa, the Middle East, and Central Asia and increased cold air outbreaks in North America and Eurasia.

This thesis examines this typical surface response to SSWs in several different contexts. We consider its relationship to other atmospheric phenomena and features, first quantifying its importance relative to the North Atlantic impacts of the El Niño-Southern Oscillation (ENSO) and then examining the role of ozone chemistry in modeling the surface response to SSWs. We also study the variability of the surface signature of SSWs, with the goal of understanding the uncertainty in magnitude and spatial pattern of surface climate patterns following SSWs and the relative roles of different sources of this uncertainty.

After providing background and context in the first chapter, the second chapter studies interactions between SSWs and the El Niño phase of ENSO. El Niño affects climate in the North Atlantic and European regions, those most affected by SSWs, through tropospheric and stratospheric pathways. One of these pathways is increased SSW frequency. However, most SSWs (about 90%) are unrelated to ENSO, and the importance for boreal winter surface climate of this frequency increase compared to other El Niño pathways remains to be quantified. We here contrast these two sources of variability using two 200-member ensembles of one-year integrations of the Whole

Atmosphere Community Climate Model, one ensemble with prescribed El Niño sea surface temperatures (SSTs) and one with neutral-ENSO SSTs. We form composites of wintertime climate anomalies, with and without SSWs, in each ensemble and contrast them to a basic state represented by neutral-ENSO winters without SSWs. This approach allows us to isolate the distinct effects of ENSO and SSWs more clearly than was done in previous work. We find that El Niño and SSWs both result in negative North Atlantic Oscillation anomalies and have comparable impacts on European precipitation, but SSWs cause larger Eurasian cooling. These results indicate the potential impact of a strong El Niño on seasonal forecasting in the North Atlantic as well as the importance of resolving the stratosphere in subseasonal and seasonal forecast models to best capture stratospheric polar vortex variability.

In the third chapter, we study the importance of interactive ozone chemistry in representing the stratospheric polar vortex and Northern Hemisphere winter surface climate variability. Modeling and observational studies have reported effects of stratospheric ozone extremes on Northern Hemisphere spring climate. Recent work has further suggested that the coupling of ozone chemistry and dynamics amplifies the surface response to midwinter SSWs. We contrast two 200-year simulations from the interactive and specified chemistry (and thus ozone) versions of the Whole Atmosphere Community Climate Model with constant year-2000 forcings. This experiment is thus designed to clearly isolate the impact of interactive ozone on polar vortex variability. In particular, we analyze the response with and without interactive chemistry to midwinter SSWs, March SSWs, and strong polar vortex events (SPVs). With interactive chemistry, the stratospheric polar vortex is stronger, and more SPVs occur, but we find little effect on the frequency of midwinter SSWs. At the surface, interactive chemistry results in a pattern resembling a more negative North Atlantic Oscillation following midwinter SSWs, but with little impact on the surface signatures of late winter SSWs and SPVs. These results suggest that including interactive ozone chemistry in model simulations is important for representing North Atlantic and European winter climate variability.

In the fourth chapter, we turn from models to reanalysis and consider the uncertainty in the surface response to SSWs. While the qualitative features of the mean surface signature of SSWs in the

North Atlantic and Europe are well-established, its uncertainties as well as other features of surface climate following SSWs are less well-understood. To address the question of robustness of the mean observed response to SSWs, we use bootstrapping with replacement to construct synthetic SSW composites from SSW events in reanalysis, creating an ensemble of composites comparable to the observed one. We then examine the differences across these synthetic composites. We find that the canonical responses of a negative North Atlantic Oscillation and associated temperature and precipitation anomalies in the North Atlantic and European regions in the months following SSWs are robust. However, the magnitude and spatial pattern of these anomalies vary considerably across the composites. We further find that this uncertainty is unrelated to vortex strength and is instead the result of unrelated tropospheric variability. These results have implications for evaluating the fidelity of forecast models in capturing the surface impact of SSWs, by comparing both the mean impact as well as the contribution from internal variability with observations.

Overall, we demonstrate the complexity of interactions of sudden stratospheric warmings with other sources of variability in the Earth system. We find that the state of the polar vortex itself, the strength of downward propagation following the SSW, and the surface response can all be affected in important ways by these other components (e.g. tropospheric variability and Arctic ozone). We close by providing broader context for these results and looking towards continuing and future work in the field.

Table of Contents

List of Figures

List of Tables

Acknowledgments

This work was only possible thanks to the guidance of Prof. Lorenzo Polvani and Dr. Gabriel Chiodo. I arrived at Columbia excited about atmospheric science but with no background, and my growth into the field is largely due to their teaching, mentorship, and patient conversation and advice. Much of what I have learned about studying the stratosphere and communicating in our field is thanks to them.

Thanks to Profs. Michael Tippett, Ron Miller, Adam Sobel, and Clara Orbe for taking the time to serve on my committee and for their input, teaching, and generosity.

Ivan Mitevski and Dr. Zane Martin were invaluable companions along the way, friends and anchors in the office, program, and atmospheric science. They helped me to feel like I belonged here, and I hope I did the same for them.

I would not have finished this degree without the support and community I found at the Center for Teaching and Learning. Thanks to the CTL grad and assessment staff: Drs. Chris Chen, Ian Althouse, Caitlin DeClerq, Mark Phillipson, and Melissa Wright. They have shaped my teaching, pushed me to reflect, and given me space both physical and virtual. Over the past year, they have been the best coworking group I could ask for. I am also appreciative of my colleagues in the first two Teaching Assessment Fellow cohorts, with whom it was a joy to shape a new program and learn a new set of tools. Finally, thanks to the CTL Grads journal club members, especially Dr. Braden Czapla, Mel Abler, and Jeff Sherman. They put up with my opinions, snark, and poor-statistics-induced frustrations, but more importantly, they generously shared their reflections on pedagogy, research, and bringing our readings into practice. They have truly been my pedagogical community for the past four years, and I am beyond grateful for it.

I owe a great deal to the mentors who have helped me in finding my academic and mathematical identity over the years. Prof. Aaron Hoffman gave me confidence, space, mentorship, friendship, and mathematics when I desperately needed them, both while I was an Olin student and after, and

he valued my opinions on teaching even when I was seventeen and figuring things out on the fly. So much of what I aspire to be to my students stems from what he was to me. Prof. Rehana Patel took a chance on me as a course assistant she barely knew, and she helped me begin to connect the dots among mathematics, teaching, confidence, and culture. Profs. Denise Troxell and Nathan Karst quickly treated me as a member of their mathematical community, and that acceptance unquestionably changed my trajectory; I am not sure I would have been in graduate school at all without their Babson-Olin graph theory group. I hope to be that kind of mentor to my students.

Many friends and communities outside of Columbia have kept me grounded over the past five years. Halie Murray-Davis, Mitch Cieminski, Jefferson Lee, Juanita Desouza, and Raagini Rameshwar have been invaluable friends, from commiserating about graduate school to sending chocolate or discussing books. I cannot imagine the past five years without Emily Wang as we both worked towards PhDs, celebrating highs and working through lows, discussing research, learning about mentoring and teaching, and finding joy together. Thanks also to my Christ Church NYC family for being my anchor in New York City, to the folks of Math Twitter, MTBoS, and TMWYF for being some of the best professional development and communities I could imagine, and to my weekly fiber arts group, especially Abi LaBounty, for being consistent community through a pandemic.

I am grateful to the 230 undergraduates whom I have taught over the past two years, the many Oliners I NINJAed before that, and the thousands more K-12 students whom I have taught for anywhere from 30 minutes to 24 weeks in the past decade. It is in large part thanks to them that I found my way here and stayed, and they are why I do this.

Rocco, canım, szerelmem. Thank you for your love and patience, for conversations at all hours of the day, for oohing and aahing at many pictures of the sky, and for all the trips back and forth. And finally, thanks to my parents, for years of teaching conversations, books, math conferences, support, love, and the rallying cry to “Solve PDE!" I didn’t quite do that here, but I came close enough.

Chapter 1: Overview of Stratospheric Polar Vortex Climatology and Variability

The stratospheric polar vortex is a strong westerly circumpolar circulation during winter, or the region of high potential vorticity over the winter polar cap. It extends from about 100 hPa through the stratosphere and into the mesosphere. The polar vortex forms as a result of thermal-wind balance and the temperature gradient in the stratosphere between the equator and the pole in winter (Schoeberl 1978). Thus, the typical life cycle of the vortex involves spinning up in the late summer or early fall, increasing in strength through winter, and then weakening and eventually returning to weak easterlies in spring. There is relatively little variation from year to year in the timing of the formation of the polar vortex; this is largely driven by the large-scale temperature gradient. There is much more variability in the strength of the vortex throughout the winter and in the timing of the return to weak easterlies, or stratospheric final warming, due to wave activity that can disrupt the vortex.

There are key differences in this vortex life cycle between the two hemispheres. In the Northern Hemisphere, the polar vortex forms in late September or early August and lasts until spring, with the final warming occurring anywhere from early March to early May but on average falling in mid-April. The maximum strength of the westerlies at 10 hPa and 60° N (roughly where the westerlies are strongest (Waugh, Sobel, et al. 2017)) is around 40 ms^{-1} on average and is typically reached in December or January. In the Southern Hemisphere, the vortex typically forms in mid-February and persists until November or early December. The vortex is at its strongest in August and September, later in winter than in the Northern Hemisphere, and the maximum wind speeds at 10 hPa and 60° S are typically around 85 ms^{-1}. The Southern Hemisphere vortex is thus much longer lasting and also significantly stronger. This is due mainly to the lower upward-propagating wave activity

resulting from the more zonal features of the Southern Hemisphere, with lower topographic and land-sea contrasts (van Loon et al. 1973). This also results in a more zonal and less variable Southern Hemisphere polar vortex.

The main topic of this thesis is extreme events of the stratospheric polar vortex and their surface impacts, and in particular how other sources of variability in the Earth system influence these extreme polar vortex states and the resulting tropospheric climate. While such extreme events with effects in the troposphere do occur in the Southern Hemisphere, they are much more frequent in the Northern Hemisphere due to the difference in variability described above. We thus focus on the Northern Hemisphere vortex for the remainder of this introduction, which will provide an overview of the polar vortex extremes, sudden stratospheric warmings and strong polar vortex events, that are of interest for the following work.

We first discuss the weak state of the vortex in Sections 1.1 and 1.2. Sudden stratospheric warmings (SSWs) are disruptions to the typically westerly flow in which the circulation breaks down and polar cap temperature in the stratosphere increases by as much as 50 K in a few days. We discuss the history of observation of these events and their basic features in Section 1.1.1 and the variety of definitions used for them in Section 1.1.2. SSWs are typically divided into two types of events based on the form of the disruption, with the vortex either displaced from the pole or splitting into two smaller vortices. We discuss these types and other classifications of SSWs in Section 1.1.3. Section 1.1.4 reviews the theory of how SSWs occur, related to upward-propagating planetary waves and stratospheric preconditioning. We discuss model representations of SSWs and their key statistics in Section 1.1.5. We then turn to the tropospheric and surface effects of SSWs in Section 1.2. In both the observations and models, SSWs are followed on average by a negative phase of the Northern Annular Mode and the North Atlantic Oscillation for up to two months after SSW onset, with associated temperature and precipitation impacts in Europe, Eurasia, and North America. We first provide a brief overview of stratosphere-troposphere coupling and then discuss the observed and modeled responses to SSWs in Sections 1.2.1 and 1.2.2 respectively. We then close the discussion of SSWs with brief comments on the large variability in this surface response,

which is the focus of the work in Chapter 4, in Section 1.2.3.

We then turn to strong polar vortex events in Section 1.3. Strong polar vortex events (SPVs) are particularly strong circumpolar westerlies, accompanied by a colder than average polar cap. We discuss these basic features in more depth in Section 1.3.1 and then review definitions of SPVs in the literature in 1.3.2. Finally, Section 1.3.3 focuses on the positive Northern Annular Mode and North Atlantic Oscillation response that is typical at the surface following an SPV.

In Section 1.4 we discuss interactions of the stratospheric polar vortex with other modes of variability, particularly the El Niño-Southern Oscillation. We discuss the relationship among stratospheric ozone, the stratospheric polar vortex, and surface climate following SSWs and SPVs in Section 1.4.1.

Section 1.5 concludes the introduction and outlines the remainder of this thesis.

1.1 Sudden Stratospheric Warmings

Sudden stratospheric warmings (SSWs) are events in which the stratospheric polar vortex breaks down in midwinter, named for the rapid spike in polar cap temperature that occurs along with this breakdown. We describe below the first observations of SSWs, their basic features, how they are defined in the literature, and the different types of events. We then turn to the theory of how SSWs occur, precursors to SSWs, and model representations of these events.

1.1.1 History and Basic Features

Sudden stratospheric warmings were first identified by Richard Scherhag from radiosonde measurements taken in Berlin in January 1952 (Scherhag 1952). The same event was identified over the northern United States, with effects on tropospheric climate in Canada and Greenland (Darling 1953). These early observations noted increases in temperature of about 50 K at 50 hPa over the course of a few days, as well as an increased frequency of easterly winds at that level as opposed to the climatological westerlies. The observed temperature increase and zonal wind reversal became the defining features of these events (Labitzke 1977; Quiroz 1975; Schoeberl 1978) and are

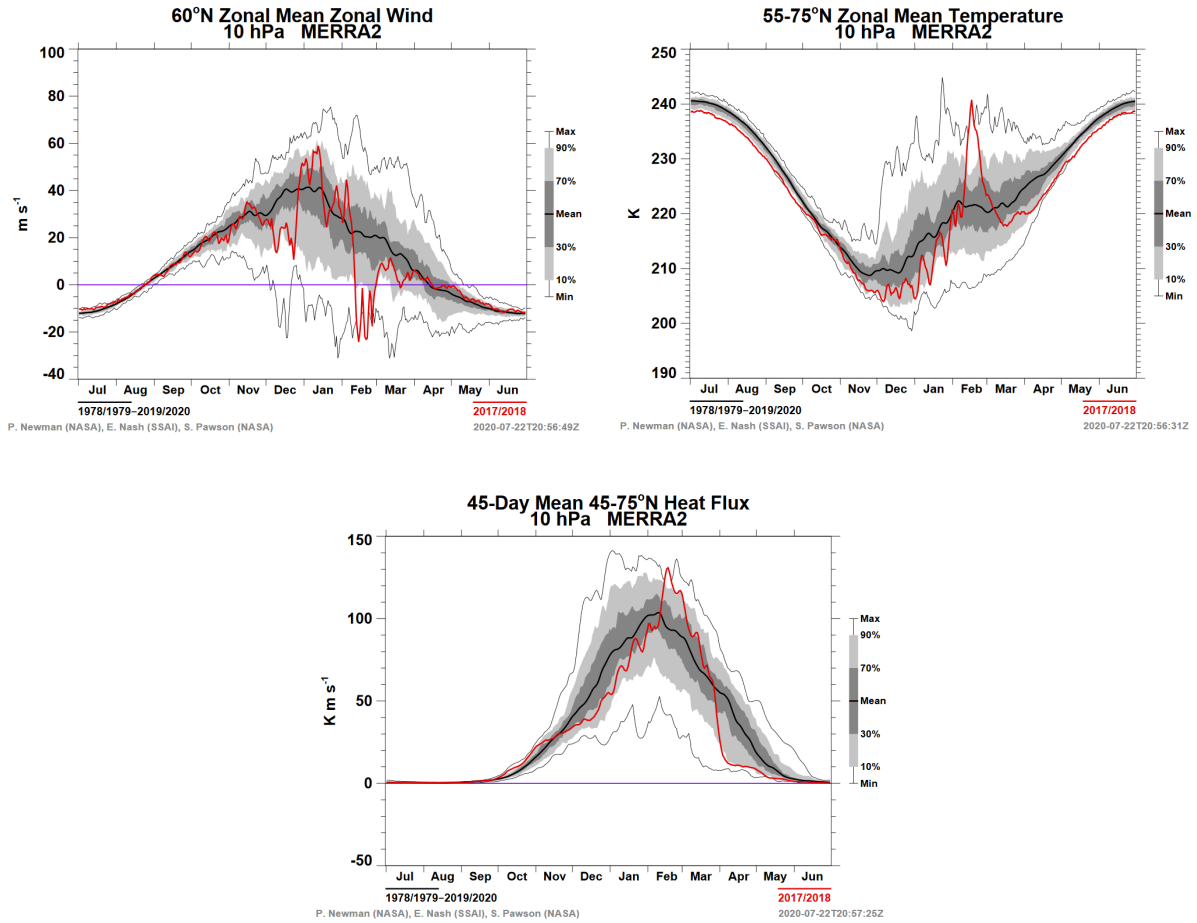

Figure 1.1: The (a) zonal mean zonal wind at 10 hPa and 60° N, (b) zonal mean temperature at 10 hPa and 55-75° N, and (c) 45-day mean midlatitude heat flux at 10 hPa, both on average over the 1978-2020 period (black, uncertainty in gray) and the 2018-19 winter (red), during which an SSW occurred in mid-February. Figures from NASA OzoneWatch.

shown in Figure 1.1. These anomalies typically originate in the upper stratosphere and descend; in the case of temperature, the anomalies can descend to the tropopause and persist for two months following the event, as is illustrated in Figure 1.2.

In terms of a potential vorticity conception of the stratospheric polar vortex, SSWs are events in which this region of high potential vorticity is strongly perturbed by wave breaking (McIntyre and Palmer 1983; McIntyre and Palmer 1984). This generally results in displacement from the pole or splitting into multiple vortices (Baldwin and Holton 1988; Butchart and Remsberg 1986). This disturbance to the vortex takes place over several days, concurrent with the temperature increase

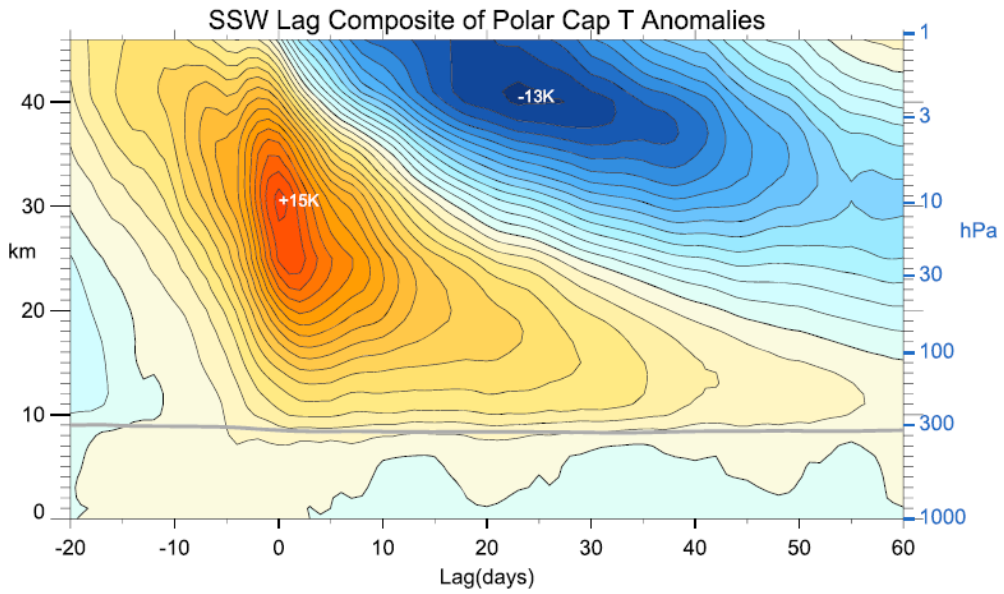

Figure 1.2: Temperature anomalies in the stratosphere and troposphere in days -20 to +60 around the SSW central date. Contours are spaced by 1 K. Figure from Baldwin, Ayarzagüena, et al. (2021).

and deceleration in zonal mean zonal winds, and the vortex often does not recover for two to three weeks (Baldwin, Ayarzagüena, et al. 2021).

SSW frequency varies by the particular definition used to identify these events. That said, the most common definitions yield an average of 6 events per decade in reanalysis over the past 60 years (Butler, Seidel, et al. 2015; Polvani, Sun, et al. 2017). Again using the most common definitions, SSWs are most frequent in the observations in January and February, with the fewest events observed in November while the vortex is still generally strengthening (Charlton and Polvani 2007a). There are not major differences in strength, measured by amplitude of the polar cap temperature anomaly at 10 hPa, of SSWs based on their timing with the exception of March SSWs, which are lower in amplitude than midwinter events (Charlton and Polvani 2007a).

1.1.2 Definitions

The literature includes a wide variety of definitions of sudden stratospheric warmings or weak polar vortex events. Here we review the main classes of such definitions. We then discuss work on

the level of agreement of these definitions and on optimal criteria for identifying SSW events.

Early definitions of SSWs relied on a combination of temperature and zonal mean zonal wind measurements. Reversal of the circulation was used as one criterion to formally distinguish between major and minor warmings, a distinction that dates to at least 1964 (McInturff 1978; WMO/IQSY 1964). The distinction between SSWs, after which the polar vortex recovers, and early and dynamical final warmings, is also found early on (WMO/IQSY 1964). Minor warmings were defined by the World Meteorological Organization Committee on Atmospheric Sciences as temperature increases of at least 25 K in less than a week, at any level of the stratosphere and any location in the winter hemisphere, that did not meet the criteria for major warmings. Major warmings were defined either as increases of at least 30 K below 10 mb or at least 40 K at or above 10 mb in under a week (WMO CAS 1978) or as temperature increases (of at least minor warming magnitude) poleward of 60° N and accompanied by a circulation reversal poleward of 60° N (McInturff 1978). Temperature increase requirements have since generally evolved into requirements of a reversal in meridional temperature gradient; these are less stringent than large (i.e. > 40 K) temperature increase criteria (Butler, Seidel, et al. 2015).

Since then, while no single definition has been canonical, measures based on an absolute threshold of zonal mean zonal wind at 10 hPa are most common, though there is some variation in the latitude(s) used. Zonal mean zonal wind reversal is an appealing definition because of its dynamical implications, limiting the upward propagation of planetary-scale stationary waves (Charney and Drazin 1961; Matsuno 1971; O'Neill and Taylor 1979; Palmer 1981); it is also relatively simple to calculate based on commonly available data. Charlton and Polvani (2007a) defined an SSW as a November-March reversal of the zonal mean zonal winds at 10 hPa and 60° N, separated from any other such reversal by at least 20 consecutive days of westerlies (see corrigendum (Charlton and Polvani 2011)). If this requirement is not met, the reversal is not considered a separate SSW from the earlier event. The definition further requires that after the reversal date, called the central date, the winds must recover to westerly for at least 10 consecutive days before 30 April. Events that do not meet this condition are considered stratospheric final warmings, the

seasonal breakdown of the vortex. This definition differs from the WMO definition mainly in the lack of temperature gradient criterion; the addition of this criterion affects the status of very few events (Charlton and Polvani 2007a).

Similar identification methods, with some variation in latitudes considered, detail, or inclusion of a temperature increase or tendency requirement, have been used elsewhere (Andrews et al. 1987; Ayarzaguena et al. 2013; Bancalá et al. 2012; Christiansen 2001; Labitzke 1981; Labitzke and Naujokat 2000). While there is little sensitivity to including the temperature gradient criterion, there is some sensitivity to latitude considered. Considering reversal at $65°N$ increases SSW frequency; considering mean reversal poleward of $60°N$ increases it further. This is because 60° N is near the edge of the polar vortex, in the surf zone. That is, when the zonal mean zonal winds at 60° N reverse, the winds poleward also reverse, and those equatorward often do not.

Another common approach to SSW identification involves empirical orthoogonal functions (EOFs) of geopotential height anomalies (Baldwin and Dunkerton 2001; Baldwin and Thompson 2009b; Gerber 2010) or zonal mean zonal wind at a particular pressure level (Limpasuvan, Thompson, et al. 2004). Baldwin and Dunkerton (2001) calculated the Northern Annular Mode (NAM) using EOFs of geopotential height anomalies at 10 hPa and identified events with a NAM index of -3 or below as weak vortex events. EOFs of vertical profiles of polar cap temperature have also been used (Hitchcock, Shepherd, and Manney 13; Hitchcock and Shepherd 2013; Kuroda et al. 2004). These methods are fundamentally different from circulation reversal definitions in being relative as opposed to absolute thresholds; they identify weak polar vortex events relative to the climatological state of the vortex (Palmeiro et al. 2015).

Similar methods to those already described include those based on polar cap-averaged geopotential height anomalies (Thompson 2001), which are similar to those based on NAM indices, and those that use tendencies of the NAM (Martineau et al. 2013), polar cap temperature (Nakagawa and Yamazaki 2006), or zonal mean zonal wind as opposed to a direct measure of those quantities. Other methods such as vortex moments or other vortex geometry-based approaches (Hannachi et al. 2011; Matthewman, Esler, et al. 2009; Mitchell, Charlton-Perez, and Gray 2011; Mitchell,

Gray, et al. 2013; Seviour, Mitchell, et al. 2013; Waugh, Randel, et al. 1999), k-means clustering (Coughlin and Gray 2009), or neural network-based approaches (Blume et al. 2012) have also been used. These definitions are a mix of absolute and relative methods; for example, vortex moment methods are absolute, and those based on NAM indices in any way are relative.

These varied definitions can have meaningful implications (Butler, Seidel, et al. 2015; Palmeiro et al. 2015). SSW frequency as calculated by these definitions varies from 3.5 events per decade to 8 or 9 events per decade. Under some definitions we see decades with almost no SSWs (notably, the 1990s); others show no such gap, classifying as major SSWs what other definitions would consider to be minor events. Seasonal distributions are largely similar across definitions, though vortex moment approaches identify a higher fraction of SSWs in March, and EOF and temperature tendency methods identify a higher fraction in December. These statistics are particularly important for considering how SSWs will change (or not change) in the future. The SSW definition used also has implications of the strength of the surface response to the event. Those definitions that capture more minor warmings show weaker coupling to the surface on average.

Butler, Seidel, et al. (2015) found that, using a zonal mean zonal wind-based definition, a threshold anywhere between reversal and < 5 ms^{-1} made little difference to SSW frequency. Requiring stronger easterly winds, however, drastically reduced the number of SSWs identified in reanalysis. The relationship to latitude was more linear; more SSWs are identified as the latitude used at which zonal mean zonal wind reversal is measured moves poleward from about 55° N. Butler and Gerber (2018) studied zonal mean zonal wind-based definitions and found that, based on several key characteristics, definitions based on winds at levels between 30 and 5 hPa, at latitudes between 55-70° N, and with decelerations to near or below 0 ms^{-1} were optimal. This supports the continued use of the Charlton and Polvani (2007a) and Charlton and Polvani (2011) definition, which is the SSW identification method that we use throughout this thesis.

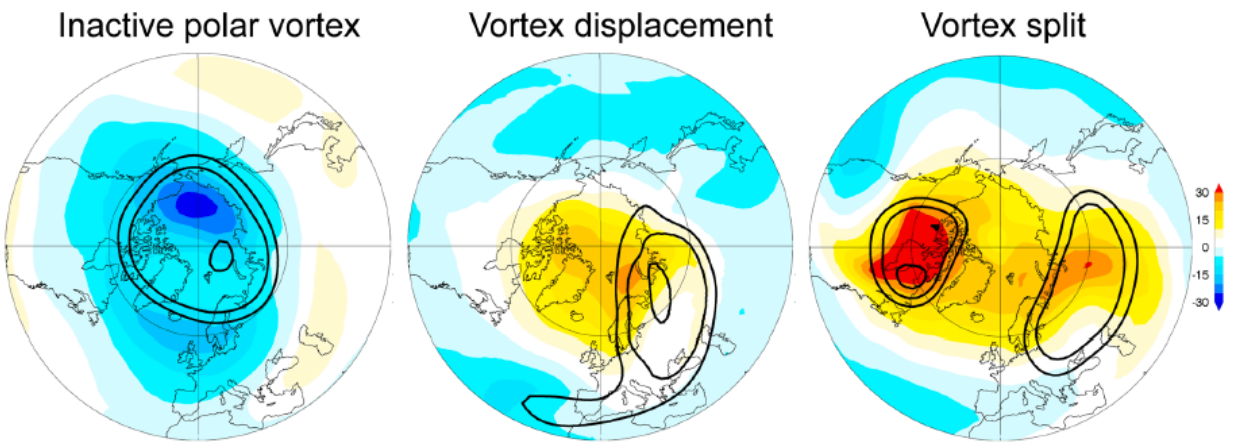

Figure 1.3: Temperature anomalies at 10 hPa (color, K) and potential vorticity at 550 K (contours for 75, 100, 125 units) for three states of the polar vortex: (a) undisturbed/strong, (b) displacement SSW, and (c) split SSW. Figure from Butler, Sjoberg, et al. (2017).

1.1.3 Types of SSWs

SSWs are often classified into one of two types of events, splits or displacements, based on the form of the vortex disruption. A split event involves the vortex splitting into two smaller vortices of equal size, and a displacement involves the vortex elongating and shifting off the pole, often forming a comma shape. This is illustrated in Figure 1.3. These different types of SSWs are of interest because they may have different precursors or mechanisms (Matthewman and Esler 2011). Whether they have different effects on the surface following the SSW is unclear (Charlton and Polvani 2007a; Karpechko, Hitchkock, et al. 2017; Maycock and Hitchcock 2015; Mitchell, Gray, et al. 2013; Nakagawa and Yamazaki 2006; Seviour, Gray, et al. 2016; White, Garfinkel, et al. 2019).

There are several ways of identifying an SSW as a split or displacement. One type of method is based on local maxima of absolute vorticity (Ayarzagüena, Palmeiro, et al. 2019; Charlton and Polvani 2007a), another is based on vortex aspect ratio and centroid (Gerber, Martineau, et al. 2021; Mitchell, Charlton-Perez, and Gray 2011; Mitchell, Gray, et al. 2013; Seviour, Mitchell, et al. 2013), and a third is based on a similar idea to the local maxima approach but uses geopotential height like the vortex geometry approach (Lehtonen and Karpechko 2016). These methods agree

on about two-thirds of SSW events. The other third are classified inconsistently and may show aspects of both a split and a displacement at different times (Gerber, Martineau, et al. 2021; Rao, Garfinkel, and White 2020b).

SSW events can also be classified as wave-1 or wave-2 events, based on the more dominant wave activity preceding them (Bancalá et al. 2012; Barriopedro and Calvo 2014; Castanheira and Barriopedro 2010; Garfinkel, Hartmann, and Sassi 2010; Tung and Lindzen 1979; Woollings et al. 2010). This is of interest because of the mechanism of some SSWs based in dynamical forcing of the stratospheric polar vortex by enhanced tropospheric wave activity, described in the next section. The classification of SSWs by wave number aligns to some extent with the split/displacement classification, with most wave-2 events being splits and most wave-1 events being displacements (Gerber, Martineau, et al. 2021). However, only just over half of events classified unambiguously as splits are wave-2 events, suggesting that split SSWs are not driven solely by wave number-2 driving and instead occur through a top-down mechanism (Albers and Birner 2014; Gerber, Martineau, et al. 2021; Watt-Meyer and Kushner 2015). We now turn to these proposed dynamical theories of SSWs.

1.1.4 Theory of SSWs

There are two broad categories of dynamical theories for how SSWs occur. The first is based on anomalous wave forcing from the troposphere and is the more traditional mechanism. The second is focused on preconditioning or resonance of the stratospheric polar vortex and is a more top-down mechanism. We have observed SSWs consistent with both mechanisms and some which do not fit neatly into either theory (Birner and Albers 2017). We briefly review each of these proposals below, though we note that many variations on each are present in the literature.

An early and one of the most-frequently cited forms of the bottom-up theory is that of Matsuno (1971). This mechanism relies on sufficiently strong and non-steady upward-propagating waves from the troposphere. Anomalously large upward-wave activity into the stratosphere results in poleward heat flux, which induces a mean meridional circulation. This results in a deceleration

of the westerly winds. For sufficiently strong wave activity, this can reverse the zonal mean flow, establishing a critical level and preventing further wave propagation (Holton 1980; Matsuno 1971). This mechanism is consistent with work showing tropospheric features that strengthen planetary wave forcing, such as blocking in some regions, often precede SSWs (e.g., Martius et al. 2009). Later work has shown that sustained wave forcing over a 40 to 60 day period is more effective in decelerating the mean flow than a single anomalous pulse of wave activity (Newman et al. 2001; Polvani and Waugh 2004; Sjoberg and Birner 2012).

The top-down mechanism suggests instead that climatological wave forcing is sufficiently strong for SSWs to occur and that the stratosphere has a much more important role in generating these events. Some features of this had been incorporated within the bottom-up paradigm, for example suggesting that preconditioning of the vortex or geometry and strength of the vortex are important to the interaction of wave activity with the mean flow (Albers and Birner 2014; McIntyre 1982; Palmer 1981). The top-down mechanism results in a disruption to the vortex due to self-tuned resonance instability (Esler and Matthewman 2011; Esler, Polvani, et al. 2006; Matthewman and Esler 2011; Plumb 1981), in which nonlinear feedbacks allow the vortex to self-tune towards resonance when forced with an off-resonant frequency. Many SSWs in observations and models occur without any anomalous tropospheric wave flux (Birner and Albers 2017; de la Cámara et al. 2019; White, Garfinkel, et al. 2019), consistent with this mechanism.

1.1.5 Modeling and Forecasting SSWs

We now turn from low-dimensional models aimed at understanding the dynamics of SSWs to climate models and forecast models used to represent and predict SSWs in the context of the rest of the atmospheric system. Here we briefly address two key questions. First, how well do climate models capture key features of statistics of SSWs? Second, how predictable are SSWs in subseasonal forecast models?

Butchart, Cionni, et al. (2010) and Mitchell, Osprey, et al. (2012) found that the zonal mean features of the polar vortex are well represented in chemistry-climate models, but geometric features

(or vortex moments) were not consistent with reanalysis. In particular, the vortex across the models was too far poleward (Mitchell, Osprey, et al. 2012). In contrast, Seviour, Gray, et al. (2016) found a wide variety of biases in vortex geometry in high-top CMIP5 models, with some vortices too far poleward and some too far equatorward. However, a too zonal vortex was a widespread bias.

While the SSW frequency in the multi-model mean of chemistry-climate models was similar to that seen in reanalysis, some models had frequencies that were much too low (Butchart, Cionni, et al. 2010; Mitchell, Osprey, et al. 2012). SSW frequency was generally better represented by high-top models that more accurately captured stratospheric variability (Butchart, Cionni, et al. 2010), consistent with the results of Charlton-Perez, Baldwin, et al. (2013) on CMIP5 models. Wu and Reichler (2020) found that the better representation of SSW frequency in models with high lids and high stratospheric resolution was related to more realistic temperatures in the tropical upper troposphere-lower stratosphere and a resulting better representation of upward-propagating wave activity. Despite these results on high-top and high vertical resolutions models, SSW frequency can still vary widely (e.g., by a factor of 2) across ensemble members of individual high-top models (Polvani, Sun, et al. 2017). Seviour, Gray, et al. (2016) further studied the frequency of split and displacement events and found that while the multi-model mean was again consistent with reanalysis, models had a wide variety of biases, often related to their mean state biases.

Extreme events of the polar vortex are not currently predictable beyond synoptic timescales. Domeisen, Butler, Charlton-Perez, et al. (2020b) found that in forecast models from the S2S (subseasonal-to-seasonal) project (Vitart et al. 2017), about 50% of ensemble members across high-top models studied captured a midwinter (DJF) SSW or an early winter weak polar vortex event at a lead time of -10 to -6 days; that increased to about 90% at a lead time of -5 to -1 days (Domeisen, Butler, Charlton-Perez, et al. 2020b; Tripathi et al. 2015). Low-top models generally performed less well, particularly for midwinter SSWs. However, there is a large amount of event-to-event variability in predictability regardless of model (Karpechko 2018; Rao, Garfinkel, and Ren 2019).

1.2 Surface Impacts of SSWs

We have already established that events in the troposphere can affect the stratosphere. However, the stratosphere does not simply respond to disturbances from the troposphere. Conditions in the stratosphere, particularly the polar stratosphere, can affect the state of tropospheric and surface climate. This is particularly important because it can give us predictability at the surface based on the state of the stratosphere. In this section, we discuss the observed and modeled composite surface response to SSWs, proposed dynamical theory for this response, and event-to-event variability in surface climate following SSWs.

1.2.1 Observed Response to SSWs

A weak vortex event results in a negative Northern Annular Mode in the upper and middle stratosphere. The Northern Annular Mode (NAM) is the first mode of climate variability at a hemispheric scale in the Northern Hemisphere, characterized by opposite signs of pressure anomalies over the polar cap and at lower latitudes. It can be defined at each level in the atmosphere. Near and at the surface, it is also known as the Arctic Oscillation (AO) and projects in the North Atlantic region onto the North Atlantic Oscillation (NAO), which is characterized by a pressure dipole between Iceland and the Azores/Iberian Peninsula. Because the NAM can be calculated at each level or height and SSWs are associated with a negative NAM index, it is a useful tool for studying potential responses to SSWs at lower levels in the atmosphere.

Baldwin and Dunkerton (2001) found that, on average, the negative NAM index associated with weak vortex events descends to the surface, resulting in a negative NAM index for up to two months after the SSW central date. This is shown in Panel (A) of Figure 1.4. This manifests as a negative NAO pattern, with a weaker and wavier eddy-driven jet stream (Kidston et al. 2015) and effects on temperature and precipitation. In particular, the temperature patterns associated with a negative NAO are colder than average temperatures and increased cold air outbreaks in northern Europe and Eurasia and the eastern United States and warmer than average temperatures

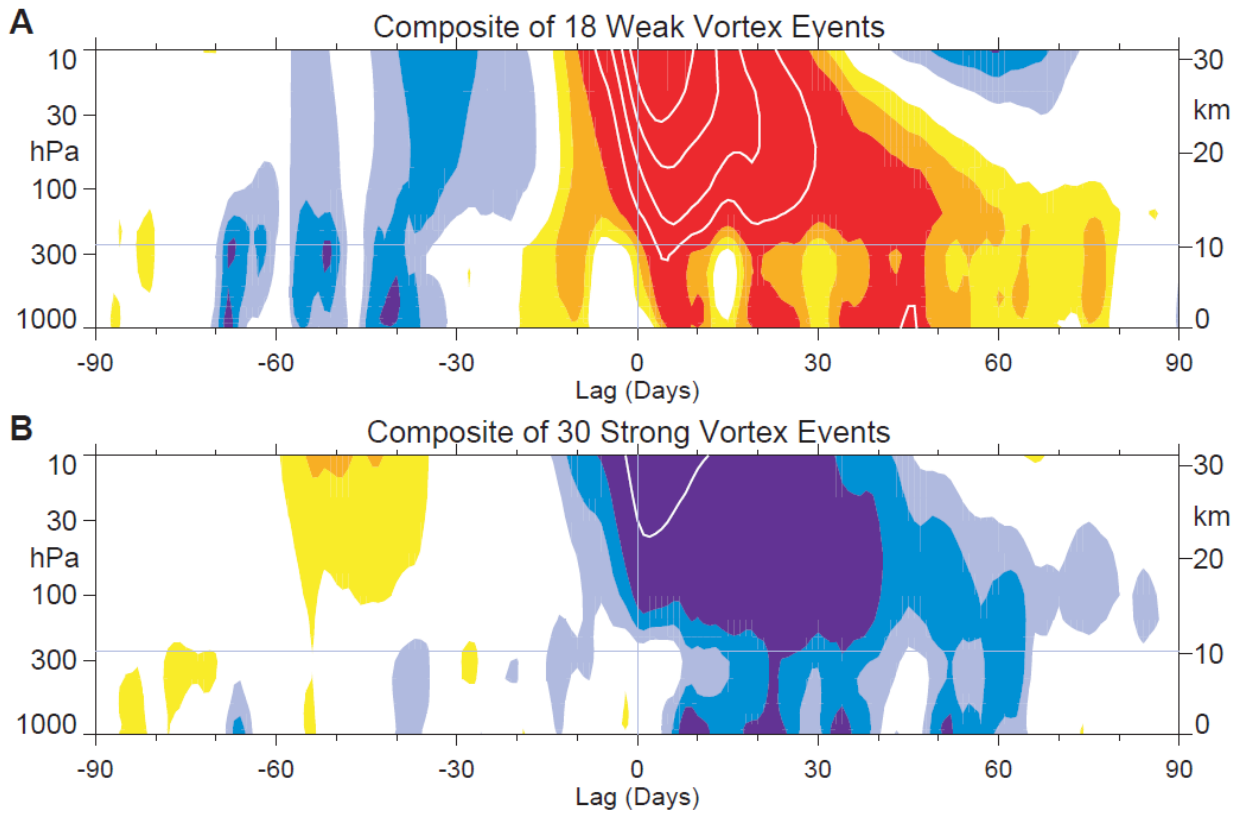

Figure 1.4: The NAM index surrounding the central date for weak and strong polar vortex events, showing the downward propagation to the surface. Contours for colors are separated by 0.25 units. White contour lines are separated by 0.5 units. Figure from Baldwin and Dunkerton (2001).

in eastern Canada, western Greenland, North Africa, the Middle East, and Central Asia (e.g., Butler, Sjoberg, et al. 2017; Domeisen and Butler 2020; King et al. 2019; Kolstad, Breiteig, et al. 2010; Scaife, Folland, et al. 2008; Thompson and Wallace 2001). The corresponding precipitation anomalies include an abnormally dry northern Europe and increased precipitation in Southern Europe (e.g., Ayarzagüena, Barriopedro, et al. 2018; Butler, Sjoberg, et al. 2017; Domeisen and Butler 2020; King et al. 2019). These composite surface climate anomalies, calculated from the JRA-55 Reanalysis, are shown in Figure 1.5 (Butler, Sjoberg, et al. 2017).

There is some evidence for impacts of SSWs on sea ice, as well. In particular, winters in reanalysis with an SSW and no strong polar vortex event were followed by increased winter sea ice concentration in the Sea of Okhotsk, increased winter and spring sea ice concentration in the Barents Sea, and increased summer sea ice concentration in the Laptev, East Siberian, and Chukchi

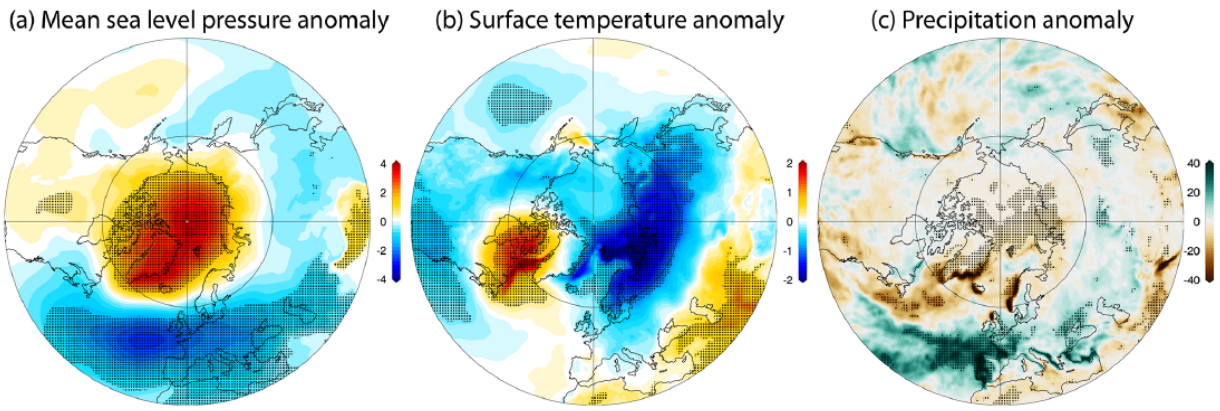

Figure 1.5: The surface response to SSWs in the JRA-55 Reanalysis: (a) sea level pressure anomaly (hPa), (b) surface temperature anomaly (K), and (c) precipitation anomaly (mm/day). Figure from Butler, Sjoberg, et al. (2017).

Seas (Smith, Polvani, and Tremblay 2018). These relationships are based on few events but are consistent with results from model simulations shown in Figure 1.6.

1.2.2 Modeled Response to SSWs

The key features of the surface response to SSW are generally reproduced by models that accurately capture stratospheric variability and heat flux extremes (Shaw et al. 2014). This includes coupled chemistry-climate models (Gerber 2010), though the signal at the surface is too persistent in some models. Haase and Matthes (2019) further found that interactive chemistry is important for representing the stratospheric polar vortex, SSWs, and the surface response to SSWs.

Figure 1.7 panels (a) and (b) show the 2m temperature response to weak vortex events in reanalysis and in the multi-model mean of a set of weeks 3-4 forecasts from forecast models initialized in weak vortex states (Domeisen, Butler, Charlton-Perez, et al. 2020a). The multi-model mean captures the key features of the observations, though the anomalies are of lower magnitude than seen in reanalysis. Initializing the forecast models in a weak vortex state leads to increased skill in eastern Russia, the Caucasus and central Asia, and the central United States. Sigmond et al. (2013) had similarly found increased skill in temperature in eastern/northern Russia and eastern Canada as well as precipition in the North Atlantic. The temperature dipole over Eurasia

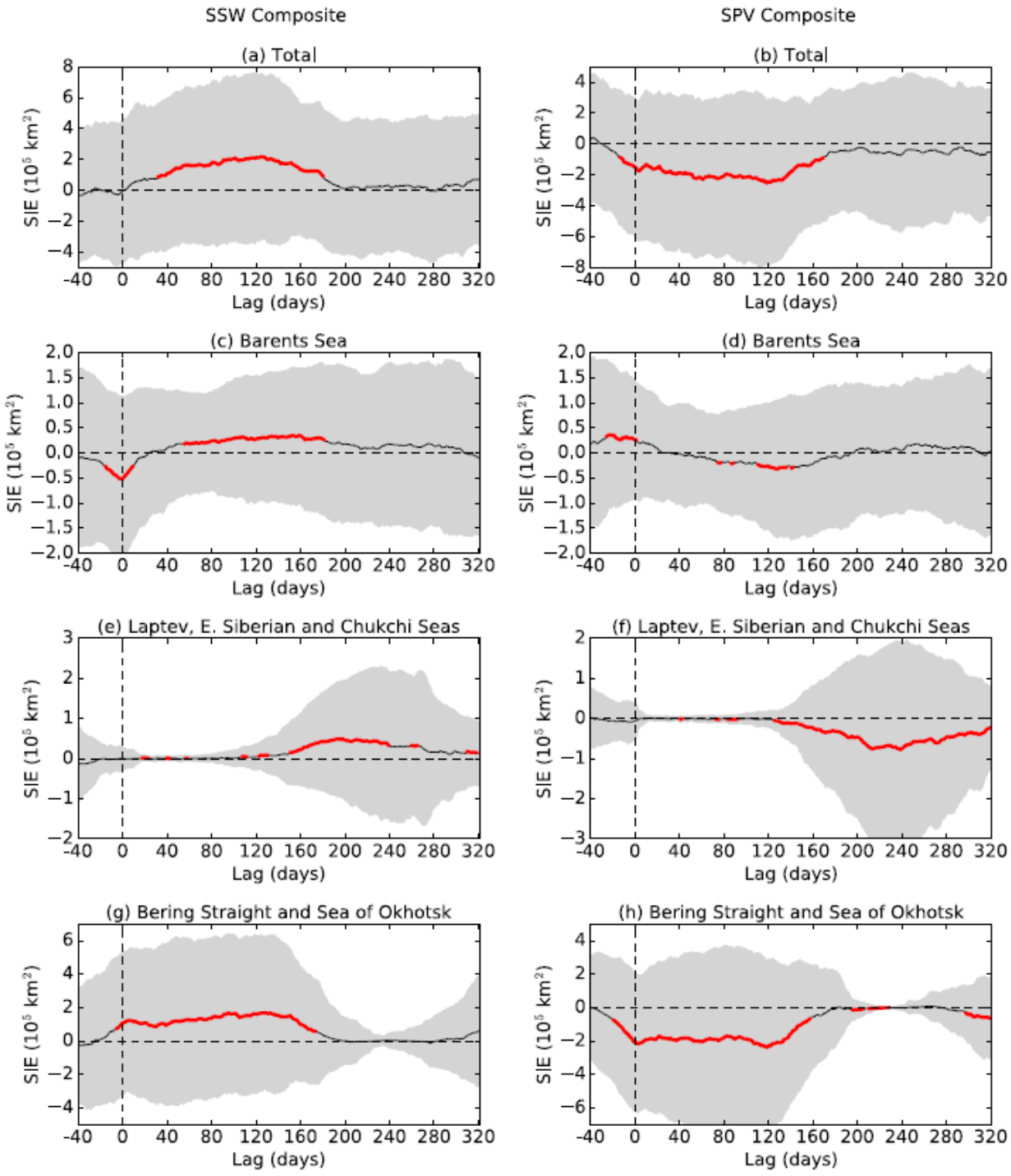

Figure 1.6: Sea ice concentration anomalies in years following winters with (left) SSWs and (right) SPVs in a simulation from the Whole Atmosphere Community Climate Model. Figure from Smith, Polvani, and Tremblay (2018).

is more zonal in the multi-model mean, with the zero-line shifted south from the reanalysis. This may contribute to decreased forecast skill in Europe, but it is difficult to determine whether this difference is due to sampling variability in the observations or to model bias. Scaife, Karpechko, et al. (2016) found that SSW members including SSWs in seasonal forecasts led to a prediction of an absolute NAO shift of -6.5 hPa on average. They further determined that excluding members with SSWs from ensembles decreased NAO prediction skill from 0.62 to 0.09; NAO prediction skill was dependent on the inclusion of SSWs. Sun, Perlwitz, et al. (2020) found that the predictive skill for the NAO following weak polar vortex events came mainly from the stratosphere as opposed to other correlated sources of variability. Overall, SSWs and other stratospheric extreme events contribute to increased predictability at the subseasonal and seasonal timescales in the North Atlantic and Europe (Butler, Charlton-Perez, et al. 2019; Dobrynin et al. 2018; Nie et al. 2019; O'Reilly et al. 2019; Tripathi et al. 2015). However, as discussed below, there is a great deal of variability in the observations in surface response to SSWs, and some forecast models overestimate NAO response to stratospheric extremes (Kolstad, Wulff, et al. 2020).

1.2.3 Variability in Surface Response to SSWs

While the mean observed response to SSWs over the past 60 years is well known, and high-top models capture the key features of this response, there is a great deal of event-to-event variability in this response. In particular, for only two-thirds to three-quarters of SSWs does the negative NAM (or equivalently, the polar cap geopotential height anomaly) descend to the troposphere and the surface (Afargan-Gerstman and Domeisen 2020; Butler, Lawrence, et al. 2020; Domeisen 2019; Karpechko, Hitchkock, et al. 2017). Even in those events that do propagate downward, the magnitude of surface anomalies and the particular spatial pattern can vary considerably. These questions of variability prompt our work in Chapter 4 of this thesis, focused on uncertainty in the composite response to SSWs. We here review work on event-to-event uncertainty in the surface response.

Prior work has suggested both stratospheric and tropospheric sources of this variability. Stronger

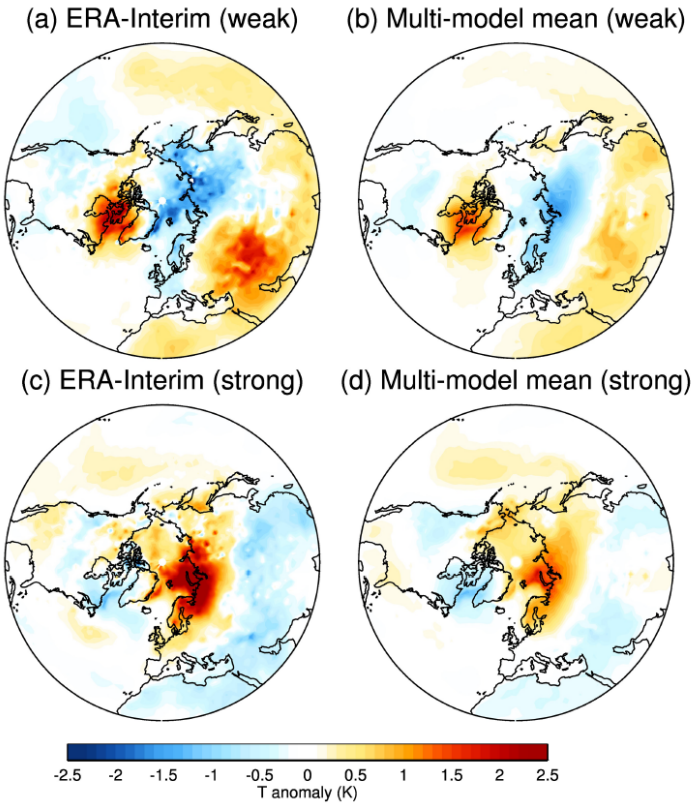

Figure 1.7: Two-meter temperature composites in weeks 3-4 following (a) the onset of an (a-b) SSW or (c-d) SPV in the (a,c) ERA-Interim reanalysis and (b,d) forecasts from subseasonal models initialized in a weak/strong polar vortex state. Figure from Domeisen, Butler, Charlton-Perez, et al. (2020a).

downward propagation of the SSW to the lower stratosphere, 100 hPa and lower, is somewhat related to the event's continued descent to the troposphere (Baldwin 2003; Christiansen 2005; Gerber, Orbe, et al. 2009; Rao, Garfinkel, and White 2020b; Siegmund 2005), perhaps related to wave activity following the SSW central date (Karpechko, Hitchkock, et al. 2017; Kodera et al. 2016), but predicting which events will and will not descend is not yet possible (Baldwin, Ayarzagüena, et al. 2021). Some work suggests that split and displacement events have different impacts on the surface, often with different blocking patterns and stronger surface signals following split events Mitchell, Gray, et al. (2013), Nakagawa and Yamazaki (2006), and Seviour, Gray, et al. (2016); other studies see little such difference (Karpechko, Hitchkock, et al. 2017; Maycock and Hitchcock 2015; White, Garfinkel, et al. 2019).

Tropospheric sources of variability in the surface signal include existing patterns or regimes in the troposphere, particularly in the North Atlantic and European region, as well as other important modes of variability such as the El Niño-Southern Oscillation (ENSO) or the Madden-Julian Oscillation (MJO). Domeisen, Grams, et al. (2020) found differing probabilities of North Atlantic weather regimes following an SSW based on the weather regime prior to the SSW. Locations of blocking or other SSW precursors may affect downward propagation or surface signal (Afargan-Gerstman and Domeisen 2020; Nakagawa and Yamazaki 2006; Peings 2019; Tyrrell et al. 2019; White, Garfinkel, et al. 2019; Zhang et al. 2019), and forcings related to the North Pacific (Drouard et al. 2013; Honda and Nakamura 2001) or sea ice (Sun, Deser, et al. 2015) also impact the anomalies at the surface following SSWs. Different ENSO phases can strengthen or diminish the negative NAO signal at the surface (Brönnimann 2007; Butler, Polvani, and Deser 2014; Butler and Polvani 2011; Calvo, Iza, et al. 2017; Oehrlein et al. 2019; Polvani, Sun, et al. 2017), though it is inconsistent or unclear in the observations and models how this is dependent on ENSO strength or type, whether the signal in the absence of a stratospheric pathway is meaningful, and whether the ENSO influence in the North Atlantic projects onto the NAO or a different pattern (Bell, Gray, Charlton-Perez, et al. 2009; García-Serrano et al. 2011; Hardiman, Dunstone, et al. 2019; Ineson and Scaife 2009; Jiménez-Esteve and Domeisen 2020; Li and Lau 2012; Mezzina et al. 2020;

Richter et al. 2015; Toniazzo and Scaife 2006; Trascasa-Castro et al. 2019; Weinberger et al. 2019; Zhou, Chen, Wang, et al. 2020; Zhou, Chen, Xie, et al. 2019). Schwartz and Garfinkel (2017) and Green and Furtado (2019) find modulations of the surface pattern following SSWs or SPVs by MJO phase, with some MJO phases resulting in constructive or destructive interference with the result of stratospheric variability or leading to a different pattern entirely. In addition to affecting the tropospheric and surface signals of extreme stratospheric events, these other features or phenomena can also impact the stratosphere directly, thus influencing surface climate through the stratospheric polar vortex, as discussed in Section 1.4.

1.3 Strong Polar Vortex Events

SSWs comprise one tail of the distribution of stratospheric polar vortex strength. At the other tail are strong polar vortex events (SPVs), or events with especially strong westerly flow around the polar cap. In this section, we outline the features of SPVs, the variety of definitions that have been used in the literature, and the surface climate following these events.

1.3.1 Basic Features

SPVs generally result from an extended period of abnormally weak planetary wave activity, allowing for a more stable polar vortex. They are not exact parallels to SSWs; the particularly strong westerlies and the lack of wave activity do not have the same rapid, dynamical nature as the wind reversal and quickly cut-off wave activity of SSWs. As a result, SPVs often occur more gradually and less dramatically, and after the event, the vortex tends to return to climatology more quickly (Limpasuvan, Hartmann, et al. 2005). However, SPVs still have important consequences, both in the stratosphere and at the surface.

SPVs are characterized by an increase in strength of the circumpolar westerlies and a corresponding decrease in stratospheric temperature over the polar cap due to thermal relaxation (Limpasuvan, Hartmann, et al. 2005). For example, in the 2019-20 winter, the Northern Hemisphere polar vortex was abnormally (and record-breakingly) strong, first briefly in January and

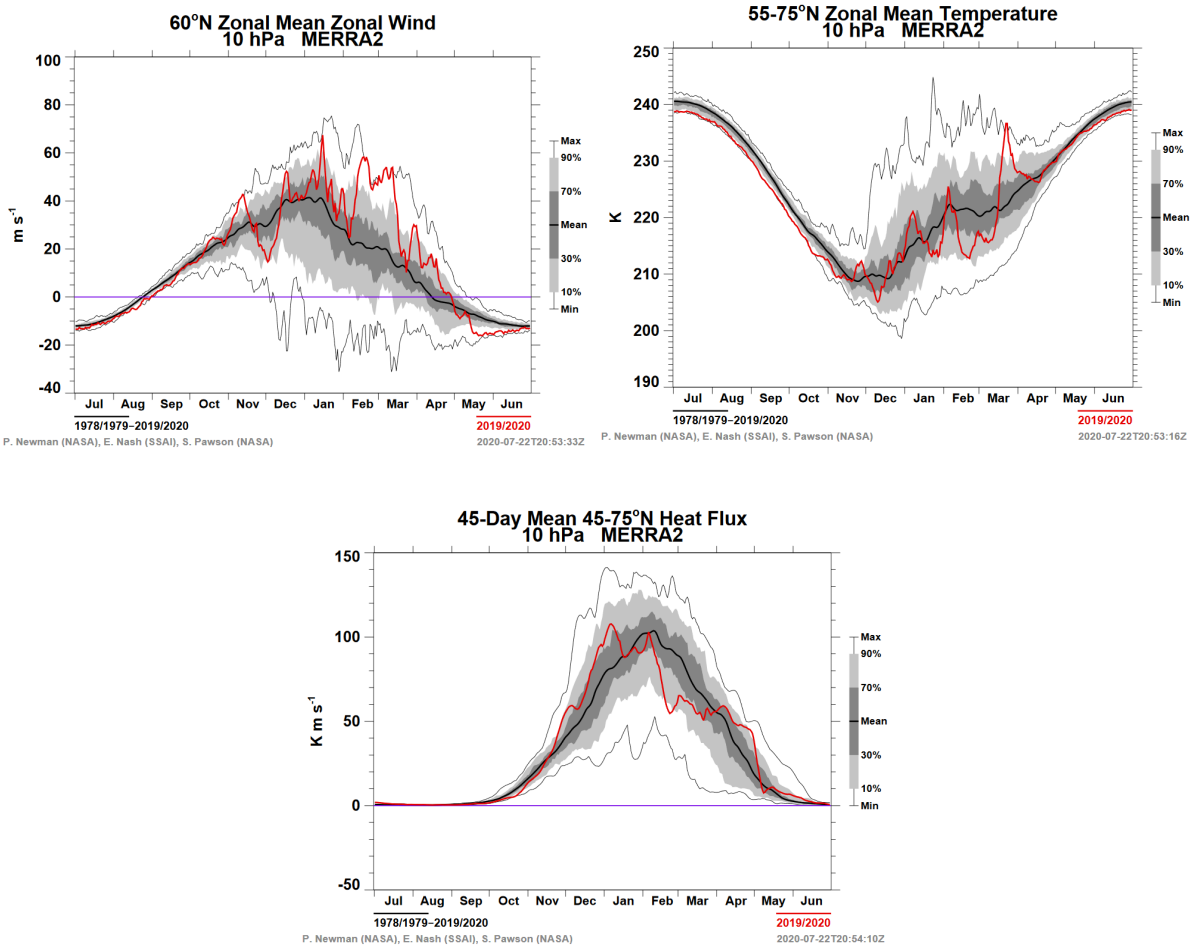

Figure 1.8: The (a) zonal mean zonal wind at 10 hPa and 60° N, (b) zonal mean temperature at 10 hPa and 55-75° N, and (c) 45-day mean midlatitude heat flux at 10 hPa, both on average over the 1978-2020 period (black, uncertainty in gray) and the 2019-20 winter (red), during which an SPV occurred in mid-February. Figures from NASA OzoneWatch.

then for a more sustained period of time in February and March (Lawrence et al. 2020). Figure 1.8 illustrates the typical life cycle of the polar vortex compared to that observed in the 2019-20 winter. The increased zonal mean zonal winds at 10 hPa are associated with lower than average temperatures and decreased 45-day mean heat flux at the same level, indicating the lower levels of wave activity that preceded the strong vortex event.

SPVs are also often associated with low ozone transport and mixing into the polar region. SPVs in the 1996-97, 2010-11, and 2019-20 winters have resulted in some of the Arctic winters and springs with the lowest recorded total column ozone levels. This is illustrated in Figure 1.9,

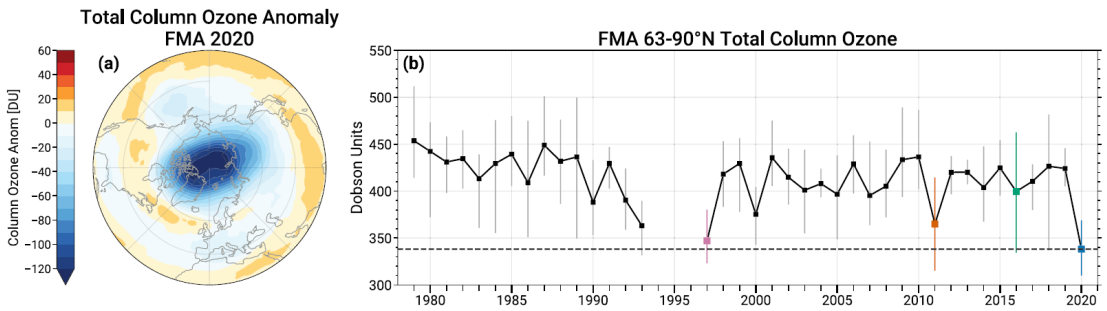

Figure 1.9: The (a) spatial total column ozone anomaly and (b) total column ozone response in Dobson units to the SPV in the 2019-20 winter compared to prior winters. Figure from Lawrence et al. (2020).

showing the total column ozone anomaly in February-April 2020 and the time series of total column ozone over the polar cap, with winters with especially extreme SPVs highlighted (Lawrence et al. 2020). The winter of 2015-16 is highlighted despite not having a particularly negative total column ozone anomaly; after a strong polar vortex through much of the winter, a dynamical (SSW-like) final warming began in early March, while there was still low sunlight (Manney and Lawrence 2016).

The Arctic stratosphere is not frequently conducive to the formation of polar stratospheric clouds (PSCs) that aid in chemical ozone destruction. However, a persistently strong polar vortex such as that seen in the 2019-20 winter can result in temperatures low enough for PSCs to form, enhancing ozone destruction.

The frequency of SPVs varies strongly by definition, and as discussed below, definitions are sometimes chosen to produce a similar number of SPVs as SSWs. Using the definition of Scaife, Karpechko, et al. (2016) and Smith, Polvani, and Tremblay (2018), about 7 SPVs occur per decade in reanalysis. The majority of these, about 4.5 events per decade, have been December events.

1.3.2 Definitions

Several definitions of SPVs have been used in the literature, and no single definition is currently standard. Many were written to intentionally parallel SSW definitions. As with SSWs, these definitions include a mix of relative and absolute thresholds at different levels.

Baldwin and Dunkerton (2001) identified strong vortex events using the same measure based on an EOF of geopotential height by which they calculated weak vortex events, choosing an annular mode threshold to yield a downward-propagating signal and sufficient events in the reanalysis data used. Limpasuvan, Hartmann, et al. (2005) also used an EOF process, but based on zonal mean zonal wind as opposed to geopotential height. Drawing on aspects of both of these definitions, Beerli and Grams (2019) modified the process used by Limpasuvan, Hartmann, et al. (2005) but applied it to the 50 hPa polar cap geopotential height anomaly instead of zonal mean zonal wind. Finally, Tripathi et al. (2015) used a simpler but still relative threshold, defining events based on zonal mean zonal winds at 10 hPa and 60° N exceeding the 80th percentile across November through March; this corresponded to 41.2 ms^{-1} in their forecast model dataset.

Scaife, Karpechko, et al. (2016) and Smith, Polvani, and Tremblay (2018) identified SPVs as the zonal mean zonal wind at 10 hPa and 60° N exceeding 48 ms^{-1}, with no new SPV defined until the winds have been below that threshold for at least 20 days. This absolute threshold was chosen by Scaife, Karpechko, et al. (2016) to produce a similar number of SPVs as SSWs in their forecast model simulations, and Smith, Polvani, and Tremblay (2018) found that also produced a similar number of SPVs as SSWs in their WACCM4 simulations and ERA-Interim. Domeisen, Butler, Charlton-Perez, et al. (2020a) used a similar definition with a threshold of 40 ms^{-1} instead. This threshold was chosen to be similar to that used in Tripathi et al. (2015), but they found that results were robust to changes in this threshold of 5 ms^{-1}.

In chapter 3 of this thesis, we will follow Scaife, Karpechko, et al. (2016) and Smith, Polvani, and Tremblay (2018) to parallel our SSW definition and because we use similar WACCM4 runs to those used by Smith, Polvani, and Tremblay (2018). However, we too find that the results are robust to changes in the value of this absolute threshold.

1.3.3 Surface Response to SPVs

SPVs, like SSWs, are followed by downward propagation of the annular mode to the lower stratosphere and frequently to the troposphere and surface. This is shown in Figure 1.4 (Baldwin

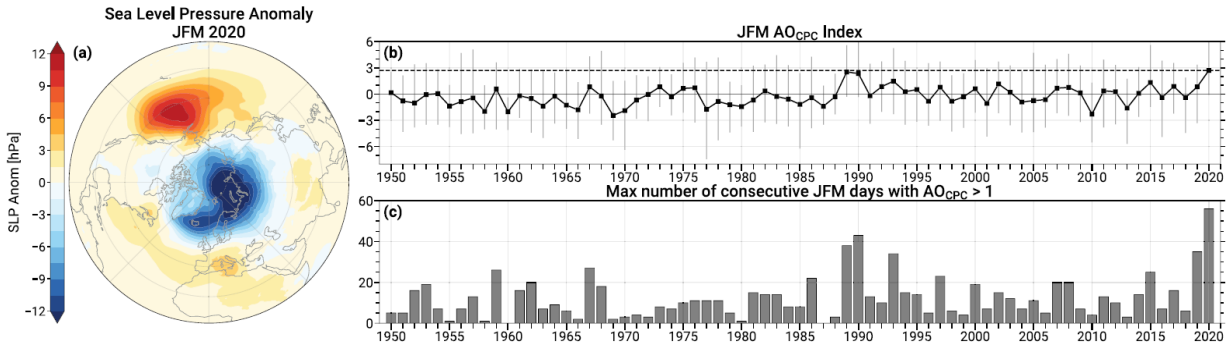

Figure 1.10: The (a) sea level pressure and (b) January-March Arctic Oscillation response to the SPV in the 2019-20 winter compared to prior winters. Figure from Lawrence et al. (2020).

and Dunkerton 2001). As with SSWs, the resulting signal at the surface can persist for up to two months following the onset of the SPV in the upper stratosphere.

In the North Atlantic and European region, this positive surface NAM projects onto the positive phases of the Arctic and North Atlantic Oscillations (Baldwin and Dunkerton 2001; Lawrence et al. 2020). This mode entails a poleward-shifted eddy-driven jet stream (Kidston et al. 2015), conditions that are warmer, wetter, and stormier than average in Northern Europe, colder and drier than average conditions in Southern Europe (Baldwin and Dunkerton 2001; Domeisen and Butler 2020; Huntingford et al. 2014; Hurrell 1995; Lawrence et al. 2020). Figure 1.10 illustrates the Arctic Oscillation response to the particularly strong 2019-20 SPV (Lawrence et al. 2020), and Figure 1.7 shows the temperature response to SPVs in ERA-Interim and an ensemble mean of forecast models (Domeisen, Butler, Charlton-Perez, et al. 2020a).

SPVs also have affects on sea ice concentration and thickness throughout the year. Smith, Polvani, and Tremblay (2018) found, in both a GCM and reanalysis, decreased sea ice extent in the Bering Straight and Sea of Okhotsk in the four to five months following an SPV and in the Laptev, East Siberian, and Chukchi Seas in the fall following an SPV (Figure 1.6). The impact on the Laptev, East Siberian, and Chukchi Seas in particular was found to be associate with sea ice thickness anomalies arising from sea ice divergence that has been linked to the AO/NAO Rigor (2002).

1.4 SSWs and Other Modes of Variability

Phenomena in the rest of the Earth system interact with the stratospheric polar vortex, either by the state of the polar vortex influencing other features of the system or those other phenomenon affecting the strength of the vortex, the frequency of extreme states, and the downward propagation following extreme events. We will focus on the mode of variability of most interest for this thesis, the El Niño-Southern Oscillation, but we first briefly discuss several other potential influences on the polar stratosphere.

The Quasi-Biennial Oscillation (QBO) is an oscillation in zonal winds between easterly and westerly in the tropical stratosphere, and a connection of the QBO and the stratospheric polar vortex has long been suggested. Early suggestions that SSWs were a direct result of the QBO phase were shown to be incorrect (Quiroz 1977). However, many studies found mean surface temperature or 1000 hPa geopotential height anomalies with many similarities to those following SSWs (SPVs) when they considered the difference between Januarys in easterly and westerly (westerly and easterly) phases of the QBO (Anstey and Shepherd 2014; EBDON 1975; Holton and Tan 1980; Thompson 2001), and in a complementary result, Limpasuvan, Thompson, et al. (2004) and Limpasuvan, Hartmann, et al. (2005) found that composites of SSWs and SPVs showed tropical stratospheric winds associated with the easterly and westerly phases of the QBO respectively. This suggests a relationship between SSW and SPV frequency and QBO phase, and this phenomenon is known as the Holton-Tan mechanism. Over 62 winters in reanalysis, Rao, Garfinkel, and White (2020b) found an SSW frequency of about 0.9 events per QBO easterly winter and about 0.5 events per QBO westerly winter, a result consistent with earlier studies (Naito et al. 2003). Several mechanisms for this effect on frequency have been proposed (Garfinkel, Shaw, et al. 2012; Holton and Tan 1980; Silverman et al. 2018; Watson and Gray 2014; White, Lu, et al. 2015).

The Madden-Julian Oscillation (MJO) is a subseasonal mode of variability in the tropical troposphere with a life cycle that can be split into eight stages (Wheeler and Hendon 2004). More than half of SSWs occur during phases 6 or 7 of the MJO, which occur about 18% of the time

(Baldwin, Ayarzagüena, et al. 2021; Schwartz and Garfinkel 2017), and other studies have found relationships to several other phases (Garfinkel, Benedict, et al. 2014; Kang and Tziperman 2017; Wang et al. 2018; Yang et al. 2019). The mechanism is again weakening the vortex through constructive interference with climatological planetary wave patterns (Garfinkel, Benedict, et al. 2014; Kang and Tziperman 2017), and models do capture a similar process (Kang and Tziperman 2017; Kang and Tziperman 2018; Schwartz and Garfinkel 2020).

Broadly, mechanisms similar to that proposed by Matsuno (1971) suggest that many SSWs should have precursors that increase planetary-scale wave activity, such as blocking (Martius et al. 2009; Peings 2019; Quiroz 1986). In line with this, some studies have suggested an effect of autumn snow cover in Eurasia in strengthening the Ural ridge and thus leading again to a weakened stratospheric polar vortex through constructive interference (Cohen, Barlow, et al. 2007; Cohen, Furtado, et al. 2014; Garfinkel, Hartmann, and Sassi 2010; Henderson et al. 2018). There is no statistically significant effect on SSW frequency (Baldwin, Ayarzagüena, et al. 2021), however, and any signal is nonstationary and only captured in some models (Furtado et al. 2015; Garfinkel, Schwartz, White, et al. 2020; Henderson et al. 2018). Finally, the solar cycle was also suggested to have an effect on the polar vortex, dependent on QBO phase (Gray et al. 2004; Labitzke and van Loon 1992; Labitzke 1987), but any such relationship is unclear in both observations and models (Baldwin, Ayarzagüena, et al. 2021; Mitchell, Misios, et al. 2015).

The El Niño-Southern Oscillation is the key driver of interannual tropospheric circulation and climate variability throughout much of the world. It also affects the stratospheric polar vortex. The vortex tends to be weaker in El Niño winters and stronger in La Niña winters, with a mechanism related to the strength of the Aleutian low and constructive or destructive interference with the climatology stationary wave pattern (Barriopedro and Calvo 2014; Garfinkel and Hartmann 2008; Ineson and Scaife 2009; Manzini, Giorgetta, et al. 2006; Smith and Kushner 2012). This relationship has been captured in both climate models and forecast models (Bell, Gray, Charlton-Perez, et al. 2009; Domeisen, Butler, Fröhlich, et al. 2015; García-Herrera et al. 2006; Ineson and Scaife 2009; Manzini 2009; Richter et al. 2015).

Despite this clear relationship to the mean strength of the vortex, the effect of ENSO on SSW frequency is not entirely straightforward. SSWs are more common in the El Niño phase than in neutral-ENSO by a factor of 30% or more. This has been seen in both reanalysis (Butler, Polvani, and Deser 2014; Garfinkel and Hartmann 2007; Polvani, Sun, et al. 2017) and modeling studies (Bell, Gray, Charlton-Perez, et al. 2009; Cagnazzo and Manzini 2009; Ineson and Scaife 2009; Oehrlein et al. 2019; Polvani, Sun, et al. 2017; Richter et al. 2015). The relationship between the frequency of events in the La Niña phase compared to the other phases is less clear. Among observed events, SSWs occur in the La Niña phase with a similar frequency as in El Niño (Butler and Polvani 2011; Domeisen, Garfinkel, et al. 2019a; Garfinkel, Butler, et al. 2012; Limpasuvan, Hartmann, et al. 2005), but this may be due to sampling variability given the short SSW record, and this relationship is sensitive to SSW, La Niña definition, and SST record (Polvani, Sun, et al. 2017; Smith, Polvani, and Tremblay 2018; Song and Son 2018). Models generally simulate a decrease in SSWs or no increase during La Niña relative to neutral-ENSO (Garfinkel, Butler, et al. 2012; Polvani, Sun, et al. 2017).

Less work has been done on SPV frequency under different ENSO conditions. Limpasuvan, Hartmann, et al. (2005) observed preferential occurrence of SPVs during La Niña as opposed to El Niño winters. This was not consistent with the results seen in a GCM in Smith, Polvani, and Tremblay (2018); the number of SPVs occurring in El Niño and La Niña were similar and both small compared to the number of events that occurred in neutral-ENSO winters.

The relationship between El Niño and SSW frequency results in a stratospheric pathway of El Niño influence on the North Atlantic and Eurasia (Bell, Gray, Charlton-Perez, et al. 2009; Butler, Polvani, and Deser 2014; Cagnazzo and Manzini 2009; Garfinkel and Hartmann 2007; Ineson and Scaife 2009; Richter et al. 2015). ENSO may, however, also have impacts on the region through the troposphere, as discussed briefly in Section 1.2.3, that could impact the surface signal following SSWs. Similarly, SSW or SPV occurrence can result in a very different climate pattern in the North Atlantic and Eurasia than predicted based on ENSO alone (Polvani, Sun, et al. 2017). Disentangling these effects is the focus of Chapter 2 of this thesis.

1.4.1 Role of Stratospheric Ozone

The most direct interaction between stratospheric ozone and the polar vortex is the link between polar vortex strength and ozone transport. Most stratospheric ozone is produced in the tropics, but it is transported to the poles, particularly the winter pole, by the Brewer-Dobson Circulation (BDC). The BDC is wave-driven by similar wave activity that affects the strength of the stratospheric polar vortex. The result is that a strong polar vortex is generally correlated with a weak BDC and low ozone transport to the poles, and vice versa (De La Cámara et al. 2018). Further, there is much less ozone mixing across a strong polar vortex edge than a weaker one, which also contributes to the higher polar cap ozone concentrations during weak compared to strong polar vortex events (Newman et al. 2001). Finally, a sufficiently cold polar cap–common in the Southern Hemisphere, but rare in the Northern Hemisphere–enhances formation of polar stratospheric clouds, which contribute to chemical ozone destruction in the spring when sunlight returns.

Thus, the occurrence of an SPV often results in particularly low winter and springtime polar cap ozone, and an SSW often results in high ozone anomalies. These ozone extremes have springtime surface impacts (Calvo, Polvani, et al. 2015; Ivy et al. 2017; Smith and Polvani 2014), with low (high) ozone extremes associated with positive (negative) NAO-like patterns in sea level pressure and surface temperature. This is partially related to a feedback between ozone anomalies and polar vortex strength and persistence into spring, but whether such a feedback is negative or positive is strongly sensitive to the background state of the polar vortex (Haase and Matthes 2019; Ivy et al. 2017; Li, Austin, et al. 2008; Lin and Fu 2013; Lin, Paynter, et al. 2017; Mahlman et al. 1994; Manzini, Steil, et al. 2003; McLandress, Jonsson, et al. 2010).

While these relationships are well-captured in interactive chemistry-climate models, these are computationally expensive to run, and climate models with prescribed monthly, zonal mean ozone chemistry are often used instead. These models cannot capture any surface impacts affected by ozone extremes. In addition to the springtime relationship noted above, Haase and Matthes (2019) found differences in SSW frequency and surface response to SSWs in simulations with and without interactive chemistry. Chapter 3 of this thesis revisits and furthers this work, considering the effect

of interactive chemistry on the representation of midwinter SSWs, late winter SSWs, and SPVs.

1.5 Conclusion

In this chapter, we introduced the stratospheric polar vortex and extreme events of that vortex, sudden stratospheric warmings (SSWs) and strong polar vortex events (SPVs). These events, SSWs in particular, their interaction with other phenomena, and the variability in their surface responses are the focus of this thesis.

The stratospheric polar vortex is a circumpolar westerly flow present in the Northern Hemisphere from about September through April, centered around 60° N, and extending throughout the stratosphere and into the mesosphere. While strongest in midwinter, this is also when the polar vortex is most variable. Sudden stratospheric warmings (SSWs) are extremely weak states of the polar vortex when the zonal mean zonal winds reverse, stratospheric polar cap temperatures rise, and the vortex splits or is displaced from the pole. Strong polar vortex events (SPVs) are on the other end of the spectrum, with strong westerly zonal mean zonal winds, a particularly cold polar cap, and very little ozone transport into the polar region.

These events propagate downward to the surface, on average projecting onto the North Atlantic Oscillation (NAO). SSWs are typically followed by the negative phase of the NAO and SPVs by the positive phase, with associated impacts on jet stream location and precipitation and temperature in Europe, Eurasia, and eastern North America. These effects at the surface can last for up to two months following the onset of the SSW or SPV in the stratosphere. Because of this response at the surface, the state of the stratospheric polar vortex and especially the occurrence of these extreme events are important for subseasonal prediction of surface climate.

Many other phenomena in the Earth system interact with the stratospheric polar vortex or with the impacts of SSWs and SPVs at the surface. We focus in particular on the El Niño-Southern Oscillation (ENSO) and stratospheric ozone. ENSO is a major driver of atmospheric circulation variability and, through its effects on wave activity, can also affect the polar stratosphere. In particular, winters in the El Niño phase tend to correspond to a weaker polar vortex and increased

SSW frequency. Thus, El Niño can affect North Atlantic climate through the stratosphere; it may also have a similar effect on the region through the troposphere. Stratospheric ozone is transported by the Brewer-Dobson Circulation to the winter pole, with increased transport when wave activity is high and the polar vortex is weak and decreased transport under strong polar vortex conditions and low wave activity. Springtime ozone extremes are associated with anomalies at the surface, but there may also be surface effects of wintertime ozone extremes associated with polar vortex variability. However, many atmospheric general circulation models do not include interactive ozone chemistry because of the computational expense of fully interactive atmospheric chemistry schemes.

This thesis is focused broadly on interactions of the extreme states of the stratospheric polar vortex with other phenomena and the resulting influence on Northern Hemisphere wintertime surface climate. We study these interactions both directly, considering the roles of particular atmospheric phenomena in variability of the polar vortex and resulting stratosphere-troposphere coupling, and indirectly, studying uncertainty in the surface response to SSWs that is partially due to these other sources of variability. The remainder of this thesis is organized as follows.

Chapters 2 and 3 present our work using simulations from Earth system models to study the interactions of the polar stratosphere with other phenomena or features of the ocean or atmosphere. In Chapter 2 we present results about the interaction and relative impacts on the North Atlantic and European region of SSWs and El Niño events. In Chapter 3 we discuss the impact on representations of the polar vortex, SSWs, and SPVs of including interactive ozone chemistry and transport in general circulation models. Our goal is to disentangle the effects of these separate but related phenomena on wintertime surface climate variability.

In Chapter 4, we turn to reanalysis and study the uncertainty in the observed surface response to SSWs. While not directly tied to interactions of SSWs with other phenomena, this work highlights the importance of tropospheric sources of variability unrelated to the stratospheric polar vortex in the observed surface climate composites following SSWs. These results will allow us to better evaluate model representations of the tropospheric response to SSWs in the future.

Chapter 5 concludes this thesis with a summary of the key findings and remarks providing context for this work in ongoing areas of research related to SSWs.

Chapter 2: Separating and quantifying the distinct impacts of El Niño and sudden stratospheric warmings on North Atlantic and Eurasian wintertime climate

Note: This chapter has been published in very near its present form as “Separating and quantifying the distinct impacts of El Niño and sudden stratospheric warmings on North Atlantic and Eurasian wintertime climate" in Oehrlein et al. (2019).

2.1 Introduction

The El Niño-Southern Oscillation (ENSO) and the occurrence of sudden stratospheric warmings (SSWs) have both been studied as important drivers of North Atlantic and Eurasian wintertime climate variability. On the one hand, the state of the stratospheric polar vortex, particularly an extreme weak vortex during SSWs, has been shown to influence the troposphere with a strong effect on the Northern Annular Mode (Baldwin and Dunkerton 2001; Charlton and Polvani 2007a; Hitchcock and Simpson 2014; Polvani and Waugh 2004). On the other hand, ENSO is the major driver of interannual climate variability and influences atmospheric circulation in many parts of the world, including the North Atlantic region (Alexander et al. 2002; Brönnimann 2007; Domeisen, Garfinkel, et al. 2019a; Horel and Wallace 1981; Rodríguez-Fonseca et al. 2016; Trenberth et al. 1998). The winter surface climate signature of El Niño over the North Atlantic resembles the negative phase of the Northern Annular Mode, similar to the effect of SSWs (Brönnimann 2007; Butler, Polvani, and Deser 2014; Calvo, Iza, et al. 2017; Polvani, Sun, et al. 2017).

However, these two sources of variability are not independent. SSWs are more common in the El Niño phase of ENSO than in the neutral phase, in both observations and stratosphere-resolving models, by a factor of about 30% (Bell, Gray, Charlton-Perez, et al. 2009; Butler and Polvani

2011; Garfinkel, Butler, et al. 2012; Polvani, Sun, et al. 2017). This suggests an SSW pathway of El Niño influence on the North Atlantic and Eurasia, which has now been well-established by both observational (Butler, Polvani, and Deser 2014; Garfinkel and Hartmann 2007) and modeling studies (Bell, Gray, Charlton-Perez, et al. 2009; Cagnazzo and Manzini 2009; Ineson and Scaife 2009; Richter et al. 2015).

The effects of El Niño on Eurasia in the absence of SSWs have been less clear. Observational composites of El Niño winters without SSWs show a negative NAO index compared to neutral-ENSO winters without SSWs, but this effect is weak compared to that of SSWs (Butler, Polvani, and Deser 2014). Seasonal prediction model studies such as Domeisen, Butler, Fröhlich, et al. (2015) and Scaife, Karpechko, et al. (2016) showed considerably decreased predictability in the North Atlantic and Europe for El Niño winters without SSWs compared to those winters with SSWs. Other studies based on climate models (Ineson and Scaife 2009; Richter et al. 2015) reported a negative NAO in a composite of El Niño winters with SSWs but a muted or different response in El Niño winters without SSWs. Also, observational (García-Serrano et al. 2011; Toniazzo and Scaife 2006) and climate model studies (Hardiman, Dunstone, et al. 2019) suggested a wave-like tropospheric response to El Niño in the North Atlantic, different from the NAO response to SSWs. However, Bell, Gray, Charlton-Perez, et al. (2009) found that in simulations with a degraded representation of the stratosphere, the negative NAO pattern in El Niño winters weakened but remained present. Li and Lau (2012) observed small negative shifts in the NAO with El Niño despite low vertical resolution in the model stratosphere and the resulting lack of a weak vortex signal. They attribute this effect to high-frequency transient eddies. Jiménez-Esteve and Domeisen (2018) also found a transient eddy-driven tropospheric pathway of El Niño that contributed to a negative NAO during mid-to-late winter in reanalysis.

To bring some clarity on both the importance of SSWs and the signal of El Niño on the North Atlantic, we here build on the work of Polvani, Sun, et al. (2017). In that paper, the distinct impacts of ENSO and SSWs on North Atlantic and Eurasian wintertime climate were analyzed using an ensemble of ten transient integrations in a high-top version of the Community Atmosphere Model,

version 5, over the period 1951-2003. They formed November-March composites of winters with and without SSWs in each ENSO phase. For key surface climate features, they found that the difference in winters with and without SSWs across all ENSO phases was greater than the difference between El Niño and La Niña winters across all stratospheric states. This supports the key role of SSWs in determining Eurasian wintertime climate independent of ENSO phase.

The aim of our work is to further clarify the respective effects of SSWs and El Niño on wintertime climate in the North Atlantic and Eurasia by carefully identifying and quantifying their separate impacts. To that end, we use two ensembles of 200 one-year model integrations, one forced with El Niño sea surface temperatures and the other with neutral-ENSO sea surface temperatures. We compare the effects of El Niño and SSWs to a basic state represented by neutral-ENSO winters without SSWs. This isolates the distinct effects of each phenomenon more cleanly than in previous studies, and the ensemble size allows us to better capture the signals of both El Niño and SSWs.

Our methodology is described in detail in Section 2.2. We then present the effects of SSWs and the tropospheric pathway of El Niño on the NAO and Northern Hemispheric surface climate in our simulation in Section 2.3. We find that the two sources of variability independently result in negative NAO anomalies and comparable effects on precipitation, while SSWs contribute much more strongly to Eurasian cooling. We conclude in Section 2.4 with a discussion of implications of the results.

2.2 Methods

The model integrations analyzed here are performed using the Community Earth System Model version 1 (CESM1), Whole Atmosphere Community Climate Model (WACCM) Marsh et al. (2013). The horizontal resolution of WACCM is 1.9° latitude by 2.6° longitude, and the model has 66 vertical levels with the model top at 5.1 $\times 10^{-6}$ hPa. Notably, WACCM accurately captures the frequency, seasonality, and dynamical features of SSWs (de la Torre et al. 2012) .

We perform two 200-member ensembles of one-year integrations initialized on June 1. June 1 is

chosen in order to simulate a realistic onset and full seasonal cycle of the stratospheric polar vortex, the growth and decay phases of El Niño warm anomalies in the tropical Pacific, and the atmospheric response to these El Niño conditions. Each ensemble of 200 atmospheric initial conditions for the integrations is generated using small air temperature perturbations, as in Kay et al. (2015). One ensemble is forced with monthly sea surface temperatures and sea ice (SSTs) corresponding to years with neutral-ENSO winters, and the other is forced with SSTs corresponding to years with El Niño winters. All members of each ensemble are forced with identical SSTs. Other forcings are consistent across the two ensembles. SSTs for neutral-ENSO integrations are constructed using the observed 1950-2014 climatology from ERSSTv5 (Huang et al. 2017). SSTs for the El Niño integrations are constructed by averaging over years in the record with warm ENSO events, defined here as the eleven winters with Oceanic Niño indices (SST anomalies in the Niño 3.4 region, 5°S-5°N and 170° − 120°W) above 1.0 K for three consecutive fall or winter three-month "seasons" (September-November, October-December, etc.). This is the NOAA Climate Prediction Center (CPC) procedure but with a higher threshold for an El Niño event, resulting in an average Niño 3.4 SST anomaly of 1.4 K over the November-March period (compared to a 1.0 K average anomaly over that period if a 0.5 K threshold is used). We use this higher threshold to focus on moderate-to-strong, realistic El Niño forcing.

We identify SSWs using the definition of Charlton and Polvani (2007a) and Charlton and Polvani (2011). An event is considered to be an SSW if the zonal mean zonal winds at 60° N and 10 hPa become easterly in extended boreal winter (NDJFM). The first day on which these winds are easterly is designated as the "central date," and no other day is considered a separate SSW event until the winds have again been westerly for at least 20 consecutive days. This definition is among the optimal thresholds for identifying SSWs as described in Butler and Gerber (2018).

To study the separate effects of El Niño and SSWs, we composite years with and without SSWs in both ensembles, and we compute anomalies with respect to neutral-ENSO years without SSWs. For composites of winters with SSWs, we take sixty day periods beginning with the central date of

the first SSW of each included year, following Baldwin and Dunkerton (2001). For the composites of El Niño winters without SSWs, we select the same sixty-day periods as in the neutral-ENSO with SSW composite, taking each sixty-day period from a randomly chosen El Niño without SSW run. We ensure that no single day appears in the composite twice. Results using sixty-day periods drawn from the El Niño with SSW composite are similar because the seasonal distributions of SSWs under neutral-ENSO and El Niño conditions are not different. In the case of neutral-ENSO without SSW, we repeat this composite-building process 500 times and take anomalies of other phases with respect to the mean of the neutral-ENSO without SSW composite distribution. We use this distribution for Monte Carlo tests of statistical significance.

We calculate the North Atlantic Oscillation (NAO) index for all integrations with the principal-component based method of Hurrell (1995). We find the principal components for the leading empirical orthogonal function of sea level pressure over the region $20° - 80°$N and 90°W-40°E. The NAO index time series for each ensemble member is calculated by normalizing the principal component time series using the mean and standard deviation of the neutral-ENSO without SSW members.

2.3 Results

Our main interest is in El Niño and SSWs as separate sources of variability. However, because El Niño increases the frequency of SSWs, we begin by analyzing the SSW frequency in our model. For both neutral-ENSO and El Niño conditions, we list in Table 2.1 the number of SSWs occurring in the 200 one-year integrations, the number of winters with SSWs, the SSW frequency, and the number of winters with multiple SSWs.

The SSW frequency (in events per decade) in the El Niño phase is 8.7, higher than the observed frequency of 8.0 found in NCEP-NCAR and ERA-40/ERA-I reanalyses of 1958-2013 (Polvani, Sun, et al. 2017). The frequency in the Neutral phase is 4.3 SSWs per decade. The corresponding observed frequencies reported in Polvani, Sun, et al. (2017) are 4.5 and 6.0 for NCEP-NCAR and ERA-40/ERA-I reanalyses respectively, so the modeled neutral-ENSO SSW frequency is near that

	EN	Neutral
Total Winters	200	200
SSW events	174	85
SSW frequency/decade	8.7	4.3
Winters with SSWs	140	72
Winters with 2 SSWs	30	11
Winters with 3 SSWs	2	1

Table 2.1: Summary of sudden stratospheric warming (SSW) events in El Niño and neutral-ENSO phases.

observed. Here, the ratio of the two frequencies is 2.0, higher than the typically reported value of 1.3 (Bell, Gray, Charlton-Perez, et al. 2009; Garfinkel, Butler, et al. 2012; Polvani, Sun, et al. 2017). The higher relative frequency of SSWs in the El Niño phase in our model is likely due to the high threshold used here to identify El Niño events. This results in stronger El Niño forcing in our model integrations, potentially deepening the North Pacific low (Garfinkel, Weinberger, et al. 2018) and increasing wave disturbance of the stratospheric polar vortex and SSW frequency (Garfinkel, Hartmann, and Sassi 2010).

We now turn to the quantification of the distinct effects of SSWs and El Niño on North Atlantic and Eurasian surface climate. Because the North Atlantic Oscillation serves as an important indicator of seasonal weather in the region (Barnston and Livezey 1987; Hurrell 1995; Loon and Rogers 1978), we first consider the impact of the two phenomena on the NAO itself. We compute anomalies from the Neutral-ENSO without SSW mean of the January-March NAO index, choosing January-March because this period best captures the wintertime surface influence of SSWs. Figure 2.1 shows distributions of JFM NAO indices for each state. All three distributions from SSW or El Niño conditions are statistically different ($p<0.01$) from the Neutral-ENSO without SSW distribution according to a Kolmogorov-Smirnov test. The mean of the neutral-ENSO with SSW distribution is -1.10, and the mean of the El Niño without SSW distribution is -1.90, so the two sources of variability independently result in negative shifts of the NAO relative to the neutral-ENSO without SSW case. Using observations, Butler, Polvani, and Deser (2014) finds negative shifts of the NAO due to El Niño, but the anomaly is about 40% of that due to SSWs. The strong

El Niño forcing in our simulations may contribute to the large response to El Niño here, but the linearity of this response is unclear, as discussed further in Section 2.4. The occurrence of both El Niño conditions and an SSW yields the most negative NAO values, with a distribution mean of -3.11. Hence, El Niño and SSWs are linearly additive in their effects on the NAO.

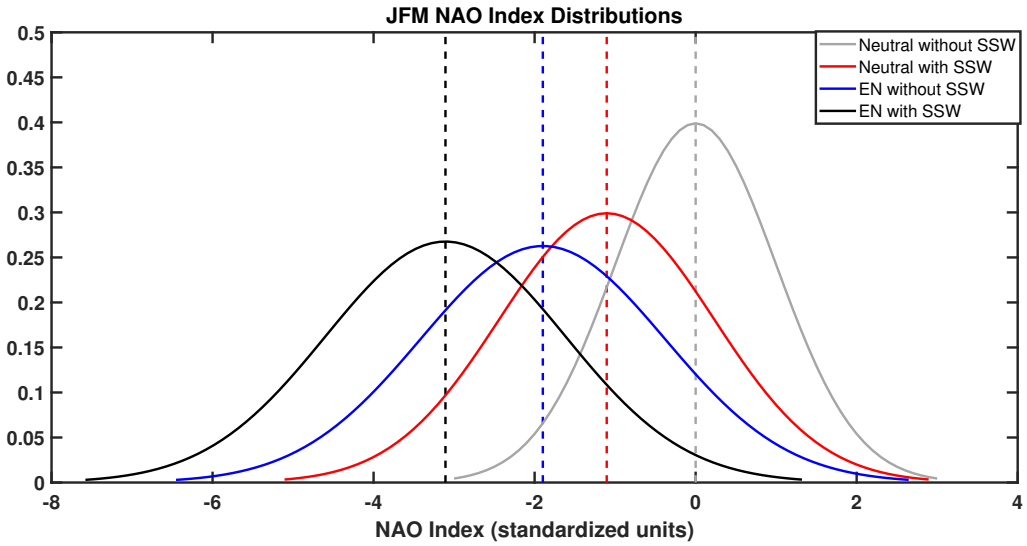

Figure 2.1: Fitted Gaussians of January-March North Atlantic Oscillation (NAO) indices for each state normalized with respect to the neutral-ENSO without SSW base state. Vertical lines indicate distribution means.

To examine the Northern Hemispheric impacts of SSWs and El Niño in more detail, we next plot composites of a few key climate anomalies for each state. Figure 2.2 shows 500 hPa geopotential height, temperature, and precipitation anomaly composites for neutral-ENSO winters with SSWs, El Niño winters without SSWs, El Niño winters with SSWs, and finally the difference between the latter two. Because all anomalies are taken with respect to neutral-ENSO winters without SSWs, Figs. 2.2a and 2.2b cleanly isolate the effects of SSWs and El Niño. We calculate statistical significance by a Monte Carlo test, considering the value at a point to be significant if the magnitude of the anomaly is equal to at least two standard deviations of the neutral-ENSO without SSW distribution. Spatial patterns for extended winter anomaly composites (November-March, not shown) are similar but of lower magnitude.

We first consider the effects of SSWs in neutral-ENSO winters, shown in column (a) of Fig.

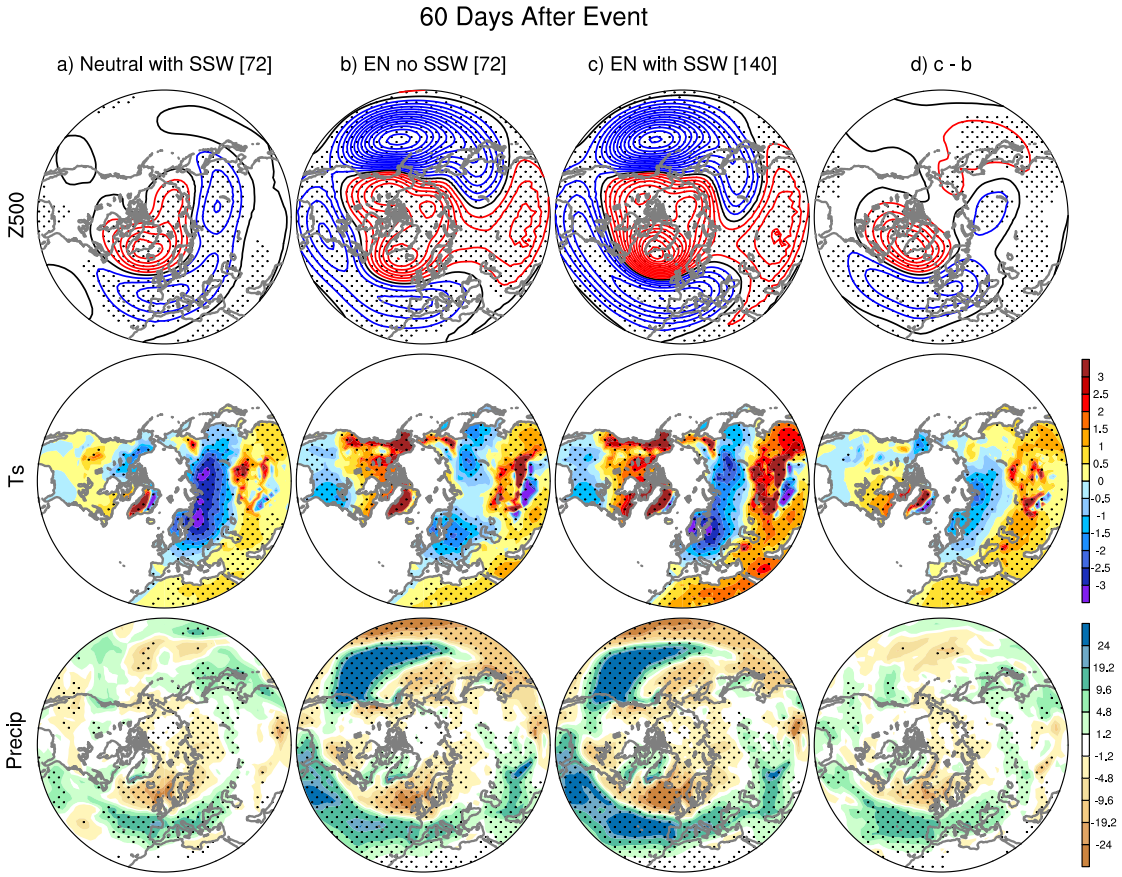

Figure 2.2: Rows are (top) mean geopotential height anomalies at 500 hPa, (middle) mean temperature anomalies at 1000 hPa (K), and (bottom) mean precipitation anomalies (mm/month). Columns are (a) neutral-ENSO winters with SSWs, (b) El Niño winters without SSWs, (c) El Niño winters with SSWs, and (d) the difference between El Niño winters with and without SSWs. Composites are computed using the 60-day methodology, anomalies are taken with respect to neutral-ENSO winters without SSWs.

2.2. There is a dipole in Z500 over the North Atlantic and Western Europe, corresponding to a negative phase of the NAO or Northern Annular Mode. We also see cold anomalies of 2-3 K over much of Northern Eurasia, particularly Siberia. Finally, there is a precipitation dipole over the

North Atlantic and Europe, with dry anomalies in Northern Europe and wet conditions in Southern Europe. These features are in good agreement with previous model and observational studies of SSWs (Baldwin and Dunkerton 2001; Butler, Polvani, and Deser 2014; Charlton and Polvani 2007a; Hitchcock and Simpson 2014; Polvani, Sun, et al. 2017).

We next turn to the impacts of El Niño alone (that is, for winters without SSWs) shown in Fig. 2.2 column (b). We first note the large anomalies over the Pacific in the Z500 field and the well-known temperature dipole over North America. These are associated with the Pacific/North America (PNA) teleconnection pattern typical of El Niño conditions (Horel and Wallace 1981). We see a Z500 dipole over the North Atlantic of similar strength as in the neutral-ENSO with SSW case. This state also shows cooling across Northern Eurasia, but it is weaker than in the neutral-ENSO with SSW case and is less concentrated in Siberia. A temperature anomaly average over Eurasia as shown in Table 2.2 allows us to more precisely quantify this difference. The temperature anomaly due to El Niño alone is a quarter of that due to SSWs alone. A similar precipitation dipole is seen as in column (a), but the increased precipitation, as with the Z500 low anomaly, extends across the Atlantic and impacts the Southern United States. The magnitudes of the anomaly over Europe are similar to those in the neutral-ENSO with SSW composite. These comparable values for precipitation in the Mediterranean region are reported in Table 2.2. The North Atlantic and Eurasian features are similar to the tropospheric pathway signals in Bell, Gray, Charlton-Perez, et al. (2009) and Cagnazzo and Manzini (2009), and Li and Lau (2012) but are greater in magnitude than in these studies, likely due to the large El Niño forcing used here. Geng et al. (2017) found cooling consistent with the temperature anomalies here in East Asia and Northern Europe during strong El Niños without downward-propagating geopotential height anomalies from the stratosphere in the observations.

The remaining columns of Figure 2 show the El Niño *with* SSW composites (column c) and the differences in the composites of El Niño with and without SSWs (column d). These composites reveal that treating the system as linearly additive captures most of the important features; we can then largely consider SSWs and the tropospheric pathway of El Niño as independent sources of

	Neutral with SSW	EN without SSW	EN with SSW
60 day Eurasian surface temperature (K)	-2.51	-0.59	-2.21
60 day Mediterranean precipitation (mm/mo)	+6.18	+6.91	+11.06

Table 2.2: Eurasian (60°-75° N, 30°-120° E) surface temperature and Mediterranean (35° – 45° N, 10° – 25° E) precipitation anomalies for neutral-ENSO and El Niño winters with and without SSWs. Means are computed using the 60-day methodology with anomalies taken with respect to neutral-ENSO winters without SSWs.

surface climate variability. The El Niño with SSW composite retains the El Niño-related features from Fig. 2.2b but with strengthening of the anomalies in regions where the SSWs have the most impact (as seen in the Fig. 2.2a composites). Comparing the columns Fig. 2.2a and Fig. 2.2d, we see similar structures and magnitudes of anomalies, but there are notable differences in the temperature. As shown in Table 2.2, the occurrence of both phenomena does not significantly change the Eurasian cooling from an SSW alone. This further supports the dominant role of SSWs on temperature variability in the region. In contrast, the regional average of Mediterranean precipitation anomalies in Table 2.2 further confirms the near-additivity of that quantity in the simulation. This additive linearity is not seen to the same extent in the observations, but that may be due to small observational sample size (Domeisen, Garfinkel, et al. 2019a).

	Neutral with SSW	EN without SSW	EN with SSW
		STOCKHOLM	
60 day Surface Temperature	-1.49	-1.34	-2.34
60 day Precipitation	-25.58	-28.09	-44.24
		PARIS	
60 day Surface Temperature	-0.45	-0.57	-1.06
60 day Precipitation	+7.81	-4.75	-1.44
		MADRID	
60 day Surface Temperature	-0.20	-0.32	-0.42
60 day Precipitation	+6.28	+11.83	+14.04

Table 2.3: Surface temperature anomalies (K) and precipitation anomalies (mm/month) for Paris, Stockholm, and Madrid in neutral-ENSO and El Niño winters with and without SSWs. Means are computed using the 60-day methodology with anomalies taken with respect to neutral-ENSO winters without SSWs.

While the latitudinal structures of the surface effects of El Niño and SSWs are dipolar, it is important to appreciate that the nodes of the precipation dipole are at different latitudes, possibly

due to the wave-like response to El Niño noted above. To illustrate the consequences of this mismatch, in Table 2.3 we consider precipitation in three particular cities: Stockholm (59.3° N), Paris (48.9° N), and Madrid (40.4° N). This selection of cities allows us to study how the anomalies change across a broad range of latitudes in Western Europe in the model as a result of these dipoles.

In Stockholm, the precipitation anomalies due to the two sources of variability lead to drier conditions and are of comparable magnitude. In Paris, however, these anomalies are of opposite signs. El Niño tends to result in drier winters in Paris, whereas SSWs lead to wetter ones. The north/south placement and extent of the precipitation anomaly dipoles for El Niño and SSWs are different, resulting in these opposite impacts in Paris. In Madrid, which is south of the nodal lines of the dipoles, both sources of variability result in wetter winters on average, and El Niño becomes relatively more important (nearly double the impact of SSWs). These results show that the superposition of two dipolar drivers of variability with nodes at different latitudes results in a complex climate response.

2.4 Summary and discussion

The climate model results presented here show that SSWs and El Niño separately play key roles in North Atlantic and Eurasian wintertime climate. Confirming prior work, we find that both SSWs and El Niño cause negative NAO anomalies and increase precipitation in Southern Europe. Both also lead to increased cooling in Northern Europe and Eurasia, but that cooling is concentrated in different regions.

Corroborating previous studies, we find a clear effect of El Niño in the absence of SSWs on the annular mode in the North Atlantic (Bell, Gray, Charlton-Perez, et al. 2009; Geng et al. 2017; Jiménez-Esteve and Domeisen 2018; Li and Lau 2012). However, the effects of this pathway of El Niño found here are larger than those seen in previous modeling or observational studies. One reason for this is that the basic state here is taken to be neutral-ENSO winters without SSWs, as opposed to a climatology, allowing us to more cleanly isolate the effect of El Niño. The second reason for this difference is the larger size of our model ensemble, resulting in a better signal-to-

noise ratio. That said, the results are robust to subsampling. Similar NAO distribution statistics to those seen in Figure 2.1 are seen in sample distributions of as few as 10 samples. This implies that the signals we observe here are meaningful and are not only discernible because of the large sample size. The third reason for the larger signal of the El Niño pathway in this work is that the El Niño forcing in our model is relatively strong, due to the 1 K threshold used for the SST composite.

Geng et al. (2017) found that strong El Niño events (anomaly of 2 K or more) in observations are associated with a shift to a negative NAO in January and cooling in Northern Europe and East Asia in the absence of significant perturbation of the stratospheric polar vortex. However, Toniazzo and Scaife (2006) and Hardiman, Dunstone, et al. (2019) found a negative NAO signal in moderate El Niño events but a wave-like response in strong (anomaly of 1.5 K or more) El Niño events in observations and a climate model; the wave-like response is consistent with the observational work of García-Serrano et al. (2011). Rao and Ren (2016a) and Rao and Ren (2016b) found significant nonlinearity in the effect of moderate (anomaly of 1 K or more) and strong (anomaly of 2 K or more) El Niños on the Arctic stratosphere in observations and WACCM simulations. The impact of El Niño variability on North Atlantic and Eurasian response, both with and without the influence of SSWs, warrants further study.

We also confirm the significant influence of SSWs on North Atlantic and Eurasian climate as described in Butler, Polvani, and Deser (2014) and Polvani, Sun, et al. (2017). The NAO and precipitation effects of SSWs are similar in magnitude to those of El Niño with an undisturbed stratosphere, and the Eurasian cooling due to SSWs is much stronger. Furthermore, the effects of SSWs are of similar magnitude in neutral-ENSO and El Niño conditions. As SSWs occur in 40 to 50% of winters even in neutral-ENSO conditions, SSWs are a key climate forcing for the North Atlantic and Eurasia whether or not ENSO is in the El Niño phase.

The results here indicate that a strong El Niño event may be important for wintertime seasonal forecasting for the North Atlantic and Eurasia not only for increasing the likelihood of SSWs, but also due to effects of El Niño through a tropospheric pathway. However, SSWs are frequent even in the neutral-ENSO phase and have surface impacts of comparable magnitude to El Niño. This

makes it critical to resolve the stratosphere in seasonal climate forecasting for the North Atlantic and Eurasia, as Butler, Arribas, et al. (2016) found that high-top forecast models better simulate both variability in the winter polar vortex and the stratospheric response to ENSO. For many measures, SSWs and El Niño had independent effects on variability, which may allow forecasts to more easily take both El Niño and the corresponding increase in SSW likelihood into account.

Chapter 3: The effect of interactive ozone chemistry on weak and strong stratospheric polar vortex events

This chapter has been published in very near its present form as “The effect of interactive ozone chemistry on weak and strong stratospheric polar vortex events" in Oehrlein et al. 2020.

3.1 Introduction

The climate impacts of stratospheric ozone extremes, particularly Antarctic ozone depletion, have been widely studied (Previdi and Polvani 2014 and references therein). While the effects are clearer and larger in the Southern Hemisphere, ozone extremes have also been shown to be associated with springtime surface anomalies in the Northern Hemisphere (Calvo, Polvani, et al. 2015; Ivy et al. 2017; Smith and Polvani 2014).

Polar cap ozone anomalies are strongly related to interannual variability in stratospheric polar vortex strength, which is larger in the Northern Hemisphere than the Southern Hemisphere. This is a result of the larger amplitudes of upward-propagating planetary waves, which perturb the stratospheric circulation. Years with low wave activity tend to correspond to a stronger vortex and a weaker Brewer-Dobson Circulation (BDC), resulting in weaker ozone transport from the tropics into the poles and decreased mixing across the vortex edge, as well as enhanced formation of polar stratospheric clouds, which contribute to increased springtime destruction of ozone. Years with high wave activity correspond to a weaker vortex and a stronger BDC, with stronger ozone transport from the tropics and increased mixing (Newman et al. 2001).

These processes are well-represented in fully interactive chemistry-climate models (Strahan and Douglass 2004). However, such models are computationally expensive compared to the more common ones, in which stratospheric ozone is simply prescribed. A number of studies

have explored the importance of interactive ozone chemistry on model representations of coupled stratosphere-troposphere variability. Smith and Polvani 2014 and Karpechko, Perlwitz, et al. 2014 found little impact of stratospheric ozone extremes on surface climate in the Northern Hemisphere using prescribed zonal mean monthly mean ozone fields. However, Calvo, Polvani, et al. 2015 found robust surface impacts associated with stratospheric ozone extremes using an interactive chemistry-climate model, suggesting the potential importance of this coupling. Further model studies are needed to disentangle the effects of ozone from those of polar vortex variability.

While the effect of polar stratospheric clouds on ozone is mainly seen in the spring when sunlight returns to the region, the variability of the polar vortex can result in wintertime ozone anomalies which may have surface impacts. The most extreme states of the polar vortex are sudden stratospheric warmings (SSWs) and strong polar vortex events (SPVs). We define these precisely in Section 2, based on extreme values of zonal mean zonal wind. Leading up to an SSW, dynamical forcing disrupts the stratospheric circulation, eventually resulting in a reversal of zonal mean zonal wind throughout much of the polar stratosphere. SSWs have surface effects for the two months following, particularly a negative North Atlantic Oscillation and cold anomalies over much of Northern Eurasia. Conversely, SPVs, in which abnormally strong westerly zonal mean zonal winds occur, are the result of anomalously weak planetary wave activity over a protracted period. As such, they are not rapid dynamical events in the same way as SSWs, but they may still have surface impacts, which is typically a positive NAO (Baldwin and Dunkerton 2001).

For the dynamical reasons described above, SSWs and SPVs tend to be associated with the occurrence of positive and negative stratospheric ozone anomalies, respectively. About two weeks prior to an SSW, the BDC accelerates, resulting in adiabatic warming of the stratosphere and enhanced isentropic eddy transport of ozone and thus increased ozone concentration over the pole (De La Cámara et al. 2018). SPVs are similarly accompanied by an anomalously weak BDC because of the lack of planetary wave activity and thus an anomalously low transport of ozone, as well.

Because they affect both stratospheric ozone and the NAO in the troposphere, extreme vor-

tex events offer an ideal case in which to study wintertime surface impacts of ozone chemistry. Haase and Matthes 2019 studied the impact of interactive versus prescribed ozone on SSWs, as well as their surface effects, in simulations of the recent past (1955-present) in an earth system model. They compared results of a simulation with interactive ozone to those of a simulation with prescribed ozone. This prescribed ozone was given daily (with no averaging/climatology) from a single historical interactive chemistry simulation. They found a stronger climatological vortex in the interactive chemistry simulation, and this was associated with a decreased SSW frequency. Further, SSWs were followed by stronger and more persistent surface anomalies in the simulation with interactive chemistry. These results suggest important surface impacts of ozone chemistry. However, their simulation was relatively short (64 winters), and the historical period they simulated includes long-term trends in ozone that may affect the results. Also, their method of prescribing ozone means that the ozone in the specified chemistry simulation was associated with dynamical variability of the interactive chemistry run, and that variability was inconsistent with the dynamical state of the specified chemistry model.

Building on the study of Haase and Matthes 2019, we here study interactions between ozone chemistry and polar vortex variability by analyzing SSWs, SPVs, and their surface impacts in two 200-year timeslice simulations with fully interactive and prescribed chemistry versions of a model. Using 200-year timeslices provides us with a large sample size of SSW and SPV events without long-term ozone trends, and we prescribe ozone based on the ozone climatology from the 200 years of the interactive chemistry simulation. Due to the larger sample size, climatological ozone distribution, and constant forcings, this set of simulations more clearly separates the impact of ozone's interannual variation on stratosphere-troposphere coupling. While we do not see decreased SSW frequency with interactive chemistry, we confirm Haase and Matthes 2019's results on the vortex climatology and response to midwinter SSWs. We further find that there is little surface effect of interactive ozone chemistry immediately following SPVs or March SSWs. However, SPVs show long-lasting effects on stratospheric ozone, with anomalies 1-2 months after the central date of a similar magnitude to those caused by midwinter SSWs.

The paper is organized as follows. Section 2 describes the model, simulations, and methodologies. Section 3 addresses our results on the impacts of interactive chemistry, considering the stratospheric mean state, midwinter SSWs, March SSWs, and SPVs. We conclude the paper with a discussion of these results.

3.2 Methods

In this study, we analyze model integrations performed with the Whole Atmosphere Community Climate Model, Version 4 (WACCM4), one atmospheric component of the Community Earth System Model (CESM1) (Marsh et al. 2013). WACCM4 is an interactive chemistry-climate model with a horizontal resolution of 1.9° in latitude and 2.6° in longitude, 66 vertical levels, and a model top at 5.1 $\times 10^{-6}$ hPa (140 km). Northern Hemisphere stratospheric variability, such as the frequency and dynamical features of SSWs, are accurately simulated in WACCM4 (Marsh et al. 2013).

We perform two model integrations, both 200-year-long timeslice integrations with forcings at constant year-2000 values to avoid long-term trends in ozone. One model integration uses the fully interactive chemistry scheme in WACCM4 (Kinnison et al. 2007). We refer to this simulation as the CHEM simulation in the analysis. The other uses the “Specified Chemistry" version of WACCM, known as SC-WACCM (Smith, Neely, et al. 2014). We refer to this prescribed chemistry simulation as the NOCHEM simulation in the analysis. In the NOCHEM simulation, ozone concentrations (and other radiatively active atmospheric constituents, including CFCs) are prescribed using zonally symmetric, monthly mean, seasonal climatology computed from the WACCM integration. These zonally symmetric monthly ozone fields are read into SC-WACCM and interpolated linearly to the day of the year. More details can be found in Smith, Neely, et al. 2014. Hence, both CHEM and NOCHEM strictly impose identical year 2000 forcings for all radiatively active species, and only differ in their treatment of ozone. The use of climatological ozone fields in NOCHEM removes the effect of extreme ozone variations on the climate system. One might consider specifying non-zonally symmetric ozone (Haase and Matthes 2019), but that comes at

the cost of a major physical inconsistency between the polar vortex and the ozone field: in other words the unperturbed (perturbed) vortex years in the model will not correspond with low (high) ozone extremes. More importantly, the vast majority of climate models in CMIP specificy zonally symmetric stratospheric ozone, including within CMIP6 (Keeble et al. 2020): hence the zonally-symmetric specified ozone case is the one of most interest in terms of evaluating the impact of interactive ozone chemistry.

We identify SSWs in the model output following the definition in Charlton and Polvani 2007a (see the corrigendum Charlton and Polvani 2011). We define an SSW as a reversal of zonal mean zonal wind at 60° N and 10 hPa from westerly to easterly during November through March, with the central date being the first day of easterly zonal mean zonal winds. No later date can be a central date until the winds have been westerly again for at least 20 days, and the winds must return to westerly for at least 10 consecutive days before April 30 (thus discarding stratospheric final warmings). This definition is optimal for identifying SSWs, as described by Butler and Gerber 2018. We focus on SSWs occurring in December-February and in March. We consider March events separately from December-February events due to different shortwave heating behavior, model bias in March SSW frequency (too frequent SSWs in our model), and different NAO structure in early spring compared to winter.

To the best of our knowledge, there is no standard definition of an SPV. Different methods have been used in the literature (Beerli and Grams 2019; Limpasuvan, Thompson, et al. 2004; Scaife, Karpechko, et al. 2016; Tripathi et al. 2015). We here follow the definition used in Scaife, Karpechko, et al. 2016 and Smith, Polvani, and Tremblay 2018, designed to be analagous to the Charlton and Polvani 2007a SSW definition and to result in a similar number of events in reanalysis. We define an SPV as zonal mean zonal wind at 60° N and 10 hPa reaching 48 m/s or higher (westerly) during November through March, with the central date being the first day of zonal mean zonal winds above 48 m/s. No later date can be a central date until the winds return below 48 m/s for at least 20 consecutive days. We focus on SPVs occurring in December-February, due to low event frequency in November and March. A separate analysis reveals that results are not sensitive

to using a 41.2 m/s threshold as in Tripathi et al. 2015.

The results we present here are based on composites of daily model output for climate variables, with composites centered around SSW or SPV central dates. For composites from either CHEM or NOCHEM simulations, we calculate significance using a Monte Carlo test based on 5000 randomly chosen central dates. We also consider the difference in CHEM or NOCHEM composites, denoted CHEM-NOCHEM; for these, we calculate significance from a two-sided two-sample t-test.

3.3 Impact of interactive chemistry

3.3.1 Stratospheric mean state and extreme events

We first consider the effect of interactive chemistry on the mean state of the stratosphere by examining the climatological Northern Hemisphere 10 hPa zonal mean zonal wind (Figure 3.1). We find stronger westerlies in CHEM than in NOCHEM in the vortex formation stage (September and early October) and in the latter half of winter (January-April), between $60° - 80°$ N. In line with this, we also find weaker downwelling in winter in the upper latitudes in CHEM than in NOCHEM (not shown). This relative strength in CHEM in late winter also corresponds to a delayed final warming by 7 days on average. These results are in agreement with those of Haase and Matthes 2019. We also found similar results in six 1955-2005 historical integrations of WACCM and SC-WACCM (with ozone specified monthly or daily from the WACCM climatology) from Neely et al. 2014 (not shown), further indicating that this feature is robust.

This is not the case in Smith, Neely, et al. 2014, where the vortex is of similar strength with interactive and prescribed ozone under constant year 1850 conditions. The difference between that study and ours is the level of chlorofluorocarbons (CFCs): these are zero in Smith, Neely, et al. 2014, which simulates pre-industrial conditions, but they are substantial in our study, which simulates year 2000 conditions. They are similarly substantial in the historical (1955-present day) simulations in Haase and Matthes 2019 and Neely et al. 2014. Because the differences between interactive and specified ozone simulations depend on the level of CFCs, a precise understanding of the mechanisms for the difference will require disentangling the dynamics and chemistry. Higher

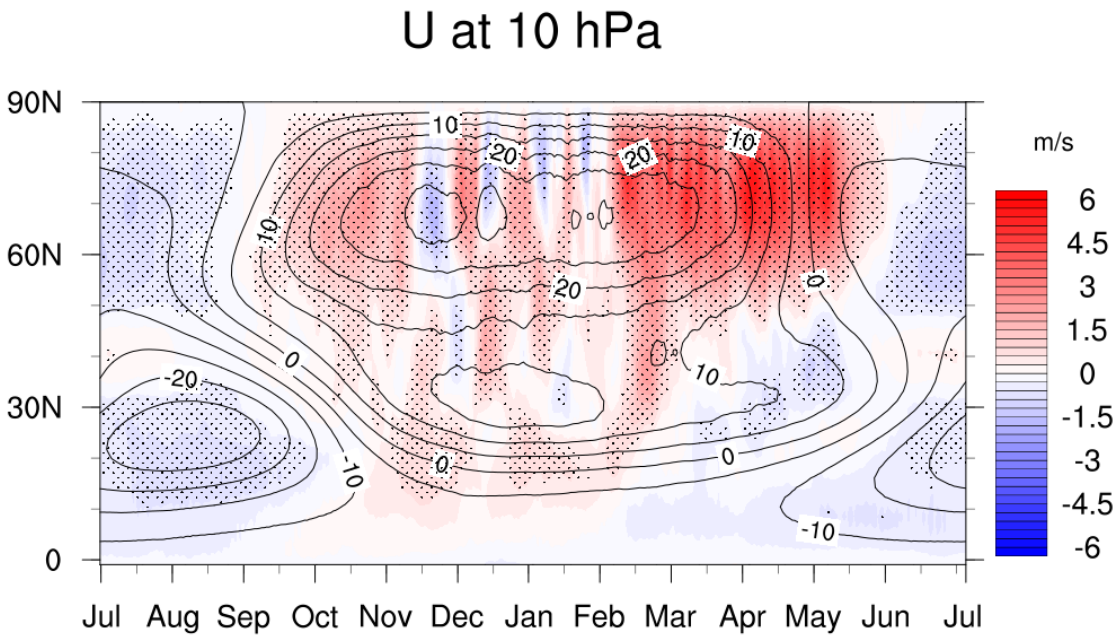

Figure 3.1: Latitude-time plot of zonal mean zonal wind at 10 hPa. Contours show NOCHEM values in m/s. Colored shading shows the difference CHEM-NOCHEM in m/s. Stippling indicates a significant CHEM-NOCHEM difference at a 95% level using a two-sample, two-tailed Welsh's t-test.

ozone variability in the presence of CFCs (Calvo, Polvani, et al. 2015) might increase the effects of the ozone-dynamics feedbacks, rendering this a very difficult problem. There are indications that these differences may be related to zonal asymmetry of ozone (Haase and Matthes 2019), further complicating the relationship. Albers and Nathan 2012 have proposed a complex mechanism to detail the coupling of zonally asymmetric ozone and dynamics in the context of a highly idealized linear model. In their model, zonal asymmetries in ozone precondition the waves, causing a reduction in planetary wave drag and a colder polar vortex. However, determining whether this mechanism is operative in our comprehensive model would be quite difficult, as the mechanism relies on many assumptions that are likely inapplicable in the presence of highly nonlinear, time-dependent, breaking waves as are observed in the winter polar stratosphere in a fully interactive model.

Because we identify extreme stratospheric events using zonal mean zonal winds at 10 hPa

and 60° N (U1060) (Butler and Gerber 2018; Charlton and Polvani 2007a), we next examine the mean state and variability of this quantity in CHEM and NOCHEM. Figure 3.2 shows the two distributions of U1060 in December through March. The average difference in DJFM between CHEM and NOCHEM is about 1.7 m/s. To determine whether this is statistically significant, we consider the average zonal mean zonal winds over each winter and treat the winters as independent. A two-sample, two-tailed Welsh's t-test of DJFM average winds in CHEM and NOCHEM yields a p-value of 0.023, so the difference, though small, is significant at a 95% level. The CHEM distribution also has a longer right tail, which is consistent with the polar vortex being stronger overall with interactive chemistry. It also indicates that we should expect more SPVs in CHEM than in NOCHEM. While there are fewer days of weak westerlies (0-20 m/s) in CHEM than in NOCHEM, the numbers of days of easterlies are similar, so we expect less of a difference in SSW frequency between the two simulations.

Indeed, this is what we find when we calculate the frequencies of weak and strong vortex events in the CHEM and NOCHEM simulations (Table 3.1). We consider December-February (DJF, midwinter) and March (late winter) separately for two reasons. First, the ozone impacts in midwinter are different from those in late winter/early spring, as shortwave effects become important in spring. Second, our model is biased in March, with too many SSWs compared to reanalysis, a feature also seen in more recent versions of this model (Gettelman et al. 2019). We see 1.4 March SSWs per decade in NOCHEM and 1.95 March SSWs per decade in CHEM compared to 0.87-1.1 per decade in the reanalysis (Butler, Sjoberg, et al. 2017).

The stronger vortex in midwinter in the CHEM simulation might lead us to expect fewer DJF SSWs in CHEM than in NOCHEM. We do see a decrease of about 10% in DJF SSWs with interactive chemistry compared to specified chemistry, but this decrease is far from being statistically significant. In contrast, in March, we see more SSWs in CHEM than in NOCHEM, potentially related to the later breakdown of the vortex.

Haase and Matthes 2019 consider the overall (November-March) number of SSWs. They report a decrease in overall SSWs with interactive chemistry of around 30%. In contrast, for November-

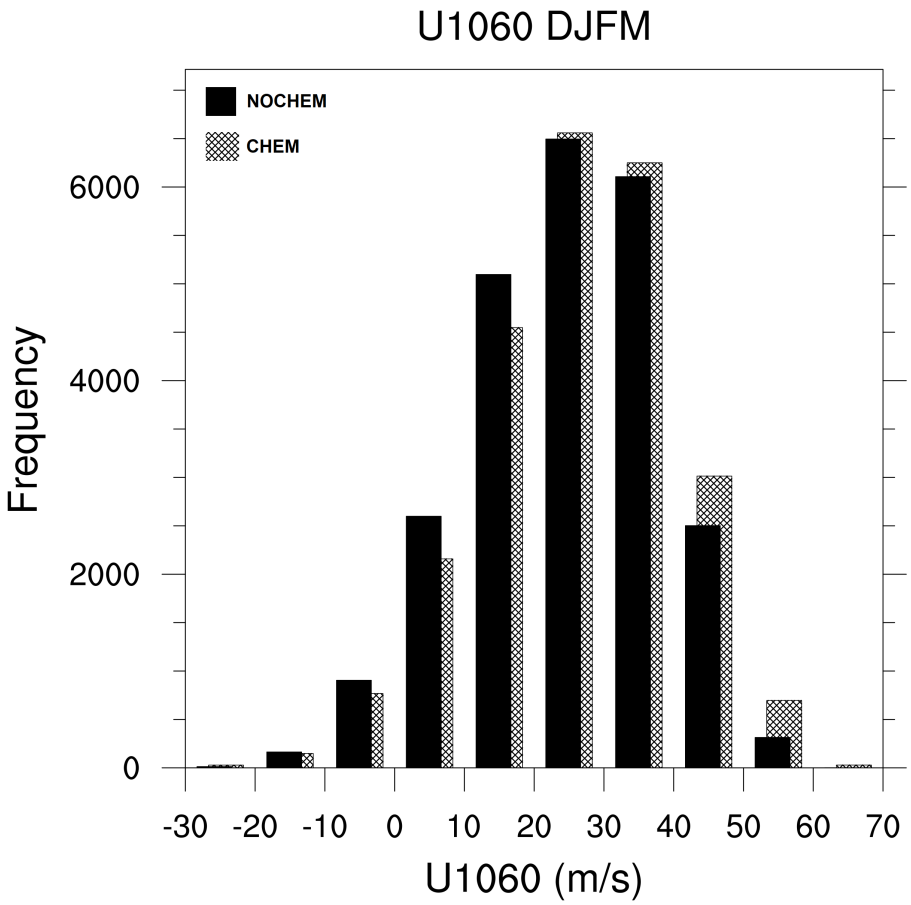

Figure 3.2: Histogram of daily values of zonal mean zonal wind at 10 hPa and 60°N in December-March for CHEM and NOCHEM. The mean of the CHEM and NOCHEM zonal mean zonal wind values are 26.1 m/s and 24.4 m/s respectively. The right tail of the CHEM distribution is longer, indicating more days of a particularly strong polar vortex.

March, we find virtually no difference in SSWs (109 events vs 111, not shown) in CHEM and NOCHEM. We note that both of these frequencies, around 5.5 events per decade, are on the lower end of what is seen across reanalyses (Butler, Sjoberg, et al. 2017; Cao et al. 2019) but very well within the spread among state-of-the-art chemistry-climate models (Ayarzagüena, Polvani, et al. 2018).

We now consider SPV frequency. The increase in DJF SPV frequency from NOCHEM to CHEM is about 29%. This is unsurprising given the stronger vortex in CHEM overall. With our definition of SPVs, the number of March strong vortex events (in either simulation) is too small

	NOCHEM	CHEM	Percent Difference	p-value
Total Winters	200	200		
DJF SSW events	75	67	-10.7%	0.45
DJF SPV events	58	74	+29.3%	0.13
March SSW events	28	39	+39.3%	0.14
March SPV events	7	5	-28.6%	0.58

Table 3.1: Summary of sudden stratospheric warming (SSW) and strong polar vortex (SPV) events in 200-year year 2000 timeslices with and without interactive chemistry (CHEM and NOCHEM respectively). We separately consider the events occurring in December through February and those occurring in March. Reported p-values are based on a two-tailed two sample t-test (Charlton and Polvani 2007b).

for a robust statistical analysis. This is because of the weaker vortex in March compared to DJF; a much larger anomalous vortex strength would be necessary to reach 48 m/s. Because of the low number of such events, we do not further study March SPVs and thus discard them from the analysis.

We now examine DJF SSWs, March SSWs, and DJF SPVs separately in each of the following three sections.

3.3.2 Midwinter sudden stratospheric warmings

We start by focusing on the surface impacts of SSWs, seeking to document any differences between the CHEM and NOCHEM simulations. After noting the impact of the events on the surface, we then consider how any differences in those impacts arise aloft.

Figure 3.3 shows composite surface level pressure anomalies in the first and second months (top and bottom respectively) following December-February SSWs in CHEM (left, 75 events) and NOCHEM (middle, 67 events), as well as the difference between the two (right). We see a strong and significant pattern resembling a negative North Atlantic Oscillation (NAO) in the first month following SSWs in both CHEM and NOCHEM, and in both cases this negative annular mode persists through the second month following the event. There is minimal difference between the

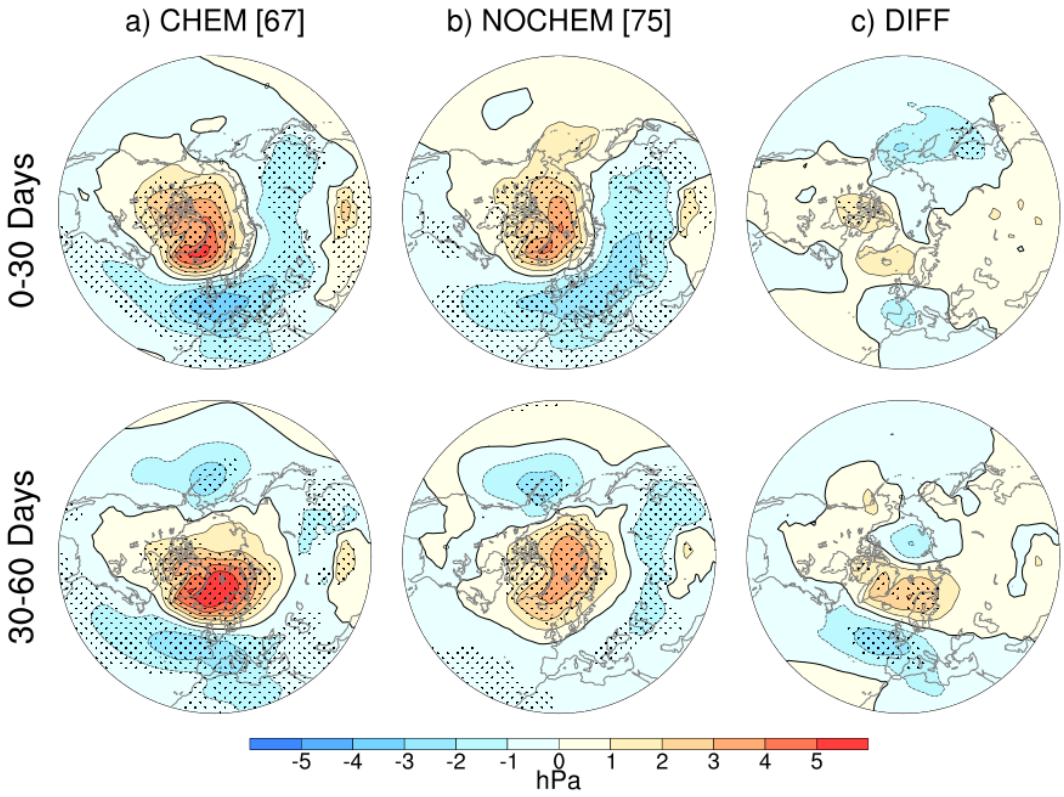

Figure 3.3: Composites of sea level pressure (SLP) anomalies (in hPa) in the 0-30 and 30-60 days following the central date of DJF SSWs in CHEM (WACCM, a) and NOCHEM (SC-WACCM, b) simulations, as well as the difference in the CHEM and NOCHEM composites (c). Significance at the 95% level using a Monte Carlo test (a,b) or a two-sided t-test (c) is indicated by stippling. The number of events included in each composite is noted in brackets above the figures.

two simulations in the first 30 days, with the CHEM simulation having only a slightly stronger signal. However, the difference is statistically significant and strongly projects onto the NAO 30-60 days after the central date. This indicates that the surface signature of SSWs is stronger and more persistent in CHEM than in NOCHEM.

To determine whether the differences at the surface following SSWs in CHEM and NOCHEM are a result of differences originating in the stratosphere, we calculate the Northern Annular Mode (NAM) for each simulation. We use a method similar to that of Gerber 2010 and Gerber and Martineau 2018; the detailed procedure is in Appendix A. We show the results of the NAM calculations in Figure 3.4. The CHEM and NOCHEM composites around SSWs have comparable NAM anomalies in the stratosphere around the central date, but in the CHEM simulation the nega-

tive anomaly persists more strongly in the lower stratosphere beyond 40 days after the central date. The CHEM-NOCHEM difference shows that this change in persistence with interactive chemistry is significant at the 95% level. There is also more descent of the anomaly to the surface in the CHEM simulation, especially at about 30 days after the central date.

This difference in descent is also seen in the CHEM-NOCHEM temperature anomalies (Figure 3.5a). The warming in the stratosphere associated with the onset of the SSW is larger with interactive chemistry. This stratospheric temperature anomaly then descends more strongly through the stratosphere and troposphere in the CHEM simulation than in the NOCHEM simulation.

We investigate the processes leading to these changes in more detail by examining the dynamical, longwave, and shortwave heating terms. The greater warming throughout the stratosphere is due to increased dynamical heating (Figure 3.5b) in CHEM compared to NOCHEM, as the higher temperature with interactive chemistry is also associated with a longwave cooling response (Figure 3.5c). The higher stratospheric temperatures result in greater longwave emission. The increase in dynamical forcing also corresponds to increased ozone transport. Ozone is a longwave emitter, so the increased dynamical forcing could directly account for part of this longwave cooling difference, as well.

The increased dynamical heating in CHEM could be related to greater wave activity necessary for an SSW to occur with a stronger mean vortex state. Figure 3.6 shows the eddy heat flux over 40-80° N over time in CHEM and NOCHEM. This is stronger by about 2 mK/s around the central date in CHEM than in NOCHEM, indicating a slightly stronger wave forcing in CHEM. The CHEM and NOCHEM means are at the upper and lower bounds of the other's confidence intervals, respectively. Further, the zonal mean zonal winds at 10 hPa and 60° N around the central date of the SSW (shown in Figure 3.7) are both stronger prior to the event and more easterly following the central date in CHEM than in NOCHEM. However, the residual vertical velocity anomalies throughout the Northern Hemisphere leading up to SSWs is nearly identical for CHEM and NOCHEM (not shown), so the increased dynamical heating in CHEM might be a result of a stronger vertical temperature gradient related to the stronger vortex in this simulation (associated

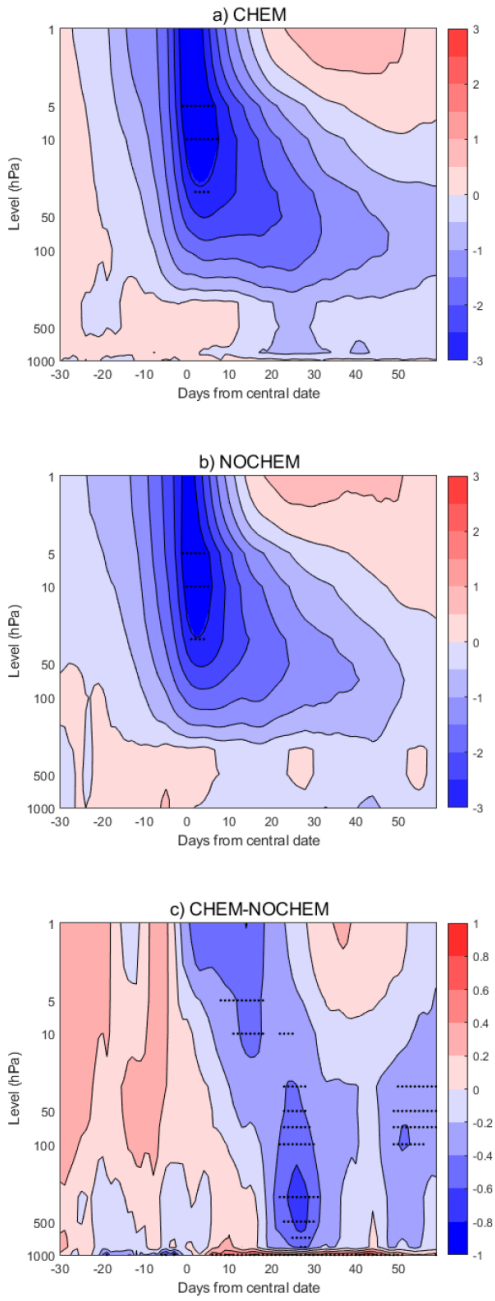

Figure 3.4: NAM anomaly composites around DJF SSW central dates in CHEM (a), NOCHEM (b), CHEM-NOCHEM (c). Stippling shows significance at the 95% level (with a Monte Carlo test for CHEM and NOCHEM and a two-tailed t-test for CHEM-NOCHEM). Contours are every 0.5 standard units for CHEM and NOCHEM and every 0.2 standard units for CHEM-NOCHEM.

with a colder polar stratosphere).

In DJF, the dynamical heating and the longwave heating are the dominant temperature tendency terms. There is also a significant shortwave heating response (Figure 3.5d), but in midwinter it

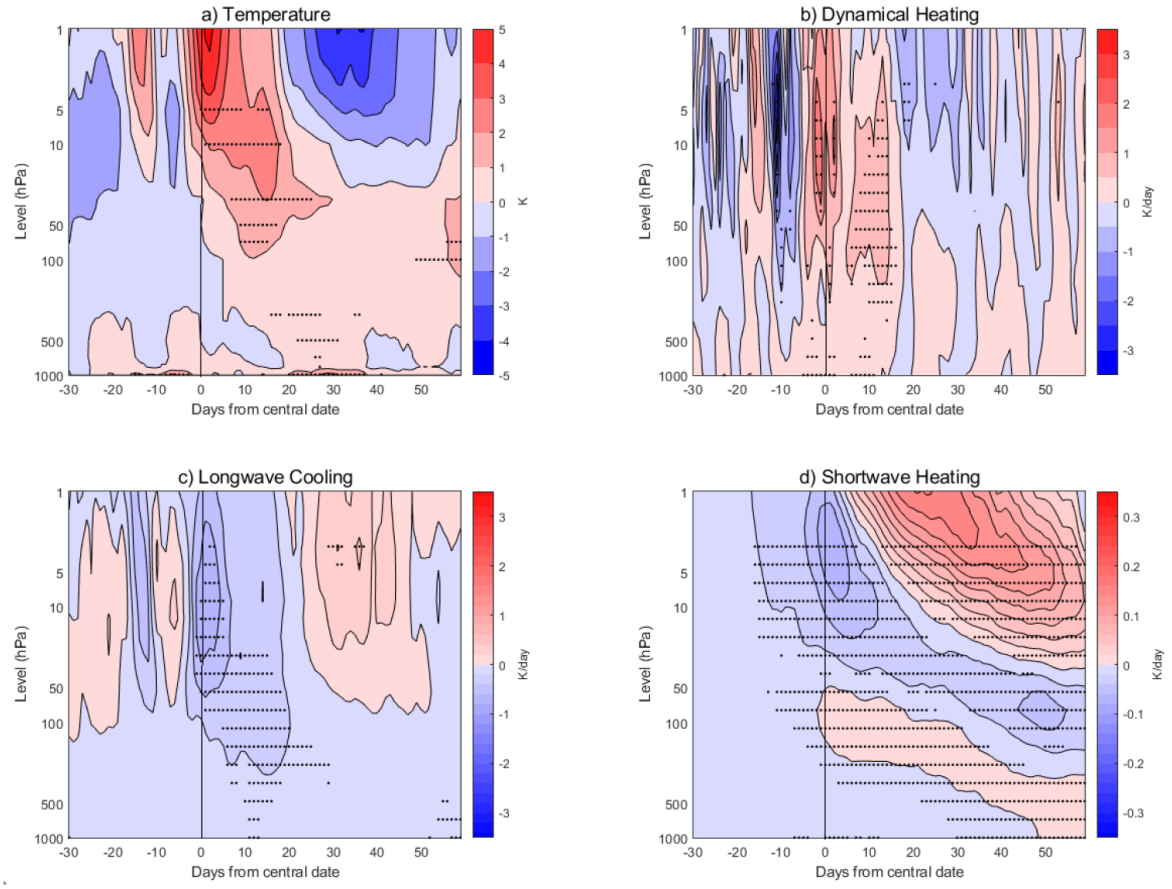

Figure 3.5: CHEM-NOCHEM differences in the temperature and heating anomalies over 60-90° N from -30 to +60 days around the SSW DJF central dates. (a): Temperature anomalies. Contours are every 1 K. (b): Dynamical heating anomalies. Contours are every 0.5 K/day. (c): Longwave heating anomalies. Contours are every 0.25 K/day. (d): Shortwave heating anomalies. Contours are every 0.02 K/day. Stippling shows significance at the 95% level under a two-tailed t-test.

is an order of magnitude smaller than the other terms, owing to the absence of incoming solar radiation to polar night. The structure in height and time is related to integrated effects of the ozone anomalies following the SSW, which show a similar structure (Kiesewetter et al. 2010). The importance of the shortwave response increases the later in winter the SSW events occurs. We illustrate this in Figure S1, showing much stronger differences in CHEM and NOCHEM shortwave anomalies for February SSWs than for December or January events.

Finally, we examine the anomaly in total ozone column around the central date of the SSW (Figure 3.7) in the CHEM simulation. We see a sharp increase in ozone in the 15 days leading up to the central date, reaching a peak of on average about 40 Dobson units above climatology just

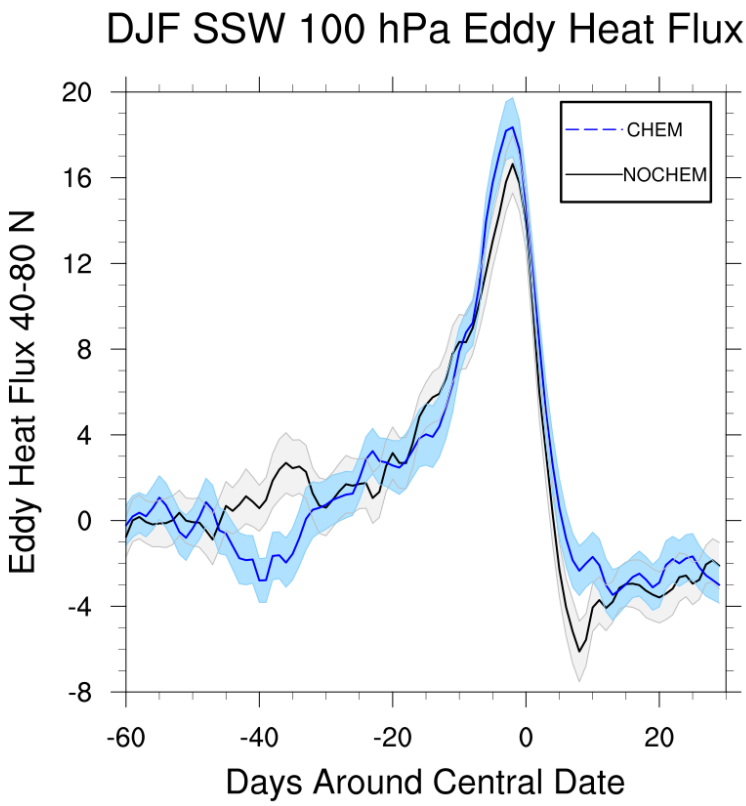

Figure 3.6: Eddy heat flux in mK/s over 40-80° N from -60 to +30 days around the SSW DJF central dates. The CHEM average is in blue, with confidence intervals shown in pale blue. The NOCHEM average is in black, with confidence intervals shown in gray.

after the central date, similar to that seen in reanalysis and a similar model by De La Cámara et al. 2018. This ozone anomaly results from transport due to the greater dynamical forcing in CHEM, as noted earlier. Following the central date, anomalies of about 20 Dobson units persist for up to 3 months following the central date. This ozone anomaly is consistent with total ozone column in reanalysis and a similar model (De La Cámara et al. 2018) and the smaller ozone depletion in years with early SSWs observed by Strahan, Douglass, and Steenrod 2016.

In summary, DJF SSWs are preceded by larger wave forcing in CHEM than in NOCHEM, partially because of the stronger mean state of the polar vortex. This then results, on average, in

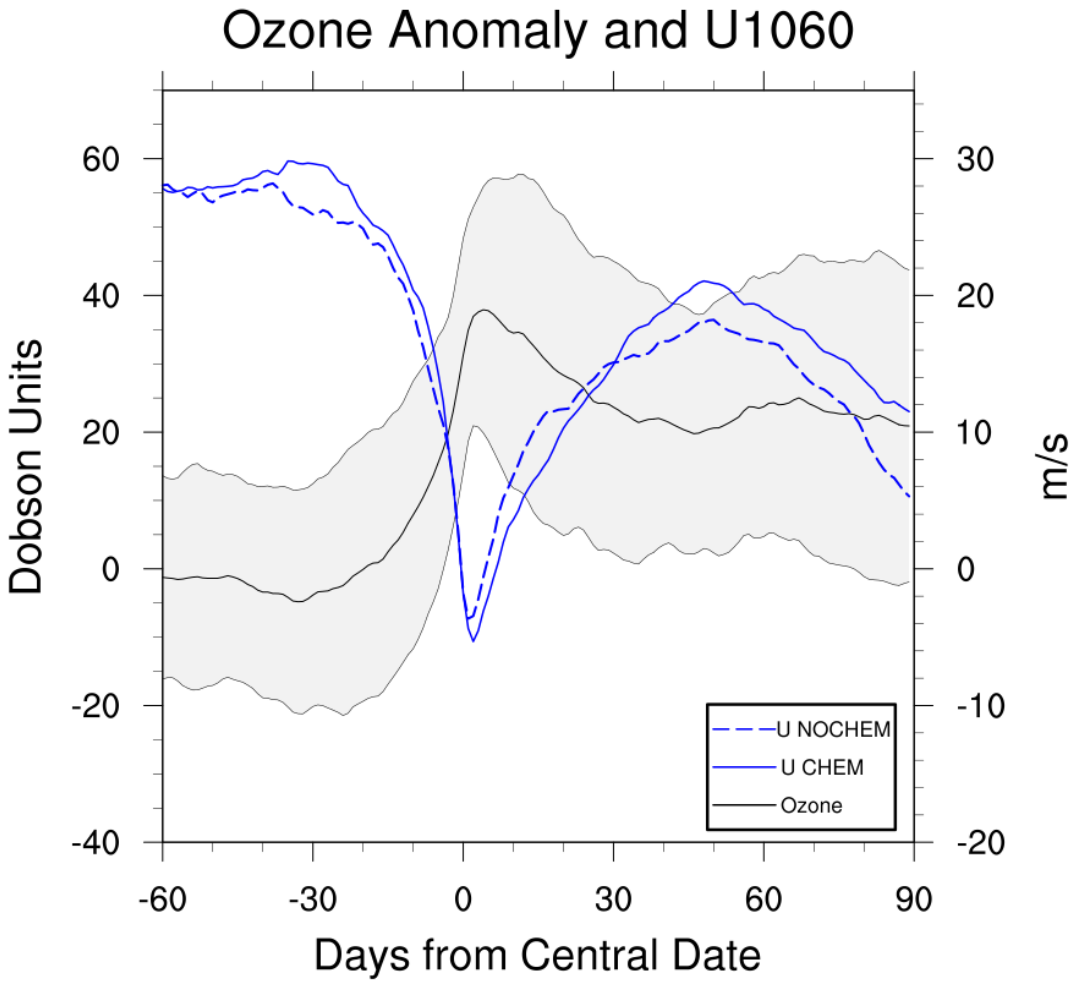

Figure 3.7: Composite of total column polar cap (over 60-90° N) ozone anomalies in Dobson units in the CHEM simulations and composites of zonal mean zonal wind at 60° N and 10 hPa in m/s from -60 to 90 days around the central date of DJF SSWs in CHEM and NOCHEM. The black line shows the mean total ozone column; 1σ from the mean is shaded. The blue solid and dashed lines shows the mean U1060 in CHEM and NOCHEM respectively.

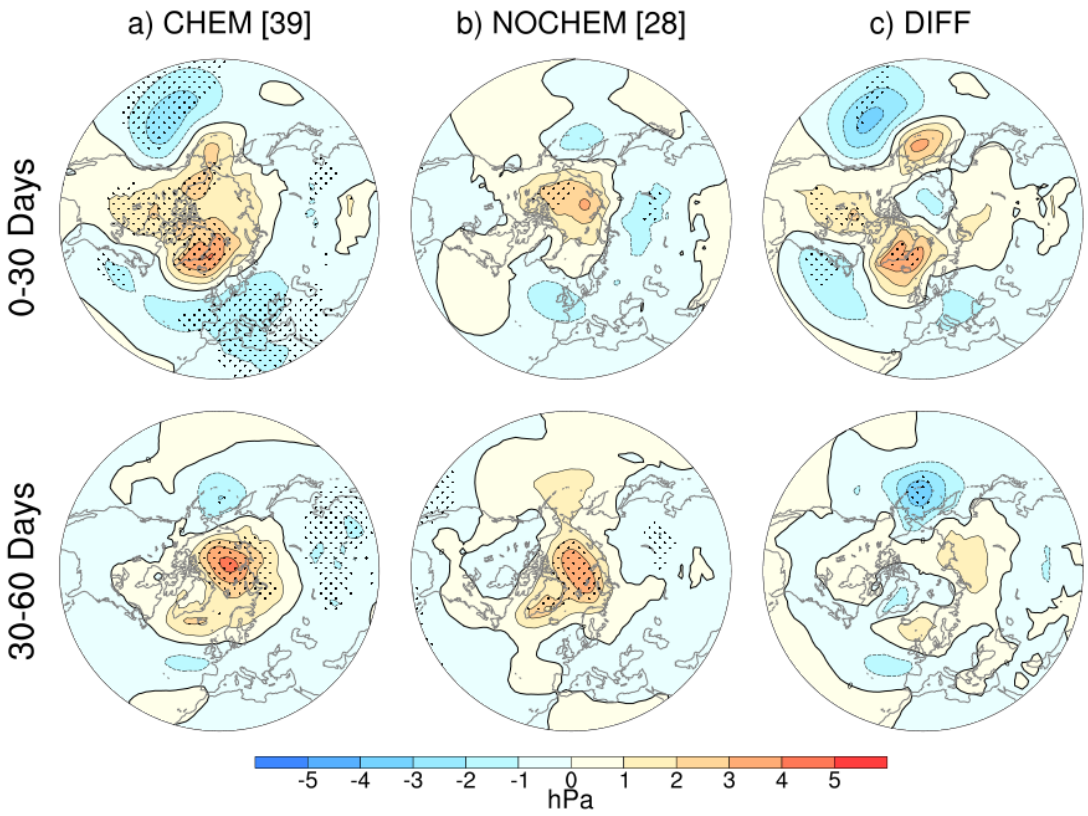

Figure 3.8: As in Figure 3, for March SSWs.

more intense SSWs, stronger stratosphere-troposphere coupling, a more negative NAO-like pattern at the surface, and long-lasting stratospheric ozone anomalies.

3.3.3 March sudden stratospheric warmings

We now turn to the March SSWs. Figure 3.8 shows the composite sea level pressure anomalies for CHEM and NOCHEM, as well as the CHEM-NOCHEM difference, for each of the first two months following the central date. Both simulations again show a negative NAO-like pattern in the two months following the SSW. There are some regions with significant difference between CHEM and NOCHEM in the first thirty days, but the pattern does not project strongly onto the NAO. Also, there is very little difference between the two composites in the second thirty days after the central date.

The surface responses seen following March SSWs, in both models, are weaker and less persis-

tent than those following DJF SSWs, and the areas of strong or significant low or high anomalies are smaller. Three factors could contribute to this: weaker SSWs, weaker stratosphere-troposphere coupling, and a shorter NAM decorrelation timescale in March than in DJF (Baldwin, Stephenson, et al. 2003; Simpson et al. 2011), resulting in weaker anomalies at the surface when averaged over several weeks. The differences between surface impacts of SSWs in CHEM and NOCHEM are also weaker for March SSWs. Thus, interactive ozone seems much less important for the surface effects of March SSWs than for DJF SSWs.

Considering the NAM in these simulations as shown in Figure S2, we see negative NAM anomalies at the surface in both the CHEM and NOCHEM simulations, consistent with the negative NAO-like pattern seen in the Figure 3.8. There is a stronger signal in the troposphere in the CHEM compared to NOCHEM March SSW simulations at around 15-20 days after the central date, which may correspond to the surface pressure differences.

The NAM anomalies suggest that March SSWs in both CHEM and NOCHEM are weaker overall than the DJF SSWs; the stratospheric NAM anomalies are smaller and less significant. The eddy heat flux show in Figure S3, however, shows weaker wave forcing preceding only the CHEM (not the NOCHEM) March SSWs compared to those in DJF. Stratosphere-troposphere coupling also seems weaker compared to that seen for DJF SSWs. Further, the difference in the NAM descent between CHEM and NOCHEM is less strong and persistent than the difference seen after midwinter SSWs.

Soon after the central date for March SSWs, the NAM signal in the stratosphere is weaker with CHEM than NOCHEM, in contrast to the midwinter SSW case. This difference appears to arise from the temperature and heating anomalies (Figure S4). The lower stratosphere is only briefly and weakly warmer in CHEM compared to NOCHEM. Shortwave heating seems to be dominant in the temperature response to March SSWs, with the CHEM-NOCHEM difference in temperature anomalies (Figure S4a) largely following the difference in shortwave heating anomalies (Figure S4d). This is in contrast to the DJF SSWs, where the shortwave heating had little effect, and dynamical heating was dominant.

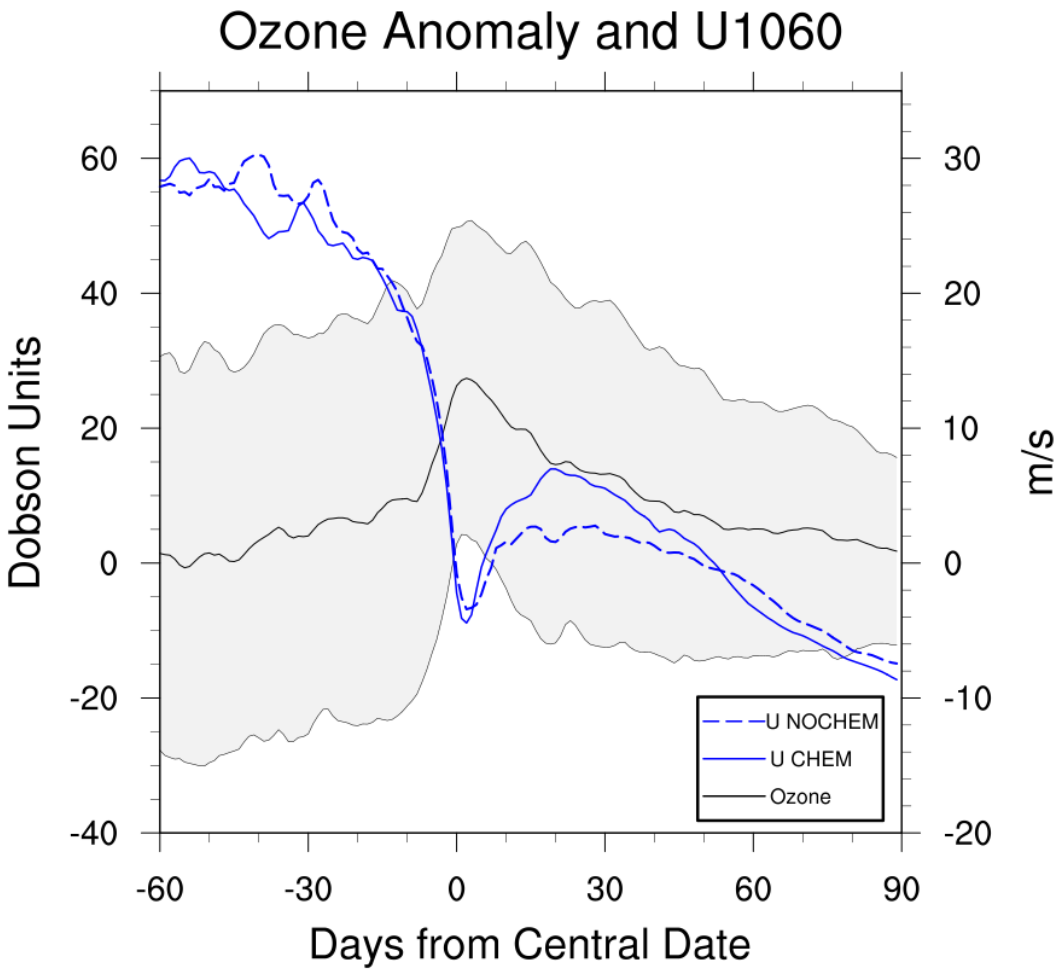

Figure 3.9: As in Figure 7, for March SSWs.

Finally, we note that unlike the DJF SSW case, the ozone anomaly for March SSWs does not persist after the event (Figure 3.9). This is related to the seasonal breakdown of the vortex, seen in the wind curves. Because these are late winter SSWs, the second month following the central date is near the expected stratospheric final warming date; the winds return to easterly about 50 days after the March SSW central date. The ozone anomaly returns to 0 Dobson units as the vortex breaks down. The maximum ozone anomaly is also about half the size of the maximum anomaly seen in DJF, consistent with the weaker nature of the March SSW events overall.

3.3.4 Midwinter strong polar vortex events

Finally, we turn our attention to strong polar vortex (SPV) events in DJF. While less extensively studied than SSWs, SPVs also impact surface climate. Baldwin and Dunkerton 2001 suggest that strong polar vortex events can have surface signals comparable to but opposite in sign to those following SSWs, and Smith, Polvani, and Tremblay 2018 found effects of Northern Hemisphere SPVs on spring and summer Arctic sea ice.

In the thirty days following the SPV central date, we see a pattern reminiscent of a weakly positive NAO in both CHEM and NOCHEM (Figure 3.10). This positive NAO-like pattern appears stronger in CHEM than in NOCHEM, but not significantly so. There is very little difference from climatology at the surface in the second month after the event in either of the simulations. This minimal difference using interactive versus specified ozone compared to the difference seen with SSWs may be related to the more zonal nature of SPVs. We specify ozone in a zonally-symmetric way, which is much more consistent with the vortex seen in an SPV than in an SSW.

The NAM anomalies following SPVs in CHEM and NOCHEM (Figure S5) have similar strength (and opposite sign) in the stratosphere to those following midwinter SSWs, but they have much weaker downward propagation, consistent with an only weakly positive NAO. The difference between the NAM anomalies in CHEM and NOCHEM confirms a more positive NAM in mid-to-lower troposphere in the first month following the SPV central date with interactive chemistry, but again, this difference is not significant and does not reach the surface.

These minimal differences in surface pressure and NAM are consistent with the similarity in the evolution of stratospheric temperature and heating rates in CHEM and NOCHEM, shown in Figure S6. The only large and significant difference is in stratospheric temperature, 40-60 days following the SPV central date, when the stratosphere is colder with interactive chemistry. This is after zonal mean zonal winds have returned to typical levels and is thus likely related to the stronger mean state of the stratospheric polar vortex with interactive chemistry compared to specified chemistry.

The zonal mean zonal winds in CHEM and NOCHEM around the SPV central dates further confirm that there is little difference in the strength of these events between CHEM and NOCHEM;

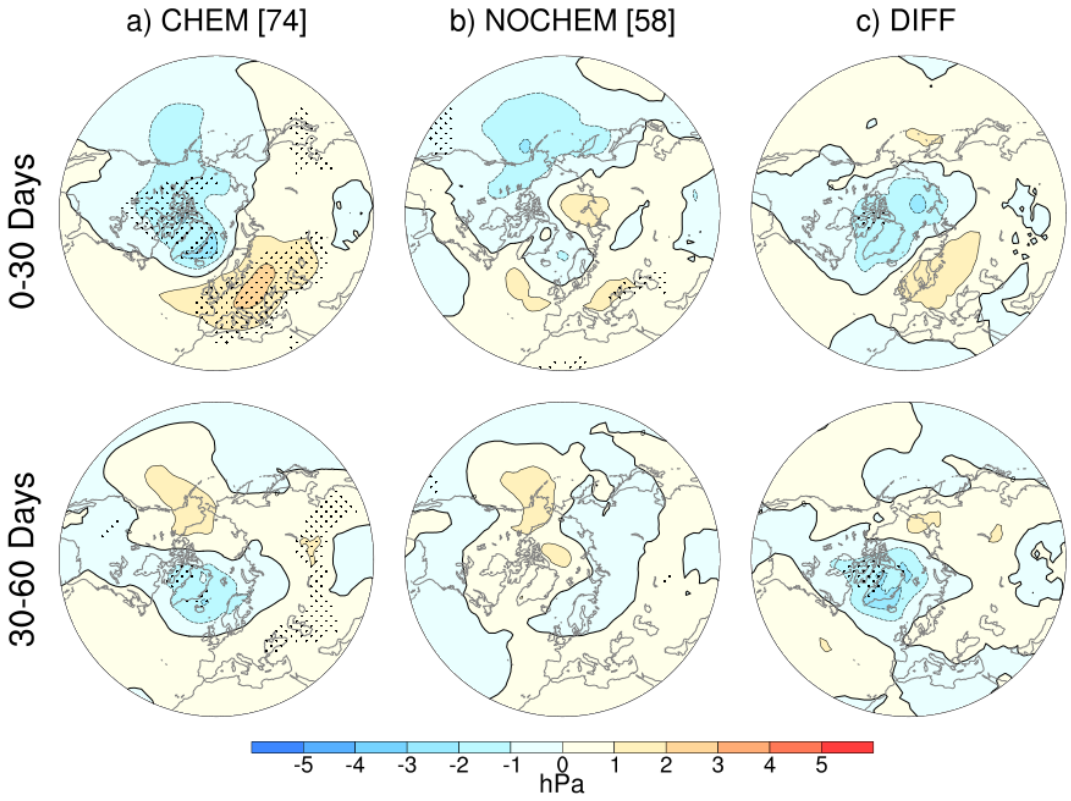

Figure 3.10: As in Figure 3, for DJF SPVs.

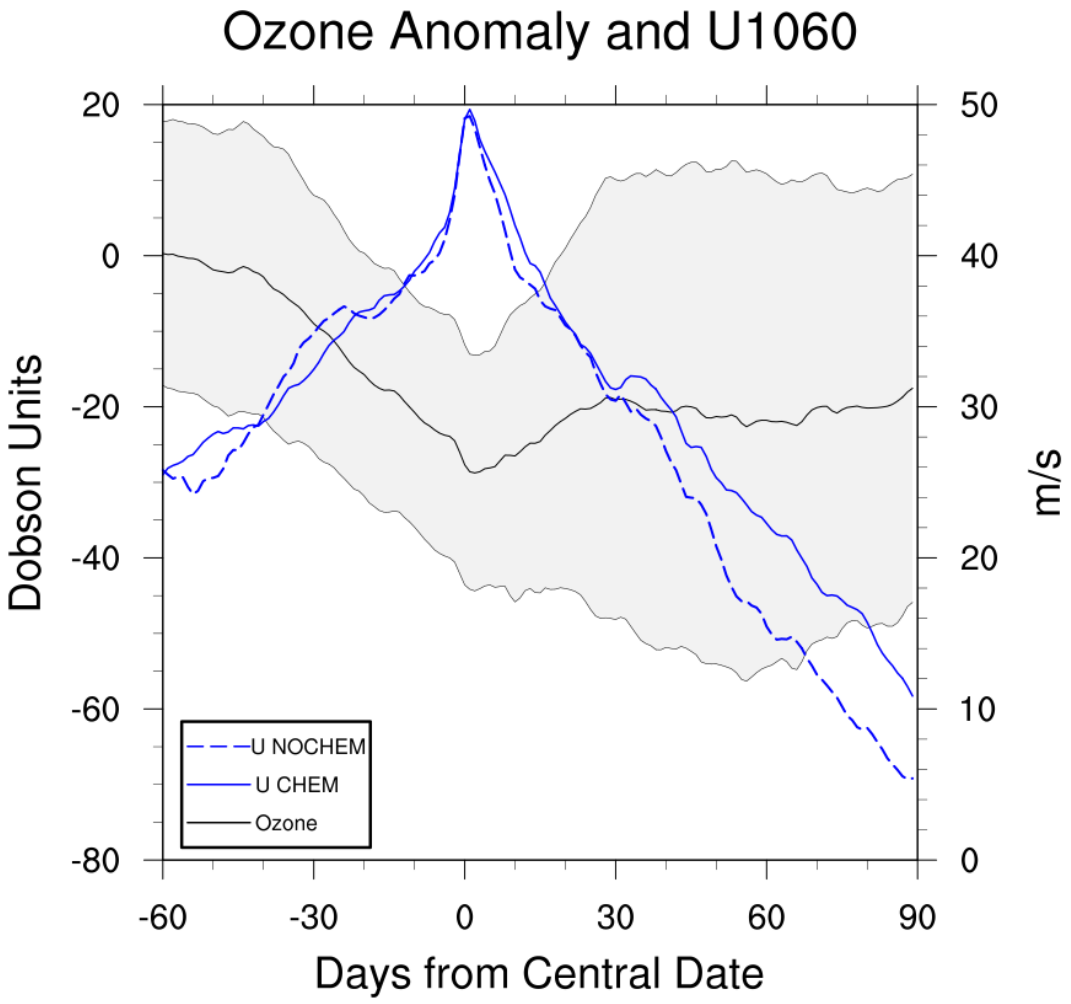

Figure 3.11: As in Figure 7, for DJF SPVs.

the winds follow nearly identical trajectories from 30 days before to 30 days after the central date. We also see a weaker ozone anomaly following SPVs than following SSWs, with a maximum absolute anomaly of about 30 Dobson units compared to 40 (Figure 3.11). The ozone decrease following SPVs is also much more gradual than the increase seen in DJF SSWs. This is consistent with the fact that SPVs are not strong and sudden dynamical events in the way that SSWs are. As with DJF SSWs, though, the anomaly does persist for three months after the central date.

3.4 Conclusions

The climate model results presented here show an important relationship between interactive ozone, the climatological state of the stratospheric polar vortex, and the Euro-Atlantic surface impacts of midwinter SSWs. However, ozone chemistry has minimal impact on the surface effects of March SSWs and of midwinter SPVs, despite long-lasting total ozone column anomalies in the latter case. Furthermore, in contrast to the results reported by Haase and Matthes 2019, we do not find significantly fewer SSWs with interactive chemistry, despite the stronger climatological polar vortex in both studies. However, we do find more frequent SPVs.

The stronger polar vortex mean state with interactive ozone chemistry also affects the surface signature of SSWs. A possible mechanism is that stronger wave forcing is necessary for an SSW to occur, and the resulting negative NAM propagates to the surface more strongly, as well. This result is also consistent with that reported by Haase and Matthes 2019, though the effects documented here are weaker. In extending this work to consider March SSWs, we found that while the same stronger dynamical forcing is present, the influence of the shortwave heating term in late winter/early spring results in a stratospheric temperature difference of opposite sign, and with little difference at the surface following March SSWs between interactive chemistry and specified chemistry simulations. We also find minimal impact on midwinter surface effects of SPVs. However, we do see persisting negative ozone anomalies that can have an important effect in spring (Ivy et al. 2017).

Previous work (Calvo, Polvani, et al. 2015; Ivy et al. 2017; Lin, Paynter, et al. 2017; Rieder et al. 2019; Smith and Polvani 2014) has shown the importance of ozone for the stratospheric polar vortex and surface springtime climate variability. Haase and Matthes 2019 further suggested that feedbacks among chemistry and dynamics are important for accurately capturing the response at the surface to SSWs, one of the major drivers of North Atlantic and European winter climate variability. By running longer simulations allowing for a cleaner quantification of the impact of interactive ozone, we find that these feedbacks are important for representing impacts of midwinter

SSWs. However, we do not find similar importance for describing surface response to March SSWs or DJF SPVs. Our results suggest that including interactive ozone chemistry may have a sizable impact on North Atlantic and European winter and spring climate variability in models.

Finally, we note that while we have only focused on winter SSWs and SPVs, stratospheric final warmings also have tropospheric effects (Ayarzagüena and Serrano 2009; Black et al. 2006; Butler, Charlton-Perez, et al. 2019; Hardiman, Butchart, et al. 2011; Thiéblemont et al. 2019; Wei et al. 2007). Those effects are dependent on the timing of the final warming, with earlier final warmings resulting in surface effects more like those seen following SSWs (Ayarzagüena and Serrano 2009; Li and Lau 2012). Interactive chemistry may thus also affect the representation and surface signature of stratospheric final warmings in models; this will be investigated in a follow-up study.

Chapter 4: Characterizing the surface impact of sudden stratospheric warmings in the context of internal variability

4.1 Introduction

The state of the stratospheric polar vortex is an important driver of wintertime climate variability in the Northern Hemisphere troposphere. In particular, the extreme weak state of the vortex seen during sudden stratospheric warmings (SSWs) has been connected to negative phases of the North Atlantic Oscillation (NAO) with associated effects at the surface for up to two months after the SSW occurs (Baldwin and Dunkerton 2001). Effects on temperature include cold anomalies and cold extremes in Northern Europe and the Eastern United States and warm anomalies in North Africa, the Middle East, Central Asia, Greenland, and Eastern Canada (e.g., Butler, Sjoberg, et al. 2017; Domeisen and Butler 2020; King et al. 2019; Kolstad, Breiteig, et al. 2010; Scaife, Folland, et al. 2008; Thompson and Wallace 2001). Common precipitation anomalies following SSWs include dry spells in northern Europe and increased precipitation in southern Europe (e.g., Ayarzagüena, Barriopedro, et al. 2018; Butler, Sjoberg, et al. 2017; Domeisen and Butler 2020; King et al. 2019).

However, there is a great deal of uncertainty in this response. Polvani, Sun, et al. (2017) found a spread of nearly a factor of 2 in SSW frequency per decade across ten ensemble members in a high-top model; given this uncertainty in frequency, we would expect similarly large spread in the surface response. The time period of SSW observations is under 70 years long (Baldwin, Ayarzagüena, et al. 2021), and the typical surface response does not follow all events. This raises the question of whether the set of SSWs we have observed are actually representative and why a surface signal is seen following some events and not others. Studies of this uncertainty have focused on variability across individual SSW events or types of events and the conditions in which they

occur. Only about two-thirds of SSWs have downward propagation to the surface and are followed by a negative NAO (Afargan-Gerstman and Domeisen 2020; Butler, Lawrence, et al. 2020; Domeisen, Garfinkel, et al. 2019a; Karpechko, Hitchkock, et al. 2017). Potential stratospheric causes for the diversity in surface response include lower stratospheric anomalies and magnitude of wave activity immediately following the central date (Karpechko, Hitchkock, et al. 2017) and differences in the type of SSW event (i.e. split/displacement or absorbing/reflecting) (Kodera et al. 2016; Mitchell, Gray, et al. 2013; Seviour, Gray, et al. 2016). However, it is unclear whether these differences in the stratosphere are important in determining the surface responses that follow (Karpechko, Hitchkock, et al. 2017; Maycock and Hitchcock 2015; White, Garfinkel, et al. 2019). Potential tropospheric causes for the uncertainty in the surface response following SSWs include jet stream location, ENSO, the MJO, and the state of the North Atlantic or Eastern Pacific prior to the event (Baldwin, Ayarzagüena, et al. 2021, and references therein).

Deser, Simpson, Phillips, et al. (2018) and Deser, Simpson, McKinnon, et al. (2017) addressed similar challenges in understanding the extratropical circulation response to the El Niño-Southern Oscillation (ENSO). Using a bootstrap resampling method, they constructed synthetic, observationally-based El Niño and La Niña composites comparable to the observed composites. Because these synthetic composites were built of resampled observed events, it is plausible that they could have occurred given different atmospheric variability unrelated to ENSO. This approach allowed them to capture both the spatial pattern and the magnitude of the uncertainty in surface impacts of ENSO. They found that SLP, temperature, and precipitation anomalies in some regions were robust across the synthetic composites but nevertheless varied in magnitude by up to a factor of 2 as well as varying in pattern; other regions showed significant responses less robustly across the composites. The diversity in the circulation responses in all of these regions was found to be unrelated to ENSO diversity and instead the result of unrelated internal atmospheric noise.

The goal of this study, building on the method of Deser, Simpson, McKinnon, et al. (2017), is to answer two questions related to uncertainty in the response to SSWs. First, how robust are the observed composite surface responses to SSWs? Second, is the variation that we see in the

composite surface response a result of diversity in the disruption in the stratosphere, or is it due to unrelated tropospheric variability? After describing our methods in the next section, we first examine a subset of the synthetic composites, as well as the observed composite, to qualitatively understand the considerable spread in both pattern and amplitude in the composite surface response following SSWs. Then, focusing on particular regions identified from those composites, we quantify the surface responses to find that the canonical and observed response is robust and distinct from what is seen in a similar winter composite that does not take the stratospheric polar vortex into account. Finally, we relate the surface anomalies to the strength of the polar vortex weakening. We find that there is little relationship between the composite vortex strength and the anomalies at the surface, and thus the uncertainty in the surface response is largely due to internal tropospheric variability. We conclude with a brief summary and a discussion of the use of these results for model evaluation.

4.2 Data and Methods

To analyse the anomalies following sudden stratosphere warmings, we use data from the Japanese 55-Year Reanalysis (JRA-55) (Japan Meteorological Agency, Japan 2013; Kobayashi et al. 2015). This reanalysis was chosen for its longer record than many other reanalyses (beginning in January 1958) and its high top and vertical resolution (Fujiwara et al. 2017). We analyze winds, sea level pressures, temperatures, precipitation, and geopotential heights from this dataset over the 1958-2019 period, calculating daily anomalies by removing from daily-mean fields a climatology calculated as the mean value of each calendar day over the full period.

We detect sudden stratospheric warmings using the definition of Charlton and Polvani (2007a) (see the corrigendum Charlton and Polvani (2011)). An event is considered to be an SSW if the zonal mean zonal winds at 10 hPa and 60°N reverse from westerly to easterly during extended boreal winter (NDJFM). The date when the zonal mean zonal winds become easterly is considered the central date, and no day within 20 days following the central date can be considered a separate SSW. If the zonal mean zonal winds do not return to westerly for at least 10 consecutive days before

April 30th, the event is considered a final stratospheric warming and is excluded. This definition is among those described in Butler and Gerber (2018) as an optimal threshold for identifying SSWs. This procedure identifies 39 SSWs in JRA-55 over the 1958-2019 period; these are listed in the leftmost column of Table S1.

We form synthetic SSW composites by randomly sampling with replacement (bootstrapping) from the 39 SSW events in the reanalysis to form new sets of 39 events. This procedure follows that of Deser, Simpson, McKinnon, et al. (2017), and we generate 2000 synthetic composites. Figure S1 shows two key sampling characteristics of this procedure: the distribution of the number of unique SSW events across the 2000 synthetic composites, and the distribution of the maximum number of times a single event is repeated in a composite. The most common number of unique events in a 39-event composite is 25 (about 64% of the available events), and the maximum number of times one event occurs is 3 or 4 in the vast majority of cases. These distributions are in agreement with probabilistic predictions of these characteristics. Surface composites are plotted with stippling for statistical significance at a 95% level, calculated using a two-tailed Student's t-test against a null hypothesis of zero response.

We compare the distributions of composite responses to SSWs in particular regions to distributions of these fields over comparable winter periods in general. To preserve any seasonality effects, we choose these periods by randomly choosing the day of an SSW central date and, separately, randomly choosing a year from the 1958-2019 period. This baseline includes winters with SSWs as well as those with strong polar vortex events or no polar vortex extremes, together composing a climatology.

We calculate the Northern Annual Mode (NAM) with a method similar to that of Gerber and Martineau (2018). The NAM is calculated at each pressure level using deseasonalized, daily-mean, geopotential height averaged over 65°-90° N, normalized to have unit variance such that a negative stratospheric NAM index indicates a weak polar vortex. A detailed procedure is available in Appendix A of Oehrlein et al. (2020).

Throughout the paper, we consider six particular surface quantities of interest. Region bound-

aries for these quantities were chosen to capture variability across composites and in some cases to follow prior work. The results are robust to changes in the exact boundaries of the region and to the method of NAO index calculation. The values of interest are computed as below:

1. North Atlantic Oscillation (NAO): Computed with a station-based-like approach. The anomalies at the northern and southern centers were calculated as area-weighted averages of SLP over 62.5°-90° N, 45° W-10° E and 35°-50° N, 45° W-10° E respectively. Each time series was individually normalized, and the results were subtracted to yield the NAO index.

2. North Atlantic Precipitation (N Atlantic Precip): Computed as an area-weighted average over 30°-50° N, 40° W-10° E.

3. North Pacific Sea-Level Pressure (N Pacific SLP): Computed as an area-weighted average over 30°-60° N, 175° E-135° W.

4. Northern Eurasian Surface Temperature (Eurasian T_s): Computed as an area-weighted average over 60°-75° N, 30°-120° E (Polvani, Sun, et al. 2017).

5. Eastern Canadian Surface Temperature (E Canadian T_s): Computed as an area-weighted average over 45°-70° N, 45°-90° W.

6. Eastern United States Surface Temperature (Eastern US T_s): Computed as an area-weighted average over 25°-42.5° N, 65°-90° W.

4.3 Results

We begin by examining the surface climate following SSWs in reanalysis and a subset of the synthetic composites. Figure 1 shows sea level pressure (SLP), surface temperature (T_s), and precipitation anomaly composites for the 60 days following SSW central dates both in the observed composite (composites A, B, and C) and across 8 of the 2000 synthetic composites (A1-8, B1-8, and C1-8), illustrating the diversity of anomaly patterns and magnitudes in these SSW composites.

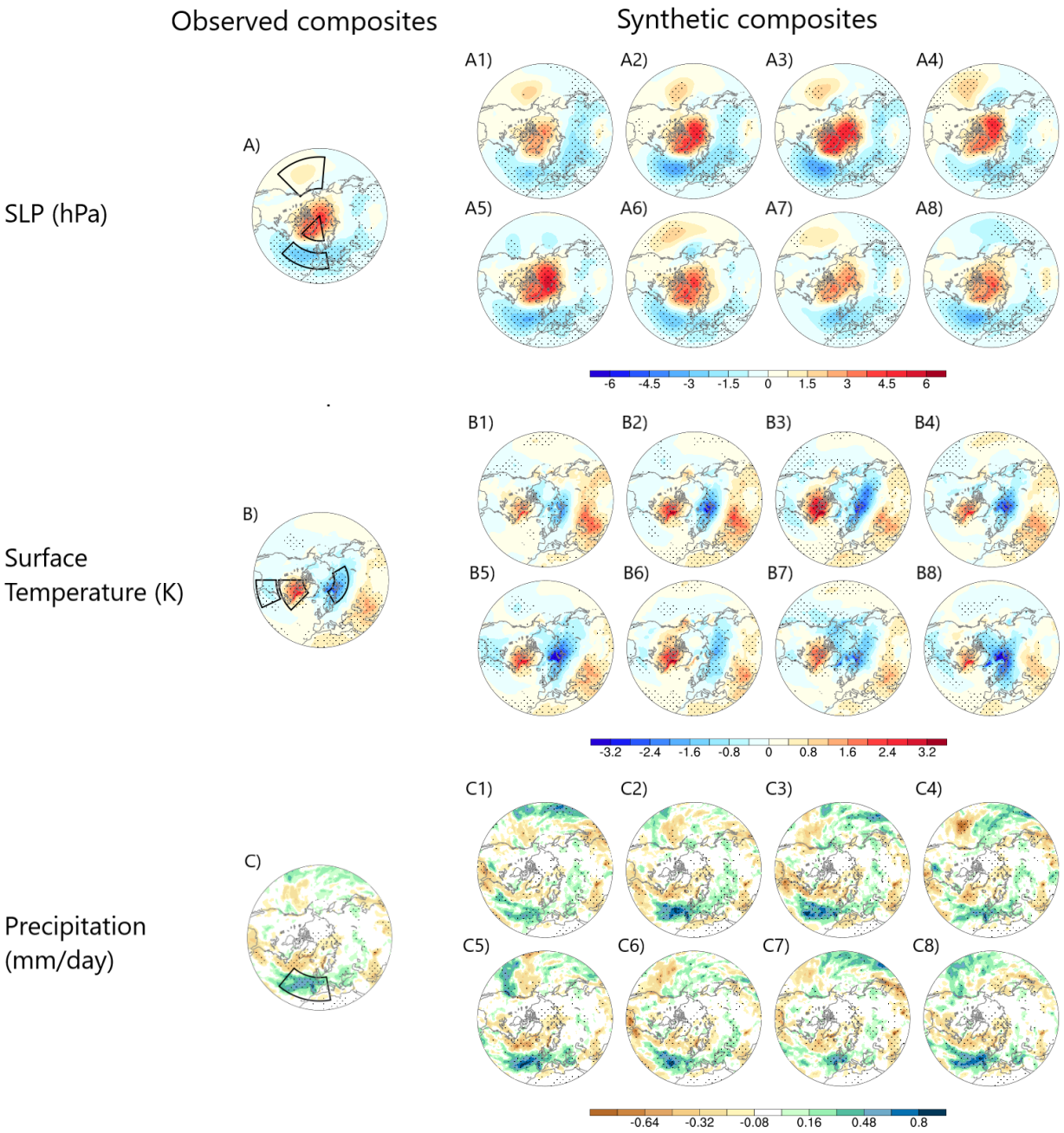

Figure 4.1: The observed composites and 8 examples of synthetic composites for sea-level pressure (SLP, A and A1-A8), surface temperature (T_s, B and B1-B8), and precipitation (C and C1-C8) in the 60 days following the SSW central date, with stippling for significance at the 95% level based on a two-tailed Student's t-test. Black boxes on the observed composites show regions of interest.

We first consider the SLP anomalies, shown in Figure 1 composites A and A1-A8. While a negative NAO-like pattern is present in all 9 of these composites, it varies from very strong (A3) to much weaker (A1) by a factor of two in both the high and low anomalies. The pattern also varies significantly, particularly in the low anomaly, which is sometimes centered over the North Atlantic (e.g. A6) and sometimes shifted towards western Europe (e.g. A7). The other main regin of interest in these composites is the North Pacific. The observed composite and 6 of the 8 synthetic composites show a high anomaly in this region, though it is not always statistically significant at the 95% level and is much weaker than the NAO-related anomalies.

We now turn to the corresponding surface temperature anomalies in Figure 1 composites B and B1-B8. Again, there are features common across all nine composites: northern Eurasian cooling, Central Asian and Middle Eastern warming, and East Canadian/Labrador Sea warming. But as with SLP, there is diversity in magnitude and pattern of these anomalies. For example, the northern Eurasian cooling is sometimes very strong (e.g. B5, B8) and sometimes much weaker (e.g. B1, B6). It can be very localized as in composite B1 or much more widespread as in B7. We also note that the observed composite and five of the synthetic composites show statistically significant cooling in the Eastern United States or just off the coast, sometimes over a small region (e.g. B6, B7) and sometimes stretching to the US Midwest (e.g. B5, B8).

Finally, Figure 1 composites C and C1-C8 show the associated precipitation anomalies. Following the NAO-like pattern above, we consistently see wet anomalies in the North Atlantic and western Europe. This again varies in magnitude, spatial extent, and center, generally following the pattern and magnitude of the low SLP anomaly. This is often accompanied by a dry anomaly further to the north and along the east coast of North America. All composites show a significant dry anomaly south of the Caspian Sea. The patterns in the Pacific are much more variable; most of the composites show dry anomalies near Japan, the Korean peninsula, and parts of eastern China, but there is no consistent pattern in the North Pacific or along the west coast of North America.

From this small sample of the composites, we identify a few key regions of interest to analyze further, shown in Figure 1 panels A, B, and C as well as in more detail in Figure S2. These are

the NAO, North Atlantic precipitation (N Atlantic Precip), North Pacific sea-level pressure (N Pacific SLP), Eurasian surface temperature (Eurasian T_s), Eastern Canadian surface temperature (E Canadian T_s), and Eastern US surface temperature (Eastern US T_s) and are described in more details in the Data and Methods section.

Along with this diversity in surface patterns following SSWs, we see a wide range of Northern Annular Mode indices in the stratosphere and troposphere in the 30 days preceding and 60 days following the central date. This is illustrated in Figure 2, showing the same eight composites of SSWs as in Figure 1 (with composite A in Figure 2 corresponding to Figure 1 composites A, B, and C, and composites B through I in Figure 2 corresponding to synthetic composites 1-8 in Figure 1 respectively). In the upper stratosphere, composites G and I have a more negative NAM than do other composites, and in composite F the maximum disturbance at 10 hPa is particularly long-lived. These differences magnify as the effects of the SSW descend to the lower stratosphere and the troposphere. The negative NAM near 100 hPa in the lower stratosphere is especially long-lived in the observations (composite A) as well as composites F and G. All composites show some descent of the negative NAM to the surface, but it varies in strength, with particularly strong descent in composites D and F and particularly weak descent in composites B and H. There is also variability in consistency of that descent across the 60 days following the central date, with the most consistent negative tropospheric NAM in composites A and D, intermittent negative tropospheric NAM in composites E, H, and I, and delayed descent in composite B.

If the spread in surface response across the composites were explained by the spread in the stratosphere, then the stratospheric portions of plots such as those in Figure 2 would explain the anomalies seen in surface composites as in Figure 1. To investigate whether this is the case, we first calculate indices or area-weighted anomalies over our regions of interest and examine the 10th and 90th percentile composites for each of these quantities, along with the corresponding NAM plot. Figure 3 shows these results for the NAO and the East Canadian surface temperature region; other regions are included in Figures S3 and S4. The events included in each composite of Figure 3 are listed in Table S1. For the two regions shown here, we see two different relationships

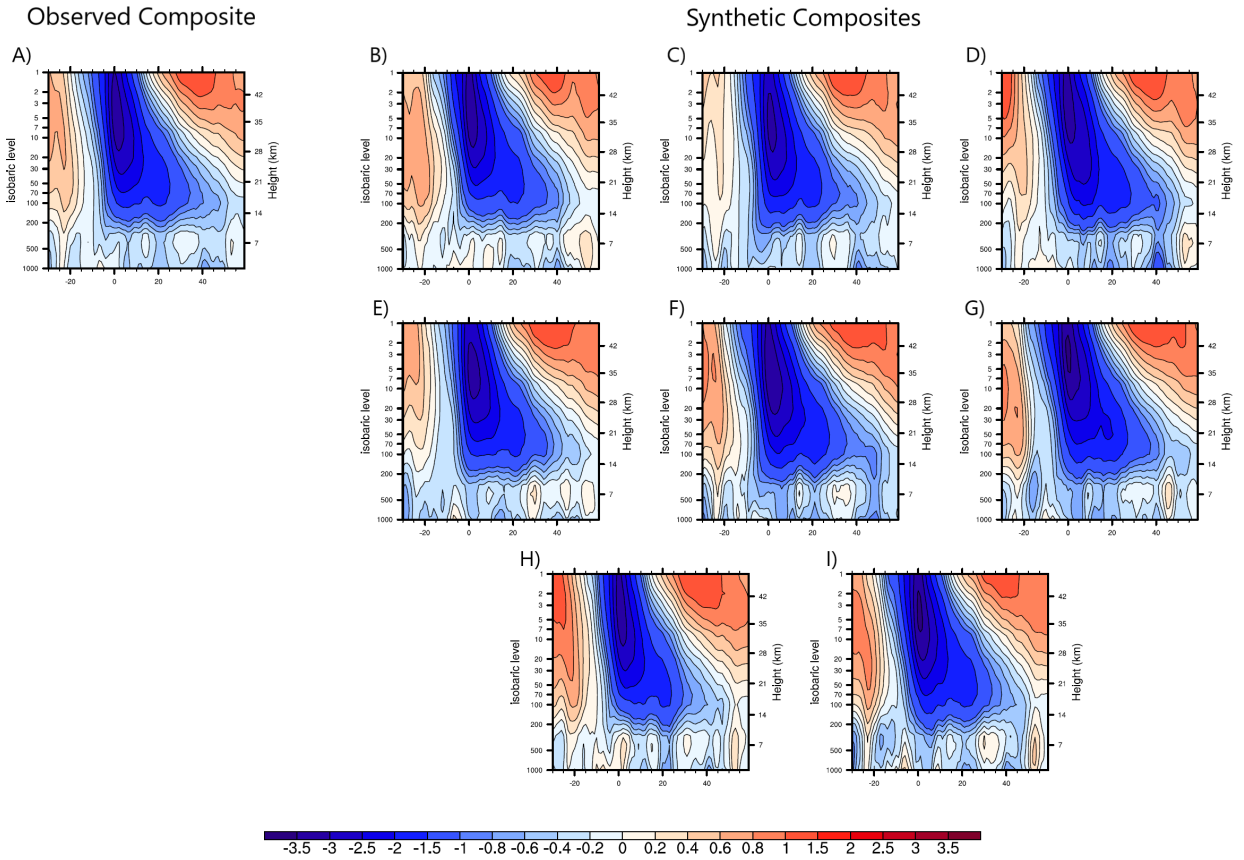

Figure 4.2: The observed composites and 8 examples of synthetic composites for NAM (standardized polar cap geopotential height anomalies) from 30 days before to 60 days after the SSW central date.

between the negative NAM index in the stratosphere and the anomaly at the surface. The stronger NAO index at the surface in Figure 3(a) is associated with a stronger negative NAM in the upper stratosphere in panel (b) compared to that in panel (d). But the opposite relationship holds for East Canadian surface temperature. We see a stronger and more widespread surface anomaly in panel (g) compared to panel (e) but a weaker negative NAM at 10 hPa in panel (h) compared to panel (f). Particularly given that we expect a correlation between this positive temperature anomaly and a negative NAO, this suggests that the strength of the composite disruption in the stratosphere does not explain the strength of the composite anomalies at the surface.

We now turn from considering individual composites to all 2000 bootstrapped composites in order to better quantify the spread in response at the surface and any relationship to diversity in the

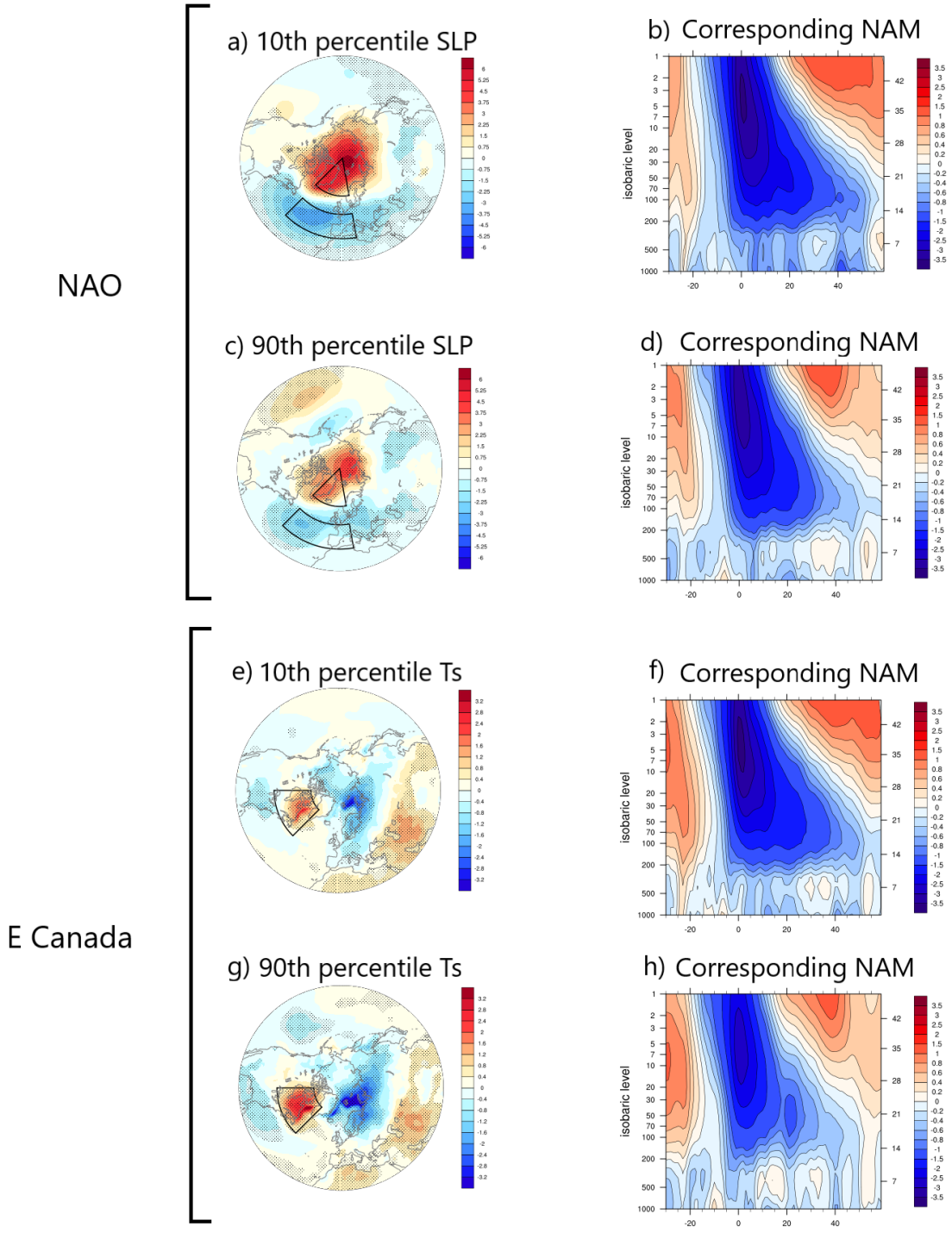

Figure 4.3: The 10th and 90th percentile composites of the NAO index and Eastern Canadian temperature anomalies in days 0-60 following the SSW central date, along with the corresponding NAM responses.

disruption in the stratospheric polar vortex. We begin by considering the uncertainty in the surface composites for our regions of interest. Figure 4 shows the indices or anomalies for each region across all 2000 composites compared to a climatological baseline of comparable winter periods. In all cases except that of North Pacific SLP (panel (c)), there are large shifts in anomalies in these regions due to SSWs, with little overlap with the baseline distributions. Some of these shifts are small, such as that of about -0.5 K in surface temperature over the Eastern US, but this is still physically meaningful as a composite result over a large region and a 60 day period. Further, all SSW distributions except North Pacific SLP and Eastern US surface temperature (panels (c) and (f)) are shifted to not overlap with 0; that is, the anomalies across all bootstrapped composites are of one sign. The Eastern US surface temperature anomaly is largely robust in this sense; it is positive in only 10 SSW composites out of 2000. The SSW composites in the North Pacific largely show positive SLP anomalies, but 404 composites (about 20%) have negative SLP anomalies, so this region shows both less separation from the baseline and a less consistent anomaly sign.

To investigate this further, we separate the observed events by El Niño-Southern Oscillation (ENSO) phase (using the Oceanic Niño Index) due to the strong influence of ENSO in the region and known interactions between ENSO and the stratospheric polar vortex (e.g., Butler and Polvani 2011; Domeisen, Garfinkel, et al. 2019b; Polvani, Sun, et al. 2017). Of the 39 events, 10 occurred in neutral-ENSO winters, 16 in El Niño (EN) winters, and 13 in La Niña (LN) winters. We form bootstrapped composites of 10 events for SSWs in all ENSO phases, comparable winters in all ENSO phases, SSWs in each ENSO phase, and comparable winters in each ENSO phase. The results are shown in Figure S5. In EN and LN, North Pacific SLP anomalies are shifted positively following SSWs compared to the baseline (by +1.3 K and +0.59 K respectively), but we see the opposite in neutral-ENSO (shift of -0.71 K). This is neither a consistent shift with SSWs across phase nor a direct relationship with ENSO, so these results do not suggest a clear influence of SSWs in the North Pacific.

For all the surface quantities of interest, in contrast to the clear shifts in mean, the shape and spread of the distributions tend to change very little from the baseline distributions to the SSW

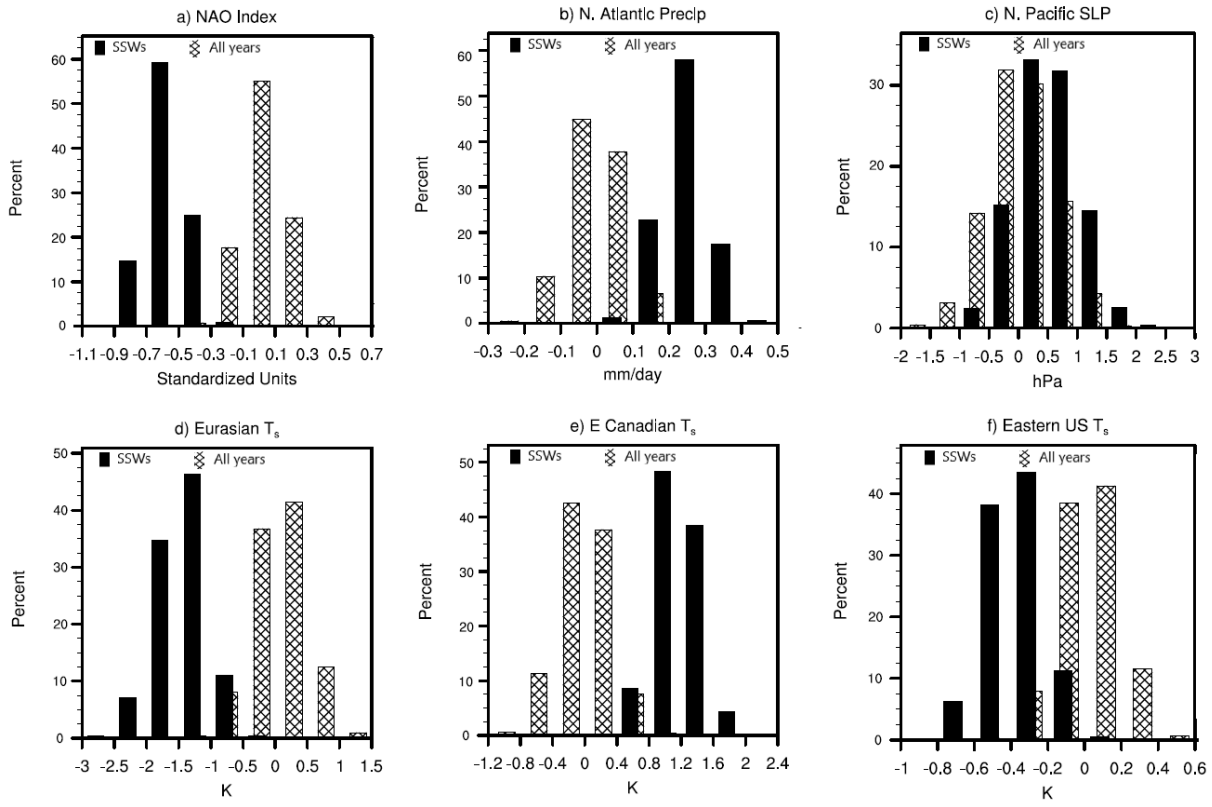

Figure 4.4: The responses in the 60 days following SSWs. Histograms show the SSW composites in black and similar composites drawn from all winters with hatching.

distributions. This suggests that the two have similar sources of variability, implying that most of the diversirty in these surface composites is not directly a result of diversity in SSW strength.

We next study this further by directly considering the relationship between the surface anomalies and vortex strength. Figure 5 shows scatterplots of the sixty-day surface anomaly in the region of interest against the 10 hPa polar cap geopotential height anomaly, averaged over 65°-90° N in the first five days after the SSW central date, for each bootstrapped composite. In all cases, there is very little relationship between the surface anomaly and the anomaly at 10 hPa, where we define and measure the strength of the SSW. Thus, the diversity in the composite responses at the surface is not the result of diversity in the composite strength of SSWs. There is some relationship between the surface anomalies and the stratospheric anomalies at 100 hPa in the first five days following the central date as shown in Figure S6, suggesting that strong and quick descent to the lower tro-

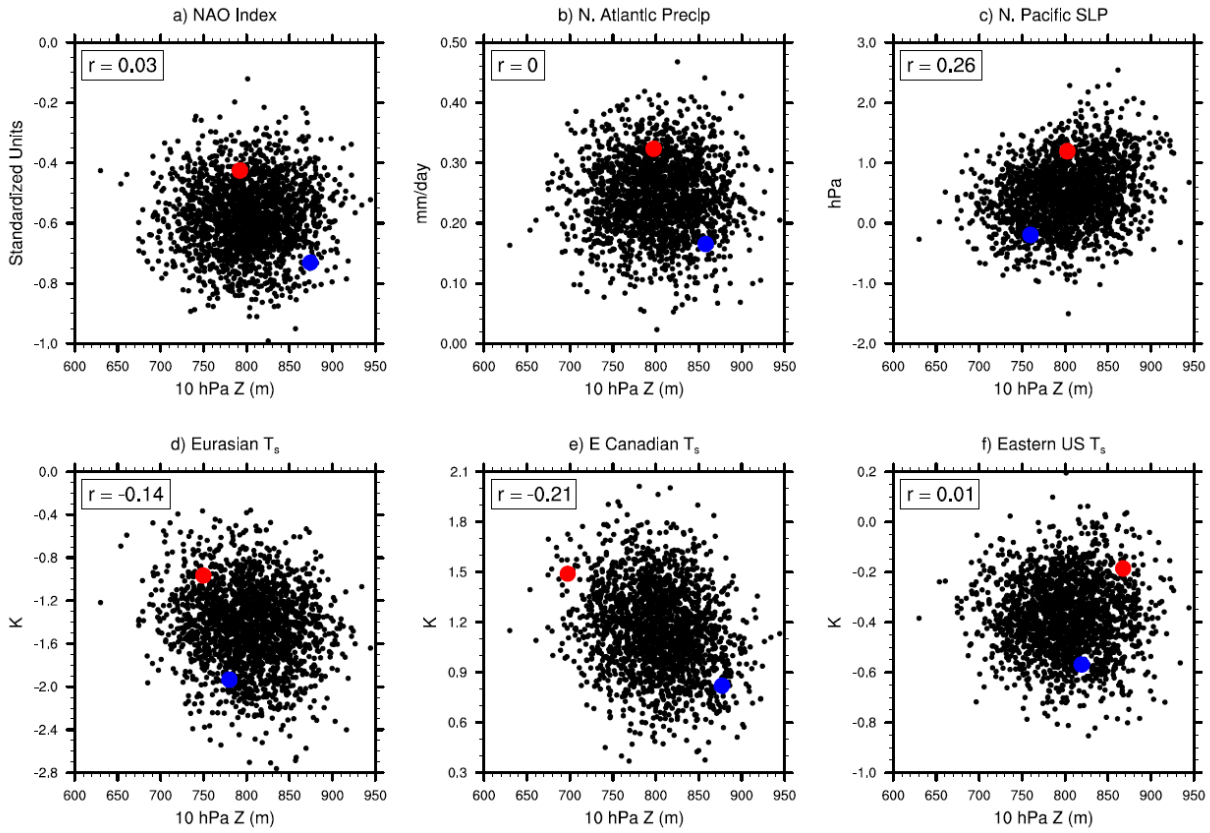

Figure 4.5: The responses of surface temperature in the 0-60 days following SSWs and relationships to the stratospheric vortex strength in days 0-5 at 10 hPa, calculated as geopotential height anomalies over the polar cap. Blue and red dots denote the 10th and 90th percentile composites by surface index/anomaly respectively.

posphere is associated with larger anomalies at the surface. However, 100 hPa is too low a level to serve as a measure of the strength of the vortex itself, and this relationship between the surface to the lower stratosphere still explains at most 25% of the variability at the surface. Looking at the correlations between the sixty-day surface anomalies and sliding windows of five-day, polar cap geopotential height anomalies across pressure levels and time periods, shown in Figure S7, we see that there are no time periods or levels in the stratosphere that explain more than about 25% of the surface variability for any of the regions of interest. The vast majority of the spread in the surface composite responses is instead the result of tropospheric internal variability.

4.4 Conclusions

Using SSW events from over 60 years, we find that the Northern Hemisphere sea-level pressure, surface temperature, and precipitation responses in the two months following SSWs show large uncertainty in both pattern and magnitude. The canonical SSW responses such as a negative NAO-like pattern in SLP and precipitation and cold anomalies across Northern Eurasia are robust but can vary by a factor of 3 or more in magnitude, and the extent and center of the anomalies also vary widely. We highlight two surface temperature regions in North America, in Eastern Canada and the Eastern United States, that also show robust anomalies. The temperature anomalies seen in Eastern Canada and the Labrador Sea are large and in some cases extend over the full Labrador Peninsular; those seen in the Eastern United States are generally lower in amplitude but can similarly stretch from just off the Atlantic coast to the Midwest United States. In other regions, such as the North Pacific, though about 80% of the composites showed a positive SLP anomaly following SSWs, the sign and significance of the composite anomaly are not robust, and there is no clear effect of SSWs on the region.

The uncertainty at the surface across regions is largely unrelated to diversity in the strength of the SSW itself; that is, a weaker polar vortex in a given composite does not correspond to stronger surface anomalies in general. This suggests that the range of patterns seen at the surface is the result of unrelated, likely tropospheric, atmospheric variability. There is some relationship between descent of geopotential height anomalies to the lower stratosphere and the strength of anomalies at the surface; this agrees with previous studies on variability across individual events (Baldwin 2003; Christiansen 2005; Gerber, Orbe, et al. 2009; Karpechko, Hitchkock, et al. 2017; Rao, Garfinkel, and White 2020b; Siegmund 2005). However, we find that this descent to the lower stratosphere still explains only a small percentage of the variability at the surface, leaving the vast majority (75% or more) to come from tropospheric sources.

These results are of use for model evaluation, allowing us to compare the patterns and amplitudes of both the model's ensemble mean SSW response and internal tropospheric variability

in that response to observations. This is helpful for distinguishing between model bias and differences due to variability unrelated to SSWs. Deser, Simpson, Phillips, et al. (2018) and Deser, Simpson, McKinnon, et al. (2017) evaluated the representation of ENSO climate impacts in the Northern Hemisphere in simulations from three models, diagnosing model bias and unrealistic internal variability in various regions, by comparing bootstrapped distributions from both observations and ensemble model simulations. Some models overpredict the strength or persistence of the negative NAO response after weak polar vortex events (Kolstad, Wulff, et al. 2020), and NAO prediction is particularly important for government, industry, and health in Europe (Charlton-Perez et al. 2021; Domeisen and Butler 2020). Thus, a careful evaluation of model response to SSWs and the interaction of that response with internal variability in comparison to the observations would be beneficial; this will be investigated in a follow-up study.

Conclusion

This chapter first summarizes the key approaches and results of the preceding chapters and then situates this thesis in the broader context of ongoing research on winter polar stratosphere-troposphere coupling.

Chapter 1 introduced the stratospheric polar vortex and the phenomenon central to this thesis, the sudden stratospheric warming (SSW). We discussed the key features of SSWs and how they are defined, and we reviewed the proposed theory, precursors, and efforts to model these events. We next discussed their surface impacts as seen in observations, reanalysis, and models, and reviewed the proposed theory around this downward propagation from the stratosphere to the surface. Further, we emphasized the variability in these surface impacts, which was the focus of the study in Chapter 4. We then turned to the other extreme of the stratospheric polar vortex, the strong polar vortex events (SPVs), briefly discussing their basic features, definitions, and surface response. We concluded Chapter 1 with a discussion of the interaction of these events, particularly SSWs, with other atmospheric features and phenomena, paying particular attention to interactions with the El Niño-Southern Oscillation (ENSO) and connections to the Brewer-Dobson Circulation and ozone transport and chemistry. These were the focus of the work in Chapters 2 and 3 respectively. In both cases, we considered interactions with both SSW occurrence and surface response following SSWs.

In Chapter 2, published as Oehrlein et al. 2019, we studied the relative contributions of El Niño and SSWs to winter climate variability in the North Atlantic and Europe. We used two ensembles of 200 one-year integrations of the Whole Atmosphere Community Climate Model (WACCM) with specified sea surface temperatures, one ensemble with neutral-ENSO conditions and one with strong El Niño conditions. We first found that the frequency of SSWs doubled under strong El Niño conditions relative to neutral-ENSO. We then formed four sets of composites representing winter climate following an SSW or in the absence of an SSW under each ENSO condition. We found similar effects on the NAO and European precipitation from SSWs alone and El Niño alone, though SSWs were followed by stronger Eurasian cooling. Further, the effects of SSWs and strong El Niño

events in the simulations were linearly additive. These results suggest that El Niño and SSWs are largely independent drivers of North Atlantic and Eurasian climate, and accurately representing both sources of variability and their interaction is important for improving seasonal forecasts.

In Chapter 3, published as Oehrlein et al. (2020), we explored the role of interactive chemistry in representations of the stratospheric polar vortex, sudden stratospheric warmings, and strong polar vortex events. We used two 200-year model simulations, one from the Whole Atmosphere Community Climate Model (WACCM), which included interactive chemistry, and one from SC-WACCM, the specified chemistry version of the same model. We confirmed results from previous work finding a stronger stratospheric polar vortex with interactive ozone chemistry. In line with that result, including interactive chemistry resulted in more strong polar vortex events. However, we found little effect on SSW frequency with interactive compared to specified chemistry, in contrast to a prior study. At the surface, interactive ozone chemistry resulted in a stronger NAO-like pattern following midwinter SSWs, and we proposed a mechanism for this difference related to the stronger climatological polar vortex and stronger wave forcing preceding the SSW. In contrast to the midwinter SSW result, there was little difference between the two simulations in the surface response to SPVs or March SSWs. This work suggests that including interactive ozone chemistry may be important for representing North Atlantic and European winter and spring climate variability in models.

In Chapter 4, we studied the uncertainty in the observed response to SSWs and the source of this uncertainty. Using an ensemble of synthetic SSW composites built from observed events, we found that the canonical responses to SSWs of a negative NAO, cooling in Northern Eurasia, and increased precipitation in the North Atlantic and southern Europe were robust across the composites. We also found similar results in North America, with cooling in the Eastern United States and warming in Eastern Canada, that are present in the literature but less thoroughly studied. While 80% of the synthetic composites showed a positive anomaly in the North Pacific, this response was not well-separated from the winter baseline, and it was not clearly due to SSWs. Finally, we found that the average strength of the SSWs (defined as geopotential height at 10 hPa near the central

date) did not explain the variability at the surface across the composites. Instead, at most 25% of this uncertainty is explained by the strength of downward propagation to the lower stratosphere, with most of the uncertainty the result of unrelated tropospheric variability. We plan to use these results to evaluate the representation of the surface effects of SSWs in models, particularly forecast models, with a similar bootstrapping method to compare both the mean impact of SSWs and the role of internal variability.

Taken as a whole, this work demonstrates the difficulty in understanding and modeling sudden stratospheric warmings and their surface impacts. This is due in part to wide variety of interactions of the stratospheric polar vortex with other phenomena in the troposphere, stratosphere, and the rest of the Earth system and in part to the large role of unrelated tropospheric variability in the surface anomalies following SSWs. With only about 40 major SSWs in the observational record, subdividing by types of events or the state of other phenomena (e.g. ENSO phase) yields relatively small sample sizes and significant uncertainty, making it difficult to either draw conclusions from the observed events or to use them to evaluate the fidelity of model simulations.

Work in the field about interactions of ENSO and the stratospheric polar vortex is ongoing. There is particular focus on whether the response to ENSO in the North Atlantic and Europe, or some portion of that response, is nonlinear or asymmetric with the phases of ENSO and ENSO strength (Jiménez-Esteve and Domeisen 2020; Mezzina et al. 2020; Trascasa-Castro et al. 2019; Weinberger et al. 2019; Zhou, Chen, Wang, et al. 2020; Zhou, Chen, Xie, et al. 2019) and whether different types of ENSO events or interactions with other oceanic or atmospheric features have different effects on the polar vortex or North Atlantic climate (Lee et al. 2019; Rao, Garfinkel, and Ren 2019; Weinberger et al. 2019; Zhou, Chen, Xie, et al. 2019). The observed relationship between ENSO and the polar vortex has weakened in recent decades, but this is likely due to sampling variability (Garfinkel, Schwartz, Butler, et al. 2019). Interactions of the stratospheric polar vortex with other sources of variability, for example the MJO (e.g. Knight et al. 2021; Lee et al. 2019) and the QBO (e.g. Dimdore-Miles et al. 2020; Lu et al. 2020; Rao, Garfinkel, and White 2020a), continue to be of interest as well.

Stratospheric final warmings also show a great deal of interannual variability in their timing and surface impacts but can be an important driver of North Atlantic spring climate (Black et al. 2006), springtime ozone concentrations (Salby and Callaghan 2007), and autumn sea ice (Kelleher et al. 2020). Final warmings that are later than average tend to be radiative events and are predictable at longer lead times than early final warmings, which are more wave-driven and resemble SSWs (Butler, Charlton-Perez, et al. 2019). However, early final warmings provide greater surface climate predictive skill, and the surface climate following early compared to late events is significantly different (Ayarzagüena and Serrano 2009; Butler, Charlton-Perez, et al. 2019). Final warming timing is related to wave-driving in the preceding winter and whether or not an SSW occurred (Butler, Charlton-Perez, et al. 2019; Hu et al. 2014; Salby and Callaghan 2007). This suggests connections to ENSO (Butler, Charlton-Perez, et al. 2019) and the Quasi-Biennial Oscillation (QBO) (Salby and Callaghan 2007; Thiéblemont et al. 2019), but it is unclear whether these impact final warmings only through SSW frequency. The strength of the response at the surface may also depend on the vertical profile of the warming in the stratosphere, but this too seems related to wave-driving and SSW occurrence in the preceding winter (Hardiman, Butchart, et al. 2011; Thiéblemont et al. 2019).

Looking to the future, it is unclear what effect, if any, climate change will have on SSW frequency, final warming timing, or their surface impacts. The results on changes to SSW frequency are inconsistent across modeling studies that have used a variety of models or model ensembles and experimental designs (Ayarzagüena, Charlton-Perez, et al. 2020; Ayarzagüena, Polvani, et al. 2018; Bell, Gray, and Kettleborough 2010; Charlton-Perez, Polvani, et al. 2008; Karpechko and Manzini 2012; Kim et al. 2017; McLandress and Shepherd 2009; Mitchell, Charlton-Perez, Gray, et al. 2012; Rao and Garfinkel 2021a; Rind et al. 1998; Scaife, Spangehl, et al. 2012). In particular, Ayarzagüena, Charlton-Perez, et al. 2020 and Rao and Garfinkel 2021a found that across CMIP5 and CMIP6 multi-model ensembles, there was no significant change in SSW frequency in the future, but there was large variation, including in sign, across individual models, scenarios, and SSW definitions. This uncertainty in sign may be due to competing effects of radiative CO_2 cool-

ing (Bell, Gray, and Kettleborough 2010) and adiabatic warming associated with a strengthened Brewer-Dobson Circulation (Butchart 2014). Rao and Garfinkel 2021a further found little effect on the lifecycle of SSWs, and any impact on SSW seasonality was unclear. They also saw no effect on polar stratosphere-troposphere coupling under moderate or high emissions scenarios, whereas Ayarzagüena, Charlton-Perez, et al. 2020 found a stronger surface pressure response to SSWs in quadruple CO_2 experiments. While many models simulate a climatologically weaker stratospheric polar vortex in the future, in some models and scenarios this is independent of changes in SSW frequency (Mitchell, Charlton-Perez, Gray, et al. 2012; Scaife, Spangehl, et al. 2012) and in others changes to SSW frequency are responsible for that weaker mean state (Bell, Gray, and Kettleborough 2010). Future changes to stratospheric final warmings have been less studied, but Rao and Garfinkel 2021b found a delay of 4-8 days in average final warming date over the next century, in agreement with Thiéblemont et al. 2019. However, this delay is comparable to the existing late bias in the final warming dates in historical simulations, and in some cases it is only present for strong emissions scenarios. They found little change in the future to final warming impacts at the surface in the Northern Hemisphere. Further work and time are necessary to determine the true balance of competing effects on the stratospheric polar vortex, its life cycle, sudden stratospheric warmings, and stratosphere-troposphere coupling as well as the role of ozone depletion and recovery compared to other changes in emissions.

Coupling of the polar stratosphere to the troposphere, particularly through sudden stratospheric warmings and final stratospheric warmings, is an important driver and predictor of North Atlantic and Eurasian climate at subseasonal-to-seasonal timescales. Understanding and predicting this coupling has implications for health, infrastructure, and shipping, among other industries (Charlton-Perez et al. 2021; Domeisen and Butler 2020). However, extreme polar stratospheric events are processes with large natural variability and relationships to a variety of other modes of variability and components of the Earth system. Continuing to deepen our understanding of the forced response to SSWs in observations will allow for better evaluation of models and knowledge of what features are important, resulting in better predictions at the subseasonal and seasonal

timescales, and more realistic representations in models will allow us to better disentangle interactions between SSWs and other sources of variability, including future climate change.

References

Afargan-Gerstman, H., & Domeisen, D. I. V. (2020). Pacific Modulation of the North Atlantic Storm Track Response to Sudden Stratospheric Warming Events. *Geophysical Research Letters*, *47*(2).

Albers, J. R., & Birner, T. (2014). Vortex Preconditioning due to Planetary and Gravity Waves prior to Sudden Stratospheric Warmings. *Journal of the Atmospheric Sciences*, *71*(11), 4028–4054.

Albers, J. R., & Nathan, T. R. (2012). Pathways for communicating the effects of stratospheric ozone to the polar vortex: Role of zonally asymmetric ozone. *Journal of the Atmospheric Sciences*, *69*(3), 785–801.

Alexander, M. A., Bladé, I., Newman, M., Lanzante, J. R., Lau, N.-C., & Scott, J. D. (2002). The atmospheric bridge: The influence of ENSO teleconnections on air - sea interaction over the global oceans. *Journal of Climate*, *15*, 2205–2231.

Andrews, D. G., Holton, J. R., & Leovy, C. B. (1987). *Middle atmosphere dynamics*. Academic Press.

Anstey, J. A., & Shepherd, T. G. (2014). High-latitude influence of the quasi-biennial oscillation. *Quarterly Journal of the Royal Meteorological Society*, *140*(678), 1–21.

Ayarzaguena, B., Langematz, U., Meul, S., Oberländer, S., Abalichin, J., & Kubin, A. (2013). The role of climate change and ozone recovery for the future timing of major stratospheric warmings. *Geophys. Res. Lett.*, *40*, 2460–2465.

Ayarzagüena, B., Barriopedro, D., Garrido-Perez, J. M., Abalos, M., Cámara, A., García-Herrera, R., Calvo, N., & Ordóñez, C. (2018). Stratospheric Connection to the Abrupt End of the 2016/2017 Iberian Drought. *Geophysical Research Letters*, *45*(22), 12, 639–12, 646.

Ayarzagüena, B., Charlton-Perez, A. J., Butler, A. H., Hitchcock, P., Simpson, I. R., Polvani, L. M., Butchart, N., Gerber, E. P., Gray, L., Hassler, B., Lin, P., Lott, F., Manzini, E., Mizuta, R., Orbe, C., Osprey, S., Saint-Martin, D., Sigmond, M., Taguchi, M., ... Watanabe, S. (2020). Uncertainty in the Response of Sudden Stratospheric Warmings and Stratosphere-Troposphere Coupling to Quadrupled CO_2 Concentrations in CMIP6 Models. *Journal of Geophysical Research: Atmospheres*, *125*(6).

Ayarzagüena, B., Palmeiro, F. M., Barriopedro, D., Calvo, N., Langematz, U., & Shibata, K. (2019). On the representation of major stratospheric warmings in reanalyses. *Atmospheric Chemistry and Physics*, *19*(14), 9469–9484.

Ayarzagüena, B., Polvani, L. M., Langematz, U., Akiyoshi, H., Bekki, S., Butchart, N., Dameris, M., Deushi, M., Hardiman, S. C., Jöckel, P., Klekociuk, A., Marchand, M., Michou, M., Morgenstern, O., O'Connor, F. M., Oman, L. D., Plummer, D. A., Revell, L., Rozanov, E., ... Zeng, G. (2018). No robust evidence of future changes in major stratospheric sudden warmings: A multi-model assessment from CCMI. *Atmospheric Chemistry and Physics*, *18*(15), 11277–11287.

Ayarzagüena, B., & Serrano, E. (2009). Monthly Characterization of the Tropospheric Circulation over the Euro-Atlantic Area in Relation with the Timing of Stratospheric Final Warmings. *Journal of Climate*, *22*(23), 6313–6324.

Baldwin, M. P. (2003). Stratospheric Memory and Skill of Extended-Range Weather Forecasts. *Science*, *301*(5633), 636–640.

Baldwin, M. P., & Dunkerton, T. J. (2001). Stratospheric harbingers of anomalous weather regimes. *Science*, *294*, 581–584.

Baldwin, M. P., Stephenson, D. B., Thompson, D. W. J., Dunkerton, T. J., Charlton, A. J., & O'Neill, A. (2003). Stratospheric memory and skill of extended-range weather forecas. *Science*, *301*, 636–640.

Baldwin, M. P., & Thompson, D. W. (2009a). A critical comparison of stratosphere-troposphere coupling indices. *Quarterly Journal of the Royal Meterological Society*, *135*, 1661–1672.

Baldwin, M. P., & Thompson, D. W. J. (2009b). A critical comparison of stratosphere–troposphere coupling indices. *Quart. J. Roy. Meteor. Soc.*, *135*, 1661–1672.

Baldwin, M. P., Ayarzagüena, B., Birner, T., Butchart, N., Butler, A. H., Charlton-Perez, A. J., Domeisen, D. I. V., Garfinkel, C. I., Garny, H., Gerber, E. P., Hegglin, M. I., Langematz, U., & Pedatella, N. M. (2021). Sudden Stratospheric Warmings. *Reviews of Geophysics*, *59*(1).

Baldwin, M. P., & Holton, J. (1988). Climatology of the Stratospheric Polar Vortex and Planetary Wave Breaking. *Journal of the Atmospheric Sciences*, *45*(7), 1123–1142.

Bancalá, S., Krüger, K., & Giorgetta, M. (2012). The preconditioning of major sudden stratospheric warmings. *J. Geophys. Res.*

Barnston, A. G., & Livezey, R. E. (1987). Classification, seasonality and persistence of low-frequency atmospheric circulation patterns. *Monthly Weather Review*, *115*, 1083–1126.

Barriopedro, D., & Calvo, N. (2014). On the Relationship between ENSO, Stratospheric Sudden Warmings, and Blocking. *Journal of Climate*, *27*(12), 4704–4720.

Beerli, R., & Grams, C. M. (2019). Stratospheric modulation of the large-scale circulation in the Atlantic–European region and its implications for surface weather events. *Quarterly Journal of the Royal Meteorological Society*, *145*(725), 3732–3750.

Bell, C. J., Gray, L. J., Charlton-Perez, A. J., Joshi, M. M., & Scaife, A. A. (2009). Stratospheric communication of El Niño teleconnections to European winter. *Journal of Climate*, *22*, 4083–4096.

Bell, C. J., Gray, L. J., & Kettleborough, J. (2010). Changes in Northern Hemisphere stratospheric variability under increased CO2 concentrations. *Quarterly Journal of the Royal Meteorological Society*, n/a–n/a.

Birner, T., & Albers, J. R. (2017). Sudden Stratospheric Warmings and Anomalous Upward Wave Activity Flux. *SOLA*, *13A*(Special_Edition), 8–12.

Black, R. X., McDaniel, B. A., & Robinson, W. A. (2006). Stratosphere-troposphere coupling during spring onset. *Journal of Climate*, *19*, 4891–4901.

Blume, C., Matthes, K., Horenko, I., & Palmer, T. N. (2012). Diagnostic study of a wavenumber-2 stratospheric sudden warming in a transformed Eulerian-mean formalism. *J. Atmos. Sci.*, *38*, 1824–1840.

Brönnimann, S. (2007). Impact of El Niño-Southern Oscillation on European climate. *Reviews of Geophysics*, *45*, RG3003.

Butchart, N. (2014). The Brewer-Dobson Circulation. *Reviews of Geophysics*, 28.

Butchart, N., Cionni, I., Eyring, V., Shepherd, T. G., Waugh, D. W., Akiyoshi, H., Austin, J., Brühl, C., Chipperfield, M. P., Cordero, E., Dameris, M., Deckert, R., Dhomse, S., Frith, S. M., Garcia, R. R., Gettelman, A., Giorgetta, M. A., Kinnison, D. E., Li, F., ... Tian, W. (2010). Chemistry–Climate Model Simulations of Twenty-First Century Stratospheric Climate and Circulation Changes. *Journal of Climate*, *23*(20), 5349–5374.

Butchart, N., & Remsberg, E. (1986). The Area of the Stratospheric Polar Vortex as a Diagnostic for Tracer Transport on an Isentropic Surface. *Journal of the Atmospheric Sciences*, *43*(13), 1319–1339.

Butler, A. H., Polvani, L. M., & Deser, C. (2014). Separating the stratospheric and tropospheric pathways of El Niño-Southern Oscillation telecoonections. *Environmental Research Letters*, *9*, 024014.

Butler, A. H., Arribas, A., Athanassiadou, M., Baehr, J., Calvo, N., Charlton-Perez, A., & et al. (2016). The Climate-system Historical Forecast Project: Do stratosphere-resolving models make better seasonal climate predictions in boreal winter? *Quarterly Journal of the Royal Meteorological Society*, *23*, 1413–1427.

Butler, A. H., Charlton-Perez, A., Domeisen, D. I., Simpson, I. R., & Sjoberg, J. (2019). Predictability of Northern Hemisphere Final Stratospheric Warmings and Their Surface Impacts. *Geophysical Research Letters*, *46*(17-18), 10578–10588.

Butler, A. H., & Gerber, E. P. (2018). Optimizing the definition of a sudden stratospheric warming. *Journal of Climate*, *31*, 2337–2344.

Butler, A. H., Lawrence, Z. D., Lee, S. H., Lillo, S. P., & Long, C. S. (2020). Differences between the 2018 and 2019 stratospheric polar vortex split events. *Quarterly Journal of the Royal Meteorological Society*, *146*(732), 3503–3521.

Butler, A. H., & Polvani, L. M. (2011). El Niño, La Niña, and stratospheric sudden warmings: A reevaluation in light of the observational record: EL NIÑO, LA NIÑA, AND SSWS. *Geophysical Research Letters*, *38*(13).

Butler, A. H., Seidel, D. J., Hardiman, S. C., Butchart, N., Birner, T., & Match, A. (2015). Defining Sudden Stratospheric Warmings. *Bulletin of the American Meteorological Society*, *96*(11), 1913–1928.

Butler, A. H., Sjoberg, J. P., Seidel, D. J., & Rosenlof, K. H. (2017). A sudden stratospheric warming compendium. *Earth System Science Data*, 14.

Cagnazzo, C., & Manzini, E. (2009). Impact of the stratosphere on the winter tropospheric teleconnections between ENSO and the North Atlantic and European region. *Journal of Climate*, *22*, 1223–1238.

Calvo, N., Iza, M., Hurwitz, M. M., Manzini, E., Peña-Ortiz, C., Butler, A. H., Cagnazzo, C., Ineson, S., & Garfinkel, C. I. (2017). Northern Hemisphere stratospheric pathway of different El Niño flavors in stratosphere-resolving CMIP5 models. *Journal of Climate*, *30*, 4351–4371.

Calvo, N., Polvani, L. M., & Solomon, S. (2015). On the surface impact of Arctic stratospheric ozone extremes. *Environmental Research Letters*, *10*(9), 094003.

Cao, C., Chen, Y.-H., Rao, J., Liu, S.-M., Li, S.-Y., Ma, M.-H., & Wang, Y.-B. (2019). Statistical Characteristics of Major Sudden Stratospheric Warming Events in CESM1-WACCM: A Comparison with the JRA55 and NCEP/NCAR reanalyses. *Atmosphere*, *10*(519).

Castanheira, J. M., & Barriopedro, D. (2010). Dynamical connection between tropospheric blockings and stratospheric polar vortex: BLOCKS AND STRATOSPHERIC POLAR VORTEX. *Geophysical Research Letters*, *37*(13), n/a–n/a.

Charlton, A. J., & Polvani, L. M. (2007a). A new look at stratospheric sudden warmings, part I: Climatology and modeling benchmarks. *Journal of Climate*, *20*, 449–469. Corrected in

Corrigendum. (2011). *Journal of Climate*, *24*, 5951. https://doi.org/10.1175/JCLI-D-11-00348.1.

Charlton, A. J., & Polvani, L. M. (2011). Corrigendum. *Journal of Climate*, *24*, 5951.

Charlton, A. J., & Polvani, L. M. (2007b). A New Look at Stratospheric Sudden Warmings. Part II: Evaluation of Numerical Modeling Simulations. *Journal of Climate*, *20*(3), 470–488.

Charlton-Perez, A. J., Polvani, L. M., Austin, J., & Li, F. (2008). The frequency and dynamics of stratospheric sudden warmings in the 21st century. *Journal of Geophysical Research*, *113*(D16), D16116.

Charlton-Perez, A. J., Baldwin, M. P., Birner, T., Black, R. X., Butler, A. H., Calvo, N., Davis, N. A., Gerber, E. P., Gillett, N., Hardiman, S., Kim, J., Krüger, K., Lee, Y.-Y., Manzini, E., McDaniel, B. A., Polvani, L., Reichler, T., Shaw, T. A., Sigmond, M., … Watanabe, S. (2013). On the lack of stratospheric dynamical variability in low-top versions of the CMIP5 models: Stratosphere in CMIP5 Models. *Journal of Geophysical Research: Atmospheres*, *118*(6), 2494–2505.

Charlton-Perez, A. J., Huang, W. T. K., & Lee, S. H. (2021). Impact of sudden stratospheric warmings on United Kingdom mortality. *Atmospheric Science Letters*, *22*(2).

Charney, J. G., & Drazin, P. G. (1961). Propagation of planetary-scale disturbances from the lower into the upper atmosphere. *Journal of Geophysical Research*, *66*(1), 83–109.

Christiansen, B. (2001). Downward propagation of zonal mean zonal wind anomalies from the stratosphere to the troposphere: Model and reanalysis. *J. Geophys. Res.*, *106*, 27 307–27 322.

Christiansen, B. (2005). Downward propagation and statistical forecast of the near-surface weather: Downward Propagation in Weather Forecast. *Journal of Geophysical Research: Atmospheres*, *110*(D14).

Cohen, J., Barlow, M., Kushner, P. J., & Saito, K. (2007). Stratosphere–troposphere coupling and links with eurasian land surface variability. *Journal of Climate*, *20*(21), 5335–5343.

Cohen, J., Furtado, J. C., Jones, J., Barlow, M., Whittleston, D., & Entekhabi, D. (2014). Linking siberian snow cover to precursors of stratospheric variability. *Journal of Climate*, *27*(14), 5422–5432.

Coughlin, K., & Gray, L. J. (2009). A continuum of sudden stratospheric warmings. *J. Atmos. Sci.*, *66*, 531–540.

Darling, E. M. (1953). Winds at 100 Mb and 50 Mb Over the United States in 1952. *Bulletin of the American Meteorological Society*, *34*(10), 458–461.

De La Cámara, A., Abalos, M., Hitchcock, P., Calvo, N., & Garcia, R. R. (2018). Response of Arctic ozone to sudden stratospheric warmings. *Atmospheric Chemistry and Physics*, *18*(22), 16499–16513.

de la Cámara, A., Birner, T., & Albers, J. R. (2019). Are sudden stratospheric warmings preceded by anomalous tropospheric wave activity? *Journal of Climate*, *32*(21), 7173–7189.

de la Torre, L., Garcia, R. R., Barriopedro, D., & Chandran, A. (2012). Climatology and characteristics of stratospheric sudden warmings in the Whole Atmosphere Community Climate Model. *Journal of Geophysical Research: Atmospheres*, *117*, D04110.

Deser, C., Simpson, I. R., Phillips, A. S., & McKinnon, K. A. (2018). How Well Do We Know ENSO's Climate Impacts over North America, and How Do We Evaluate Models Accordingly? *Journal of Climate*, *31*(13), 4991–5014.

Deser, C., Simpson, I. S., McKinnon, K. A., & Phillips, A. S. (2017). The Northern Hemisphere extratropical circulation response to ENSO: How well do we know it and how do we evaluate models accordingly? *Journal of Climate*, *30*, 5059–5082.

Dimdore-Miles, O., Gray, L., & Osprey, S. (2020). *Origins of Multi-decadal Variability in Sudden StratosphericWarmings* (preprint). Atmospheric teleconnections incl. stratosphere–troposphere coupling.

Dobrynin, M., Domeisen, D. I. V., Müller, W. A., Bell, L., Brune, S., Bunzel, F., Düsterhus, A., Fröhlich, K., Pohlmann, H., & Baehr, J. (2018). Improved teleconnection-based dynamical seasonal predictions of boreal winter. *Geophysical Research Letters*, *45*(8), 3605–3614.

Domeisen, D. I., Butler, A. H., Fröhlich, K., Bittner, M., Müller, W. A., & Baehr, J. (2015). Seasonal predictability over Europe arising from El Niño and stratospheric variability in the MPI-ESM seasonal prediction system. *Journal of Climate*, *28*, 256–271.

Domeisen, D. I. V., & Butler, A. H. (2020). Stratospheric drivers of extreme events at the Earth's surface. *Communications Earth & Environment*, *1*(1), 59.

Domeisen, D. I. V., Butler, A. H., Charlton-Perez, A. J., Ayarzagüena, B., Baldwin, M. P., Dunn-Sigouin, E., Furtado, J. C., Garfinkel, C. I., Hitchcock, P., Karpechko, A. Y., Kim, H., Knight, J., Lang, A. L., Lim, E.-P., Marshall, A., Roff, G., Schwartz, C., Simpson, I. R., Son, S.-W., & Taguchi, M. (2020a). The Role of the Stratosphere in Subseasonal to Seasonal Prediction: 2. Predictability Arising From Stratosphere-Troposphere Coupling. *Journal of Geophysical Research: Atmospheres*, *125*(2).

Domeisen, D. I. V., Garfinkel, C. I., & Butler, A. H. (2019a). The teleconnection of el niño southern oscillation to the stratosphere. *Reviews of Geophysics*, *57*.

Domeisen, D. I. V., Grams, C. M., & Papritz, L. (2020). The role of North Atlantic–European weather regimes in the surface impact of sudden stratospheric warming events. *Weather and Climate Dynamics*, *1*(2), 373–388.

Domeisen, D. I. (2019). Estimating the Frequency of Sudden Stratospheric Warming Events From Surface Observations of the North Atlantic Oscillation. *Journal of Geophysical Research: Atmospheres*, *124*(6), 3180–3194.

Domeisen, D. I., Butler, A. H., Charlton-Perez, A. J., Ayarzagüena, B., Baldwin, M. P., Dunn-Sigouin, E., Furtado, J. C., Garfinkel, C. I., Hitchcock, P., Karpechko, A. Y., Kim, H., Knight, J., Lang, A. L., Lim, E.-P., Marshall, A., Roff, G., Schwartz, C., Simpson, I. R., Son, S.-W., & Taguchi, M. (2020b). The Role of the Stratosphere in Subseasonal to Seasonal Prediction: 1. Predictability of the Stratosphere. *Journal of Geophysical Research: Atmospheres*, *125*(2).

Domeisen, D. I., Garfinkel, C. I., & Butler, A. H. (2019b). The Teleconnection of El Niño Southern Oscillation to the Stratosphere. *Reviews of Geophysics*, *57*(1), 5–47.

Drouard, M., Rivière, G., & Arbogast, P. (2013). The North Atlantic Oscillation response to large-scale atmospheric anomalies in the northeastern Pacific. *J. Atmos. Sci.*, *70*, 2854–2874.

EBDON, R. A. (1975). The quasi-biennial oscillation and its association with tropospheric circulation patterns. *Meteorol. Mag.*, *104*(1239), 282–297.

Esler, J. G., & Matthewman, N. J. (2011). Stratospheric Sudden Warmings as Self-Tuning Resonances. Part II: Vortex Displacement Events. *Journal of the Atmospheric Sciences*, *68*(11), 2505–2523.

Esler, J. G., Polvani, L. M., & Scott, R. K. (2006). The Antarctic stratospheric sudden warming of 2002: A self-tuned resonance? *Geophysical Research Letters*, *33*(12), L12804.

Fujiwara, M., Wright, J. S., Manney, G. L., Gray, L. J., Anstey, J., Birner, T., Davis, S., Gerber, E. P., Harvey, V. L., Hegglin, M. I., Homeyer, C. R., Knox, J. A., Krüger, K., Lambert, A., Long, C. S., Martineau, P., Molod, A., Monge-Sanz, B. M., Santee, M. L., … Zou, C.-Z. (2017). Introduction to the SPARC Reanalysis Intercomparison Project (S-RIP) and overview of the reanalysis systems. *Atmospheric Chemistry and Physics*, *17*(2), 1417–1452.

Furtado, J. C., Cohen, J. L., Butler, A. H., Riddle, E. E., & Kumar, A. (2015). Eurasian snow cover variability and links to winter climate in the CMIP5 models. *Climate Dynamics*, *45*(9), 2591–2605.

García-Herrera, R., Calvo, N., Garcia, R. R., & Giorgetta, M. A. (2006). Propagation of enso temperature signals into the middle atmosphere: A comparison of two general circulation models and era-40 reanalysis data. *Journal of Geophysical Research: Atmospheres*, *111*(D6).

García-Serrano, J., Rodríguez-Fonseca, B., Bladé, I., Zurita-Gotor, P., & de la Cámara, A. (2011). Rotational atmospheric circulation during north atlantic-european winter: The influence of enso. *Climate Dynamics*, *37*, 1727–1743.

Garfinkel, C. I., & Hartmann, D. L. (2008). Different enso teleconnections and their effects on the stratospheric polar vortex. *Journal of Geophysical Research: Atmospheres*, *113*(D18).

Garfinkel, C. I., Benedict, J. J., & Maloney, E. D. (2014). Impact of the MJO on the boreal winter extratropical circulation. *Geophysical Research Letters*, *41*(16), 6055–6062.

Garfinkel, C. I., Butler, A. H., Waugh, D., Hurwitz, M., & Polvani, L. M. (2012). Why might stratospheric sudden warmings occur with similar frequency in El Niño and La Niña winters? *Journal of Geophysical Research: Atmospheres*, *117*, D19106.

Garfinkel, C. I., & Hartmann, D. L. (2007). Effects of the El Niño-Southern Oscillation and the quasi-biennial oscillation on polar temperatures in the stratosphere. *Journal of Geophysical Research: Atmospheres*, *112*, D19112.

Garfinkel, C. I., Hartmann, D. L., & Sassi, F. (2010). Tropical precursors of anomalous Northern Hemispheric polar vortices. *Journal of Climate*, *23*, 3282–3299.

Garfinkel, C. I., Schwartz, C., Butler, A. H., Domeisen, D. I. V., Son, S.-W., & White, I. P. (2019). Weakening of the Teleconnection From El Niño–Southern Oscillation to the Arctic Stratosphere Over the Past Few Decades: What Can Be Learned From Subseasonal Forecast Models? *Journal of Geophysical Research: Atmospheres*, *124*(14), 7683–7696.

Garfinkel, C. I., Schwartz, C., White, I. P., & Rao, J. (2020). Predictability of the early winter Arctic oscillation from autumn Eurasian snowcover in subseasonal forecast models. *Climate Dynamics*, *55*(3), 961–974.

Garfinkel, C. I., Shaw, T. A., Hartmann, D. L., & Waugh, D. W. (2012). Does the Holton–Tan mechanism explain how the Quasi-Biennial Oscillation modulates the Arctic polar vortex? *Journal of the Atmospheric Sciences*, *69*(5), 1713–1733.

Garfinkel, C. I., Weinberger, I., White, I. P., Oman, L. D., Aquila, V., & Lim, Y.-K. (2018). The salience of nonlinearities in the boreal winter response to ENSO: North Pacific and North America. *Climate Dynamics*.

Geng, X., Zhang, W., Stuecker, M. F., & Jin, F.-F. (2017). Strong sub-seasonal wintertime cooling over East Asia and Northern Europe associated with super El Niño events. *Scientific Reports*, *7*(3770).

Gerber, E. P. (2010). Stratosphere-troposphere coupling and annular mode variability in chemistry-climate models. *J. Geophys. Res.*, *115*.

Gerber, E. P., & Martineau, P. (2018). Quantifying the variability of annular modes: Reanalysis uncertainty vs. sampling uncertainty. *Atmospheric Chemistry and Physics*, *18*, 17099–17117.

Gerber, E. P., Orbe, C., & Polvani, L. M. (2009). Stratospheric influence on the tropospheric circulation revealed by idealized ensemble forecasts. *Geophysical Research Letters*, *36*(24), L24801.

Gerber, E. P., Martineau, P., Ayarzagüena, B., Barriopedro, D., Bracegirdle, J., Butler, A. H., Calvo, N., Hardiman, S. C., Hitchcock, P., Iza, M., Langematz, U., Lu, H., Marshall, G., Orr, A., Palmeiro, F. M., Son, S.-W., & Taguchi, M. (2021). Extratropical Stratosphere–Troposphere Coupling. *Stratosphere-troposphere processes and their role in climate (SPARC) reanalysis intercomparison project (S-RIP)*. SPARC.

Gettelman, A., Mills, M. J., Kinnison, D. E., Garcia, R. R., Smith, A. K., Marsh, D. R., Tilmes, S., Vitt, F., Bardeen, C. G., McInerney, J., Liu, H.-L., Solomon, S. C., Polvani, L. M., Emmons, L. K., Lamarque, J.-F., Richter, J. H., Glanville, A. S., Bacmeister, J. T., Phillips, A. S., ... Randel, W. J. (2019). The Whole Atmosphere Community Climate Model Version 6 (WACCM6). *Journal of Geophysical Research Atmospheres*.

Gray, L. J., Crooks, S., Pascoe, C., Sparrow, S., & Palmer, M. (2004). Solar and qbo influences on the timing of stratospheric sudden warmings. *Journal of the Atmospheric Sciences*, *61*(23), 2777–2796.

Green, M. R., & Furtado, J. C. (2019). Evaluating the joint influence of the madden-julian oscillation and the stratospheric polar vortex on weather patterns in the northern hemisphere. *Journal of Geophysical Research: Atmospheres*, *124*(22), 11693–11709.

Haase, S., & Matthes, K. (2019). The importance of interactive chemistry for stratosphere–troposphere coupling. *Atmospheric Chemistry and Physics*, *19*(5), 3417–3432.

Hannachi, A., Mitchell, D., Gray, L., & Charlton-Perez, A. (2011). On the use of geometric moments to examine the continuum of sudden stratospheric warmings. *J. Atmos. Sci.*, *68*, 657–674.

Hardiman, S. C., Dunstone, N. J., Scaife, A. A., Smith, D. M., Ineson, S., Lim, J., & Fereday, D. (2019). The impact of strong el niño and la niña events on the north atlantic. *Geophysical Review Letters*, *46*, 2874–2883.

Hardiman, S. C., Butchart, N., Charlton-Perez, A. J., Shaw, T. A., Akiyoshi, H., Baumgaertner, A., Bekki, S., Braesicke, P., Chipperfield, M., Dameris, M., Garcia, R. R., Michou, M., Pawson, S., Rozanov, E., & Shibata, K. (2011). Improved predictability of the troposphere using stratospheric final warmings. *Journal of Geophysical Research*, *116*(D18), D18113.

Henderson, G. R., Peings, Y., Furtado, J. C., & Kushner, P. J. (2018). Snow–atmosphere coupling in the Northern Hemisphere. *Nature Climate Change*, *8*(11), 954–963.

Hitchcock, P., Shepherd, T. G., & Manney, G. L. (13). Statistical characterization of Arctic polar-night jet oscillation events. *J. Climate*, *26*, 2096–2116.

Hitchcock, P., & Simpson, I. R. (2014). The downward influence of stratospheric sudden warmings. *Journal of the Atmospheric Sciences*, *71*, 3856–3876.

Hitchcock, P., & Shepherd, T. G. (2013). Zonal-Mean Dynamics of Extended Recoveries from Stratospheric Sudden Warmings. *Journal of the Atmospheric Sciences*, *70*(2), 688–707.

Holton, J. (1980). The dynamics of sudden stratospheric warmings. *Annual Review of Earth and Planetary Sciences*, *8*(1), 169–190.

Holton, J. R., & Tan, H.-C. (1980). The influence of the equatorial quasi-biennial oscillation on the global circulation at 50 mb. *Journal of Atmospheric Sciences*, *37*(10), 2200–2208.

Honda, M., & Nakamura, H. (2001). Interannual seesaw between the aleutian and icelandic lows. part ii: Its significance in the interannual variability over the wintertime northern hemisphere. *Journal of Climate*, *14*(24), 4512–4529.

Horel, J. D., & Wallace, J. M. (1981). Planetary-scale atmospheric phenomena associated with the southern oscillation. *Monthly Weather Review*, *109*, 813–829.

Hu, J., Ren, R., & Xu, H. (2014). Occurrence of Winter Stratospheric Sudden Warming Events and the Seasonal Timing of Spring Stratospheric Final Warming. *Journal of the Atmospheric Sciences*, *71*(7), 2319–2334.

Huang, B., Thorne, P. W., Banzon, V. F., Boyer, T., Chepurin, G., Lawrimore, J. H., Menne, M. J., Smith, T. M., Vose, R. S., & Zhang, H.-M. (2017). Extended Reconstructed Sea Surface Temperature, Version 5: Updates, validations, and intercomparisons. *Journal of Climate*, *30*, 8179–8205.

Huntingford, C., Marsh, T., Scaife, A. A., Kendon, E. J., Hannaford, J., Kay, A. L., Lockwood, M., Prudhomme, C., Reynard, N. S., Parry, S., Lowe, J. A., Screen, J. A., Ward, H. C., Roberts, M., Stott, P. A., Bell, V. A., Bailey, M., Jenkins, A., Legg, T., ... Allen, M. R. (2014). Potential influences on the United Kingdom's floods of winter 2013/14. *Nature Climate Change*, *4*(9), 769–777.

Hurrell, J. W. (1995). Decadal trends in the North Atlantic Oscillation: Regional temperatures and precipitation. *Science*, *269*(5224), 676–679.

Ineson, S., & Scaife, A. (2009). The role of the stratosphere in the European climate response to El Niño. *Nature Geoscience*, *2*, 32–36.

Ivy, D. J., Solomon, S., Calvo, N., & Thompson, D. W. J. (2017). Observed connections of Arctic stratospheric ozone extremes to Northern Hemisphere surface climate. *Environmental Research Letters*, *12*(2), 024004.

Japan Meteorological Agency, Japan. (2013). *JRA-55: Japanese 55-year Reanalysis, Daily 3-Hourly and 6-Hourly Data*. Research Data Archive at the National Center for Atmospheric Research, Computational; Information Systems Laboratory.

Jiménez-Esteve, B., & Domeisen, D. I. V. (2018). The tropospheric pathway of the ENSO-North Atlantic teleconnection. *Journal of Climate*, *31*, 4563–4584.

Jiménez-Esteve, B., & Domeisen, D. I. V. (2020). Nonlinearity in the tropospheric pathway of ENSO to the North Atlantic. *Weather and Climate Dynamics*, *1*(1), 225–245.

Kang, W., & Tziperman, E. (2017). More Frequent Sudden Stratospheric Warming Events due to Enhanced MJO Forcing Expected in a Warmer Climate. *Journal of Climate*, *30*(21), 8727–8743.

Kang, W., & Tziperman, E. (2018). The Role of Zonal Asymmetry in the Enhancement and Suppression of Sudden Stratospheric Warming Variability by the Madden–Julian Oscillation. *Journal of Climate*, *31*(6), 2399–2415.

Karpechko, A. Y., Perlwitz, J., & Manzini, E. (2014). A model study of the tropospheric impacts of the Arctic ozone depletion of 2011. *Journal of Geophysical Research*, *119*, 7999–8014.

Karpechko, A. Y., Hitchkock, P., Peters, D. H. W., & Schneider, A. (2017). Predictability of downward propagation of major sudden stratospheric warmings. *Quarterly Journal of the Royal Meteorological Society*, *143*, 1459–1470.

Karpechko, A. Y., & Manzini, E. (2012). Stratospheric influence on tropospheric climate change in the Northern Hemisphere: Stratospheric Impact on Climate Change. *Journal of Geophysical Research: Atmospheres*, *117*(D5), n/a–n/a.

Karpechko, A. Y. (2018). Predictability of sudden stratospheric warmings in the ecmwf extended-range forecast system. *Monthly Weather Review*, *146*(4), 1063–1075.

Kay, J., Deser, C., Phillips, A., Mai, A., Hannay, C., Strand, G., & et al. (2015). The Community Earth System Model (CESM) Large Ensemble Project. *Bulletin of the American Meteorological Society*, *96*(8), 1333–1349.

Keeble, J., Hassler, B., Banerjee, A., Checa-Garcia, R., Chiodo, G., Davis, S., Eyring, V., Griffiths, P. T., Morgenstern, O., Nowack, P., Zeng, G., Zhang, J., Bodeker, G., Cugnet, D., Danabasoglu, G., Deushi, M., Horowitz, L. W., Li, L., Michou, M., … Wu, T. (2020). Evaluating stratospheric ozone and water vaporchanges in CMIP6 models from 1850-2100. *Atmos. Chem. Phys. Discuss*, *in review*.

Kelleher, M. E., Ayarzagüena, B., & Screen, J. A. (2020). Interseasonal Connections between the Timing of the Stratospheric Final Warming and Arctic Sea Ice. *Journal of Climate*, *33*(8), 3079–3092.

Kidston, J., Scaife, A. A., Hardiman, S. C., Mitchell, D. M., Butchart, N., Baldwin, M. P., & Gray, L. J. (2015). Stratospheric influence on tropospheric jet streams, storm tracks and surface weather. *Nature Geoscience*, *8*(6), 433–440.

Kiesewetter, G., Sinnhuber, B.-M., Vountas, M., Weber, M., & Burrows, J. P. (2010). A long-term stratospheric ozone data set from assimilation of satellite observations: High-latitude ozone anomalies. *Journal of Geophysical Research*, *115*(D10307).

Kim, J., Son, S.-W., Gerber, E. P., & Park, H.-S. (2017). Defining Sudden Stratospheric Warming in Climate Models: Accounting for Biases in Model Climatologies. *Journal of Climate*, *30*(14), 5529–5546.

King, A. D., Butler, A. H., Jucker, M., Earl, N. O., & Rudeva, I. (2019). Observed Relationships Between Sudden Stratospheric Warmings and European Climate Extremes. *Journal of Geophysical Research*, 19.

Kinnison, D. E., Brasseur, G. P., Walters, S., Garcia, R. R., Marsh, D. R., Sassi, F., Harvey, V. L., Randall, C. E., Emmons, L., Lamarque, J. F., Hess, P., Orlando, J. J., Tie, X. X., Randel, W., Pan, L. L., Gettelman, A., Granier, C., Diehl, T., Niemeier, U., & Simmons, A. J. (2007). Sensitivity of chemical tracers to meteorological parameters in the MOZART-3 chemical transport model. *Journal of Geophysical Research Atmospheres*, *112*, D20302.

Knight, J., Scaife, A., Bett, P. E., Collier, T., Dunstone, N., Gordon, M., Hardiman, S., Hermanson, L., Ineson, S., Kay, G., McLean, P., Pilling, C., Smith, D., Stringer, N., Thornton, H., & Walker, B. (2021). Predictability of European Winters 2017/2018 and 2018/2019: Contrasting influences from the Tropics and stratosphere. *Atmospheric Science Letters*, *22*(1).

Kobayashi, S., Ota, Y., Harada, Y., Ebita, A., Moriya, M., Onoda, H., Onogi, K., Kamahori, H., Kobayashi, C., Endo, H., Miyaoka, K., & Takahashi, K. (2015). The JRA-55 Reanalysis: General Specifications and Basic Characteristics. *Journal of the Meteorological Society of Japan. Ser. II*, *93*(1), 5–48.

Kodera, K., Mukougawa, H., Maury, P., Ueda, M., & Claud, C. (2016). Absorbing and reflecting sudden stratospheric warming events and their relationship with tropospheric circulation: Absorbing and Reflecting Sudden Warmings. *Journal of Geophysical Research: Atmospheres*, *121*(1), 80–94.

Kolstad, E. W., Breiteig, T., & Scaife, A. A. (2010). The association between stratospheric weak polar vortex events and cold air outbreaks in the Northern Hemisphere. *Quarterly Journal of the Royal Meteorological Society*, 8.

Kolstad, E. W., Wulff, C. O., Domeisen, D. I. V., & Woollings, T. (2020). Tracing North Atlantic Oscillation Forecast Errors to Stratospheric Origins. *Journal of Climate*, *33*(21), 9145–9157.

Kuroda, Y., Kodera, K., Andrews, D. G., Holton, J. R., & Leovy, C. B. (2004). Role of the Polar-night Jet Oscillation on the formation of the Arctic Oscillation in the Northern Hemisphere winter [Publisher: Academic Press]. *J. Geophys. Res.*, *109*, D11112.

Labitzke, K. (1981). Stratospheric-mesospheric midwinter disturbances: A summary of observed characteristics. *J. Geophys. Res.*, *86*, 9665–9678.

Labitzke, K., & Naujokat, B. (2000). *The lower arctic stratosphere in winter since 1952* (15). World Climate Research Programme SPARC Office, Switzerland.

Labitzke, K., & van Loon, H. (1992). On the association between the QBO and the extratropical stratosphere. *Journal of Atmospheric and Terrestrial Physics*, *54*(11), 1453–1463.

Labitzke, K. (1977). Interannual Variability of the Winter Stratosphere in the Northern Hemisphere. *Monthly Weather Review*, *105*, 762–770.

Labitzke, K. (1987). Sunspots, the QBO, and the stratospheric temperature in the north polar region. *Geophysical Research Letters*, *14*(5), 535–537.

Lawrence, Z. D., Perlwitz, J., Butler, A. H., Manney, G. L., Newman, P. A., Lee, S. H., & Nash, E. R. (2020). The Remarkably Strong Arctic Stratospheric Polar Vortex of Winter 2020: Links to Record-Breaking Arctic Oscillation and Ozone Loss. *Journal of Geophysical Research: Atmospheres*, *125*(22).

Lee, R. W., Woolnough, S. J., Charlton-Perez, A. J., & Vitart, F. (2019). ENSO Modulation of MJO Teleconnections to the North Atlantic and Europe. *Geophysical Research Letters*, *46*(22), 13535–13545.

Lehtonen, I., & Karpechko, A. Y. (2016). Observed and modeled tropospheric cold anomalies associated with sudden stratospheric warmings. *Journal of Geophysical Research*, 20.

Li, F., Austin, J., & Wilson, J. (2008). The strength of the brewer–dobson circulation in a changing climate: Coupled chemistry–climate model simulations. *Journal of Climate*, *21*(1), 40–57.

Li, Y., & Lau, N.-C. (2012). Impact of ENSO on the atmospheric variability over the North Atlantic in late winter–role of transient eddies. *Journal of Climate*, *25*, 320–342.

Limpasuvan, V., Hartmann, D. L., Thompson, D. W. J., Jeev, K., & Yung, Y. L. (2005). Stratosphere-troposphere evolution during polar vortex intensification. *Journal of Geophysical Research Atmospheres*, *110*, D24101.

Limpasuvan, V., Thompson, D. W. J., & Hartmann, D. L. (2004). The life cycle of the Northern Hemisphere sudden stratospheric warmings. *Journal of Climate*, *17*, 2584–2596.

Lin, P., & Fu, Q. (2013). Changes in various branches of the Brewer–Dobson circulation from an ensemble of chemistry climate models. *Journal of Geophysical Research: Atmospheres*, *118*(1), 73–84.

Lin, P., Paynter, D., Polvani, L., Correa, G. J. P., Ming, Y., & Ramaswamy, V. (2017). Dependence of model-simulated response to ozone depletion on stratospheric polar vortex climatology: Response To Ozone Depends On Climatology. *Geophysical Research Letters*, *44*(12), 6391–6398.

Loon, H. V., & Rogers, J. C. (1978). The seesaw in winter temperatures between Greenland and Northern Europe. Part i: General description. *Monthly Weather Review*, *106*, 296–310.

Lu, H., Hitchman, M. H., Gray, L. J., Anstey, J. A., & Osprey, S. M. (2020). On the role of Rossby wave breaking in the quasi-biennial modulation of the stratospheric polar vortex during boreal winter. *Quarterly Journal of the Royal Meteorological Society*, *146*(729), 1939–1959.

Mahlman, J. D., Umscheid, L. J., & Pinto, J. P. (1994). Transport, radiative, and dynamical effects of the Antarctic ozone hole: A GFDL "SKYHI" model experiment. *Journal of Atmospheric Sciences*, *51*(4), 489–508.

Manney, G. L., & Lawrence, Z. D. (2016). The major stratospheric final warming in 2016: Dispersal of vortex air and termination of Arctic chemical ozone loss. *Atmospheric Chemistry and Physics*, *16*(23), 15371–15396.

Manzini, E., Giorgetta, M. A., Esch, M., Kornblueh, L., & Roeckner, E. (2006). The influence of sea surface temperatures on the northern winter stratosphere: Ensemble simulations with the maecham5 model. *Journal of Climate*, *19*(16), 3863–3881.

Manzini, E., Steil, B., Brühl, C., Giorgetta, M. A., & Krüger, K. (2003). A new interactive chemistry-climate model: 2. Sensitivity of the middle atmosphere to ozone depletion and increase in greenhouse gases and implications for recent stratospheric cooling. *Journal of Geophysical Research*, *108*(D14, 4229).

Manzini, E. (2009). ENSO and the stratosphere. *Nature Geoscience*, *2*(11), 749–750.

Marsh, D. R., Mills, M. J., Kinnison, D. E., Lamarque, J.-F., Calvo, N., & Polvani, L. M. (2013). Climate Change from 1850 to 2005 Simulated in CESM1(WACCM). *Journal of Climate*, *26*(19), 7372–7391.

Martineau, P., Son, S.-W., Baldwin, M. P., Thompson, D. W. J., Christiansen, B., Matthewman, N. J., Esler, J. G., Charlton-Perez, A. J., Polvani, L. M., Mitchell, D. M., Charlton-Perez,

A. J., Gray, L. J., Hannachi, A., Mitchell, D., Gray, L., Charlton-Perez, A., Coughlin, K., Gray, L. J., Labitzke, K., ... Albers, J. R. (2013). Stratospheric-mesospheric midwinter disturbances: A summary of observed characteristics [Publisher: Amer. Meteor. Soc.]. *J. Geophys. Res. Atmos.*, *86*, 9665–9678.

Martius, O., Polvani, L. M., & Davies, H. C. (2009). Blocking precursors to stratospheric sudden warming events. *Geophysical Research Letters*, *36*(14).

Matsuno, T. (1971). A dynamical model of the stratospheric sudden warming. *Journal of the Atmospheric Sciences*, *28*(8), 1479–1494.

Matthewman, N. J., Esler, J. G., Charlton-Perez, A. J., & Polvani, L. M. (2009). A new look at stratospheric sudden warmings. part iii: Polar vortex evolution and vertical structure. *J. Climate*, *22*, 1566–1585.

Matthewman, N. J., & Esler, J. G. (2011). Stratospheric Sudden Warmings as Self-Tuning Resonances. Part I: Vortex Splitting Events. *Journal of the Atmospheric Sciences*, *68*(11), 2481–2504.

Maycock, A. C., & Hitchcock, P. (2015). Do split and displacement sudden stratospheric warmings have different annular mode signatures?: Annular Mode Signatures of SSWs. *Geophysical Research Letters*, *42*(24), 10, 943–10, 951.

McInturff, R. M. (1978). *Stratospheric warmings: Synoptic, dynamic and general-circulation aspects* (tech. rep. NASA-RP-1017).

McIntyre, M. E., & Palmer, T. N. (1983). Breaking planetary waves in the stratosphere. *Nature*, *305*(5935), 593–600.

McIntyre, M., & Palmer, T. (1984). The 'surf zone' in the stratosphere. *Journal of Atmospheric and Terrestrial Physics*, *46*(9), 825–849.

McIntyre, M. E. (1982). How well do we understand the dynamics of stratospheric warmings? *Journal of the Meteorological Society of Japan. Ser. II*, *60*(1), 37–65.

McLandress, C., Jonsson, A. I., Plummer, D. A., Reader, M. C., Scinocca, J. F., & Shepherd, T. G. (2010). Separating the dynamical effects of climate change and ozone depletion. part i: Southern hemisphere stratosphere.

McLandress, C., & Shepherd, T. G. (2009). Impact of Climate Change on Stratospheric Sudden Warmings as Simulated by the Canadian Middle Atmosphere Model. *Journal of Climate*, *22*(20), 5449–5463.

Mezzina, B., García-Serrano, J., Bladé, I., Palmeiro, F. M., Batté, L., Ardilouze, C., Benassi, M., & Gualdi, S. (2020). Multi-model assessment of the late-winter extra-tropical response to El Niño and La Niña. *Climate Dynamics*.

Mitchell, D. M., Charlton-Perez, A. J., & Gray, L. J. (2011). Characterizing the variability and extremes of the stratospheric polar vortices using 2d moment analysis. *J. Atmos. Sci.*, *68*, 1194–1213.

Mitchell, D. M., Charlton-Perez, A. J., Gray, L. J., Akiyoshi, H., Butchart, N., Hardiman, S. C., Morgenstern, O., Nakamura, T., Rozanov, E., Shibata, K., Smale, D., & Yamashita, Y. (2012). The nature of Arctic polar vortices in chemistry-climate models: Polar Vortices in Chemistry-Climate Models. *Quarterly Journal of the Royal Meteorological Society*, *138*(668), 1681–1691.

Mitchell, D. M., Misios, S., Gray, L. J., Tourpali, K., Matthes, K., Hood, L., Schmidt, H., Chiodo, G., Thiéblemont, R., Rozanov, E., Shindell, D., & Krivolutsky, A. (2015). Solar signals in cmip-5 simulations: The stratospheric pathway. *Quarterly Journal of the Royal Meteorological Society*, *141*(691), 2390–2403.

Mitchell, D. M., Gray, L. J., Anstey, J., Baldwin, M. P., & Charlton-Perez, A. J. (2013). The Influence of Stratospheric Vortex Displacements and Splits on Surface Climate. *Journal of Climate*, *26*(8), 2668–2682.

Mitchell, D. M., Osprey, S. M., Gray, L. J., Butchart, N., Hardiman, S. C., Charlton-Perez, A. J., & Watson, P. (2012). The Effect of Climate Change on the Variability of the Northern Hemisphere Stratospheric Polar Vortex. *Journal of the Atmospheric Sciences*, *69*(8), 2608–2618.

Naito, Y., Taguchi, M., & Yoden, S. (2003). A Parameter Sweep Experiment on the Effects of the Equatorial QBO on Stratospheric Sudden Warming Events. *Journal of the Atmospheric Sciences*, *60*, 16.

Nakagawa, K. I., & Yamazaki, K. (2006). What kind of stratospheric sudden warming propagates to the troposphere? *Geophysical Research Letters*, *33*(4), L04801.

Neely, R. R., Marsh, D. R., Smith, K. L., Davis, S. M., & Polvani, L. M. (2014). Biases in southern hemisphere climate trends induced by coarsely specifying the temporal resolution of stratospheric ozone. *Geophysical Research Letters*, *41*(23), 8602–8610.

Newman, P. A., Nash, E. R., & Rosenfield, J. E. (2001). What controls the temperature of the Arctic stratosphere during the spring? *Journal of Geophysical Research*, *106*(D17), 19999–20010.

Nie, Y., Scaife, A. A., Ren, H.-L., Comer, R. E., Andrews, M. B., Davis, P., & Martin, N. (2019). Stratospheric initial conditions provide seasonal predictability of the north atlantic and arctic oscillations. *Environmental Research Letters*, *14*(3), 034006.

Oehrlein, J., Chiodo, G., & Polvani, L. M. (2019). Separating and quantifying the distinct impacts of El Niño and sudden stratospheric warmings on North Atlantic and Eurasian wintertime climate. *Atmospheric Science Letters*, *20*(7).

Oehrlein, J., Chiodo, G., & Polvani, L. M. (2020). The effect of interactive ozone chemistry on weak and strong stratospheric polar vortex events. *Atmospheric Chemistry and Physics*, *20*(17), 10531–10544.

O'Neill, A., & Taylor, B. F. (1979). A study of the major stratospheric warming of 1976/77. *Quarterly Journal of the Royal Meteorological Society*, *105*(443), 71–92.

O'Reilly, C. H., Weisheimer, A., Woollings, T., Gray, L. J., & MacLeod, D. (2019). The importance of stratospheric initial conditions for winter north atlantic oscillation predictability and implications for the signal-to-noise paradox. *Quarterly Journal of the Royal Meteorological Society*, *145*(718), 131–146.

Palmeiro, F. M., Barriopedro, D., García-Herrera, R., & Calvo, N. (2015). Comparing Sudden Stratospheric Warming Definitions in Reanalysis Data*. *Journal of Climate*, *28*(17), 6823–6840.

Palmer, T. N. (1981). Diagnostic study of a wavenumber-2 stratospheric sudden warming in a transformed Eulerian-mean formalism. *J. Atmos. Sci.*, *38*.

Peings, Y. (2019). Ural blocking as a driver of early-winter stratospheric warmings. *Geophysical Research Letters*, *46*(10), 5460–5468.

Plumb, R. A. (1981). Instability of the distorted polar night vortex: A theory of stratospheric warmings. *Journal of Atmospheric Sciences*, *38*(11), 2514–2531.

Polvani, L. M., Sun, L., Butler, A. H., Richter, J. H., & Deser, C. (2017). Distinguishing stratospheric sudden warmings from ENSO as key drivers of wintertime climate variability over the North Atlantic and Eurasia. *Journal of Climate*, *30*, 1959–1969.

Polvani, L. M., & Waugh, D. W. (2004). Upward wave activity flux as a precursor to extreme stratospheric events and subsequent anomalous surface weather regimes. *Journal of Climate*, *17*, 3548–3554.

Previdi, M., & Polvani, L. M. (2014). Climate system response to stratospheric ozone depletion and recovery. *Quarterly Journal of the Royal Meteorological Society*, *140*, 2401–2419.

Quiroz, R. S. (1975). The Stratospheric Evolution of Sudden Warmings in 1969–74 Determined from Measured infrared Radiation Fields. *Journal of the Atmospheric Sciences*, *32*, 211–224.

Quiroz, R. S. (1977). The tropospheric-stratospheric polar vortex breakdown of January 1977. *Geophysical Research Letters*, *4*(4), 151–154.

Quiroz, R. S. (1986). The association of stratospheric warmings with tropospheric blocking. *Journal of Geophysical Research: Atmospheres*, *91*(D4), 5277–5285.

Rao, J., & Garfinkel, C. I. (2021a). CMIP5/6 models project little change in the statistical characteristics of sudden stratospheric warmings in the 21st century. *Environmental Research Letters*, *16*(3), 034024.

Rao, J., & Garfinkel, C. I. (2021b). Projected changes of stratospheric final warmings in the Northern and Southern Hemispheres by CMIP5/6 models. *Climate Dynamics*.

Rao, J., Garfinkel, C. I., & Ren, R. (2019). Modulation of the Northern Winter Stratospheric El Niño–Southern Oscillation Teleconnection by the PDO. *Journal of Climate*, *32*(18), 5761–5783.

Rao, J., Garfinkel, C. I., & White, I. P. (2020a). How Does the Quasi-Biennial Oscillation Affect the Boreal Winter Tropospheric Circulation in CMIP5/6 Models? *Journal of Climate*, *33*(20), 8975–8996.

Rao, J., Garfinkel, C. I., & White, I. P. (2020b). Predicting the Downward and Surface Influence of the February 2018 and January 2019 Sudden Stratospheric Warming Events in Subseasonal to Seasonal (S2S) Models. *Journal of Geophysical Research: Atmospheres*, *125*(2).

Rao, J., & Ren, R. (2016a). Asymmetry and nonlinearity of the influence of ENSO on the northern winter stratosphere: 1. Observations. *Journal of Geophysical Research: Atmospheres*, *121*, 9000–9016.

Rao, J., & Ren, R. (2016b). Asymmetry and nonlinearity of the influence of ENSO on the northern winter stratosphere: 2. Model study with WACCM. *Journal of Geophysical Research: Atmospheres*, *121*, 9017–9032.

Richter, J. H., Deser, C., & Sun, L. (2015). Effects of stratospheric variability on El Niño teleconnections. *Environmental Research Letters*, *10*, 124021.

Rieder, H. E., Chiodo, G., Fritzer, J., Wienerroither, C., & Polvani, L. M. (2019). Is interactive ozone chemistry important to represent polar cap stratospheric temperature variability in Earth-System Models? *Environmental Research Letters*, *14*(4), 044026.

Rigor, I. G. (2002). Response of Sea Ice to the Arctic Oscillation. *Journal of Climate*, *15*, 16.

Rind, D., Shindell, D., Lonergan, P., & Balachandran, N. K. (1998). Climate Change and the Middle Atmosphere. Part III: The Doubled CO2 Climate Revisited [Publisher: American Meteorological Society Section: Journal of Climate]. *Journal of Climate*, *11*(5), 876–894.

Rodríguez-Fonseca, B., Suárez-Morena, R., Ayarzagüena, B., López-Parages, J., Gómara, I., Villamayor, J., Mohino, E., Losada, T., & Castaño-Tierno, A. (2016). A review of ENSO influence on the North Atlantic, a non-stationary signal. *Atmosphere*, *7*, 87.

Salby, M. L., & Callaghan, P. F. (2007). Influence of planetary wave activity on the stratospheric final warming and spring ozone. *Journal of Geophysical Research*, *112*(D20), D20111.

Scaife, A. A., Karpechko, A. Y., Baldwin, M. P., Brookshaw, A., Butler, A. H., Eade, R., & et al. (2016). Seasonal winter forecasts and the stratosphere. *Atmospheric Science Letters*, *17*, 51–56.

Scaife, A. A., Folland, C. K., Alexander, L. V., Moberg, A., & Knight, J. R. (2008). European Climate Extremes and the North Atlantic Oscillation. *Journal of Climate*, *21*(1), 72–83.

Scaife, A. A., Spangehl, T., Fereday, D. R., Cubasch, U., Langematz, U., Akiyoshi, H., Bekki, S., Braesicke, P., Butchart, N., Chipperfield, M. P., Gettelman, A., Hardiman, S. C., Michou, M., Rozanov, E., & Shepherd, T. G. (2012). Climate change projections and stratosphere–troposphere interaction. *Climate Dynamics*, *38*(9-10), 2089–2097.

Scherhag, R. (1952). Die explosionsartigen Stratospherenerwarmingen des Spatwinters 1951/52. *Berichte des Deutschen Wetterdienstes in der US-Zone*, *6*(38), 51–63.

Schoeberl, M. R. (1978). Stratospheric warmings: Observations and theory. *Reviews of Geophysics*, *16*(4), 521–538.

Schwartz, C., & Garfinkel, C. I. (2017). Relative roles of the MJO and stratospheric variability in North Atlantic and European winter climate: Extratropical Impact of MJO Versus SSW. *Journal of Geophysical Research: Atmospheres*, *122*(8), 4184–4201.

Schwartz, C., & Garfinkel, C. I. (2020). Troposphere-stratosphere coupling in subseasonal-to-seasonal models and its importance for a realistic extratropical response to the madden-julian oscillation [e2019JD032043 10.1029/2019JD032043]. *Journal of Geophysical Research: Atmospheres*, *125*(10), e2019JD032043.

Seviour, W. J. M., Mitchell, D. M., & Gray, L. J. (2013). A practical method to identify displaced and split stratospheric polar vortex events. *Geophys. Res. Lett.*, *40*, 5268–5273.

Seviour, W. J. M., Gray, L. J., & Mitchell, D. M. (2016). Stratospheric polar vortex splits and displacements in the high-top CMIP5 climate models: Vortex Splits and Displacements in CMIP5. *Journal of Geophysical Research: Atmospheres*, *121*(4), 1400–1413.

Shaw, T. A., Perlwitz, J., & Weiner, O. (2014). Troposphere-stratosphere coupling: Links to North Atlantic weather and climate, including their representation in CMIP5 models. *Journal of Geophysical Research: Atmospheres*, *119*(10), 5864–5880.

Siegmund, P. (2005). Stratospheric Polar Cap Mean Height and Temperature as Extended-Range Weather Predictors. *Monthly Weather Review*, *133*(8), 2436–2448.

Sigmond, M., Scinocca, J. F., Kharin, V. V., & Shepherd, T. G. (2013). Enhanced seasonal forecast skill following stratospheric sudden warmings. *Nature Geoscience*, *6*, 98–102.

Silverman, V., Harnik, N., Matthes, K., Lubis, S. W., & Wahl, S. (2018). Radiative effects of ozone waves on the Northern Hemisphere polar vortex and its modulation by the QBO. *Atmospheric Chemistry and Physics*, *18*(9), 6637–6659.

Simpson, I. R., Hitchcock, P., Shepherd, T. G., & Scinocca, J. F. (2011). Stratospheric variability and tropospheric annular-mode timescales. *Geophysical Research Letters*, *38*(L20806).

Sjoberg, J. P., & Birner, T. (2012). Transient tropospheric forcing of sudden stratospheric warmings. *Journal of the Atmospheric Sciences*, *69*(11), 3420–3432.

Smith, K. L., Neely, R. R., Marsh, D. R., & Polvani, L. M. (2014). The Specified Chemistry Whole Atmosphere Community Climate Model (SC-WACCM). *Journal of Advances in Modeling Earth Systems*, *6*(3), 883–901.

Smith, K. L., & Polvani, L. M. (2014). The surface impacts of Arctic stratospheric ozone anomalies. *Environmental Research Letters*, *9*(7), 074015.

Smith, K. L., & Kushner, P. J. (2012). Linear interference and the initiation of extratropical stratosphere-troposphere interactions. *Journal of Geophysical Research: Atmospheres*, *117*(D13).

Smith, K. L., Polvani, L. M., & Tremblay, L. B. (2018). The Impact of Stratospheric Circulation Extremes on Minimum Arctic Sea Ice Extent. *Journal of Climate*, *31*(18), 7169–7183.

Song, K., & Son, S.-W. (2018). Revisiting the ENSO–SSW relationship. *Journal of Climate*, *31*(6), 2133–2143.

Strahan, S. E., & Douglass, A. R. (2004). Evaluating the credibility of transport processes in simulations of ozone recovery using the Global Modeling Initiative three-dimensional model. *Journal of Geophysical Research Atmospheres*, *109*, D05110.

Strahan, S. E., Douglass, A. R., & Steenrod, S. D. (2016). Chemical and dynamical impacts of stratospheric sudden warmings on Arctic ozone variability. *Journal of Geophysical Research Atmospheres*, *121*, 11836–11851.

Sun, L., Deser, C., & Tomas, R. A. (2015). Mechanisms of stratospheric and tropospheric circulation response to projected arctic sea ice loss. *Journal of Climate*, *28*(19), 7824–7845.

Sun, L., Perlwitz, J., Richter, J. H., Hoerling, M. P., & Hurrell, J. W. (2020). Attribution of NAO Predictive Skill Beyond 2 Weeks in Boreal Winter. *Geophysical Research Letters*, *47*(22).

Thiéblemont, R., Ayarzagüena, B., Matthes, K., Bekki, S., Abalichin, J., & Langematz, U. (2019). Drivers and Surface Signal of Interannual Variability of Boreal Stratospheric Final Warmings. *Journal of Geophysical Research: Atmospheres*, *124*(10), 5400–5417.

Thompson, D. W. J. (2001). Regional Climate Impacts of the Northern Hemisphere Annular Mode. *Science*, *293*(5527), 85–89.

Thompson, D. W. J., & Wallace, J. M. (1998). The Arctic Oscillation signature in the wintertime geopotential height and temperature fields. *Geophysical Research Letters*, *25*, 1297–1300.

Thompson, D. W. J., & Wallace, J. M. (2001). Regional Climate Impacts of the Northern Hemisphere Annular Mode. *Science*, *293*(5527), 85–89.

Toniazzo, T., & Scaife, A. A. (2006). The influence of ENSO on winter North Atlantic climate. *Geophysical Research Letters*, *33*, L24704.

Trascasa-Castro, P., Maycock, A. C., Scott Yiu, Y. Y., & Fletcher, J. K. (2019). On the Linearity of the Stratospheric and Euro-Atlantic Sector Response to ENSO. *Journal of Climate*, *32*(19), 6607–6626.

Trenberth, K. E., Branstator, G. W., Karoly, D., Kumar, A., Lau, N.-C., & Ropelewski, C. (1998). Progress during TOGA in understanding and modeling global teleconnections associated with tropical sea surface temperatures. *Journal of Geophysical Research: Atmospheres*, 14291–14324.

Tripathi, O. P., Charlton-Perez, A., Sigmond, M., & Vitart, F. (2015). Enhanced long-range forecast skill in boreal winter following stratospheric strong vortex conditions. *Environmental Research Letters*, *10*(10), 104007.

Tung, K. K., & Lindzen, R. S. (1979). A Theory of Stationary Long Waves. Part 1: A Simple Theory of Blocking. *Monthly Weather Review*, *107*, 714–734.

Tyrrell, N. L., Karpechko, A. Y., Uotila, P., & Vihma, T. (2019). Atmospheric circulation response to anomalous siberian forcing in october 2016 and its long-range predictability. *Geophysical Research Letters*, *46*(5), 2800–2810.

van Loon, H., Jenne, R. L., & Labitzke, K. (1973). Zonal harmonic standing waves. *Journal of Geophysical Research*, *78*(21), 4463–4471.

Vitart, F., Ardilouze, C., Bonet, A., Brookshaw, A., Chen, M., Codorean, C., Déqué, M., Ferranti, L., Fucile, E., Fuentes, M., Hendon, H., Hodgson, J., Kang, H.-S., Kumar, A., Lin, H., Liu, G., Liu, X., Malguzzi, P., Mallas, I., … Zhang, L. (2017). The Subseasonal to Seasonal (S2S) Prediction Project database. *Bulletin of the American Meteorological Society*, *98*(1), 163–173.

Wang, F., Tian, W., Xie, F., Zhang, J., & Han, Y. (2018). Effect of Madden–Julian Oscillation Occurrence Frequency on the Interannual Variability of Northern Hemisphere Stratospheric Wave Activity in Winter. *Journal of Climate*, *31*(13), 5031–5049.

Watson, P. A. G., & Gray, L. J. (2014). How does the quasi-biennial oscillation affect the stratospheric polar vortex? *Journal of the Atmospheric Sciences*, *71*(1), 391–409.

Watt-Meyer, O., & Kushner, P. J. (2015). The Role of Standing Waves in Driving Persistent Anomalies of Upward Wave Activity Flux. *Journal of Climate*, *28*(24), 9941–9954.

Waugh, D. W., Randel, W. J., Pawson, S., Newman, P. A., & Nash, E. R. (1999). Persistence of the lower stratospheric polar vortices. *Journal of Geophysical Research: Atmospheres*, *104*(D22), 27191–27201.

Waugh, D. W., Sobel, A. H., & Polvani, L. M. (2017). What Is the Polar Vortex and How Does It Influence Weather? *Bulletin of the American Meteorological Society*, *98*(1), 37–44.

Wei, K., Chen, W., & Huang, R. H. (2007). Dynamical diagnosis of the breakup of the stratospheric polar vortex in the Northern Hemisphere. *Sci. China Ser. D*, *50*(9), 1369–1379.

Weinberger, I., Garfinkel, C. I., White, I. P., & Oman, L. D. (2019). The salience of nonlinearities in the boreal winter response to ENSO: Arctic stratosphere and Europe. *Climate Dynamics*, *53*(7-8), 4591–4610.

Wheeler, M. C., & Hendon, H. H. (2004). An All-Season Real-Time Multivariate MJO Index: Development of an Index for Monitoring and Prediction. *Monthly Weather Review*, *132*, 16.

White, I., Garfinkel, C. I., Gerber, E. P., & Jucker, M. (2019). The Downward Influence of Sudden Stratospheric Warmings: Association with Tropospheric Precursors. *Journal of Climate*, *32*, 24.

White, I. P., Lu, H., Mitchell, N. J., & Phillips, T. (2015). Dynamical response to the qbo in the northern winter stratosphere: Signatures in wave forcing and eddy fluxes of potential vorticity. *Journal of the Atmospheric Sciences*, *72*(12), 4487–4507.

WMO CAS. (1978).

WMO/IQSY. (1964). *1964: International Years of the Quiet Sun (IQSY), 1964–1965: Alert messages with special references to stratwarms.* (tech. rep. No. 6).

Woollings, T., Charlton-Perez, A., Ineson, S., Marshall, A. G., & Masato, G. (2010). Associations between stratospheric variability and tropospheric blocking. *Journal of Geophysical Research: Atmospheres*, *115*(D6).

Wu, Z., & Reichler, T. (2020). Variations in the Frequency of Stratospheric Sudden Warmings in CMIP5 and CMIP6 and Possible Causes. *Journal of Climate*, *33*(23), 10305–10320.

Yang, C., Li, T., Xue, X., Gu, S.-y., Yu, C., & Dou, X. (2019). Response of the Northern Stratosphere to the Madden-Julian Oscillation During Boreal Winter. *Journal of Geophysical Research: Atmospheres*, *124*(10), 5314–5331.

Zhang, R., Tian, W., Zhang, J., Huang, J., Xie, F., & Xu, M. (2019). The corresponding tropospheric environments during downward-extending and nondownward-extending events of stratospheric Northern Annular Mode anomalies. *Journal of Climate*, *32*(6), 1857–1873.

Zhou, X., Chen, Q., Wang, Z., Xu, M., Zhao, S., Cheng, Z., & Feng, F. (2020). Longer Duration of the Weak Stratospheric Vortex During Extreme El Niño Events Linked to Spring Eurasian Coldness. *Journal of Geophysical Research: Atmospheres*, *125*(16).

Zhou, X., Chen, Q., Xie, F., Li, J., Li, M., Ding, R., Li, Y., Xia, X., & Cheng, Z. (2019). Nonlinear response of Northern Hemisphere stratospheric polar vortex to the Indo–Pacific warm pool (IPWP) Niño. *Scientific Reports*, *9*(1), 13719.

Appendix A: Northern Annular Mode Calculation

We calculate the NAM using a method similar to that of Gerber 2010 and Gerber and Martineau 2018. The specific procedure is as follows:

1. We average model output to find a time series of daily, zonal mean geopotential height $Z(t, \lambda, p)$ as a function of time t, latitude λ, and pressure p.

2. For every day and pressure level, we remove the global mean geopotential height $\bar{Z}^{\text{global}}(t, p)$. This helps to remove the global changes so that the index instead mainly captures meridional differences or shifts (Gerber 2010). (While not the case for the simulations used in this study, this step would remove much of the global warming signal if it were present.)

3. For each day, latitude, and pressure level, we remove the average for that calendar day over the whole period; that is, we remove the climatology to find an anomalous height.

4. For each day, latitude, and pressure, we remove the linear trend over the period.

5. For each day and pressure level, we compute a polar cap average. Here we are interested in the NAM, and we take the average from 65-90°N. This is a proxy for the annular mode as shown in Baldwin and Thompson 2009a.

6. We multiply by -1 so that a positive polar cap geopotential height anomaly yields a negative NAM, for consistency with the convention of Thompson and Wallace 1998.

7. We normalize the index by its standard deviation at each pressure level.

Appendix B: Supplementary Figures to “The effect of interactive ozone chemistry on weak and strong stratospheric polar vortex events"

In this supplementary section, we show the seasonality of the shortwave heating anomalies induced by the CHEM (interactive chemistry) simulation compared to NOCHEM (specified chemistry) in the occurrence of SSWs (Fig. S1). Given that March SSWs behave differently from those occurring in midwinter, we show the evolution of these events separately from that of the DJF SSWs. In particular, here we show the NAM evolution (Fig. S2), evolution of temperature and the individual heating terms (Fig. S3), and the wave forcing (Fig. S4). (These figures are parallel to Figures 4, 5, and 6 for midwinter SSWs in the main text). Finally, we show the same sequence (NAM, temperature and heating terms) for SPVs in midwinter in Figs. S5-S6.

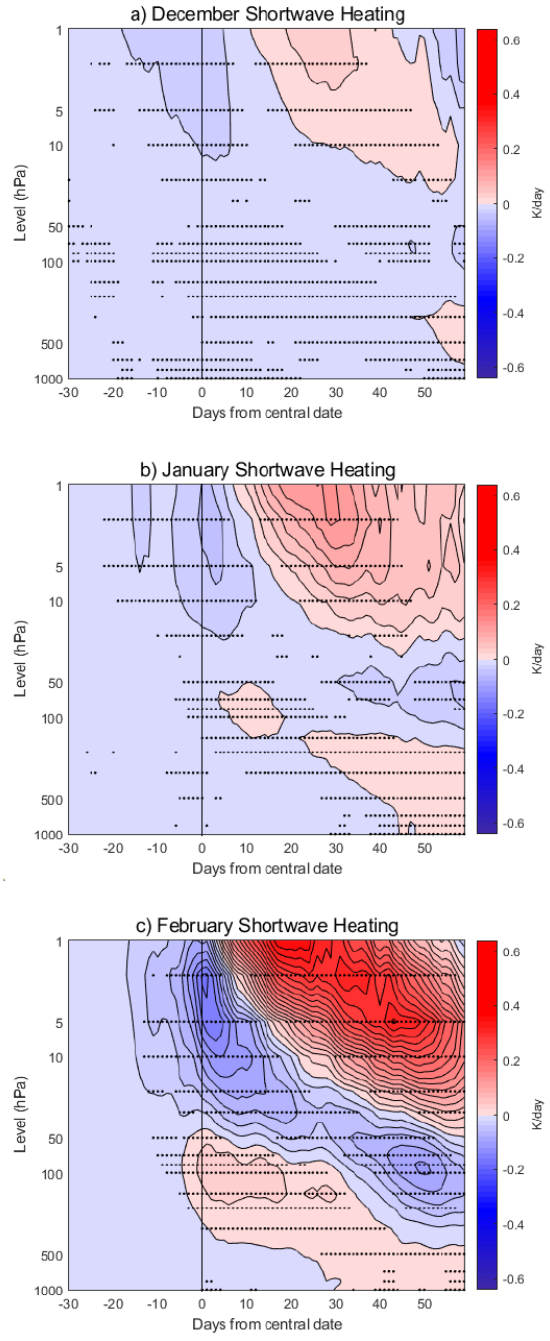

Figure S3.1: CHEM-NOCHEM difference in shortwave heating anomalies from -30 to +60 days around the SSW central dates in December (a), January (b), and February (c).

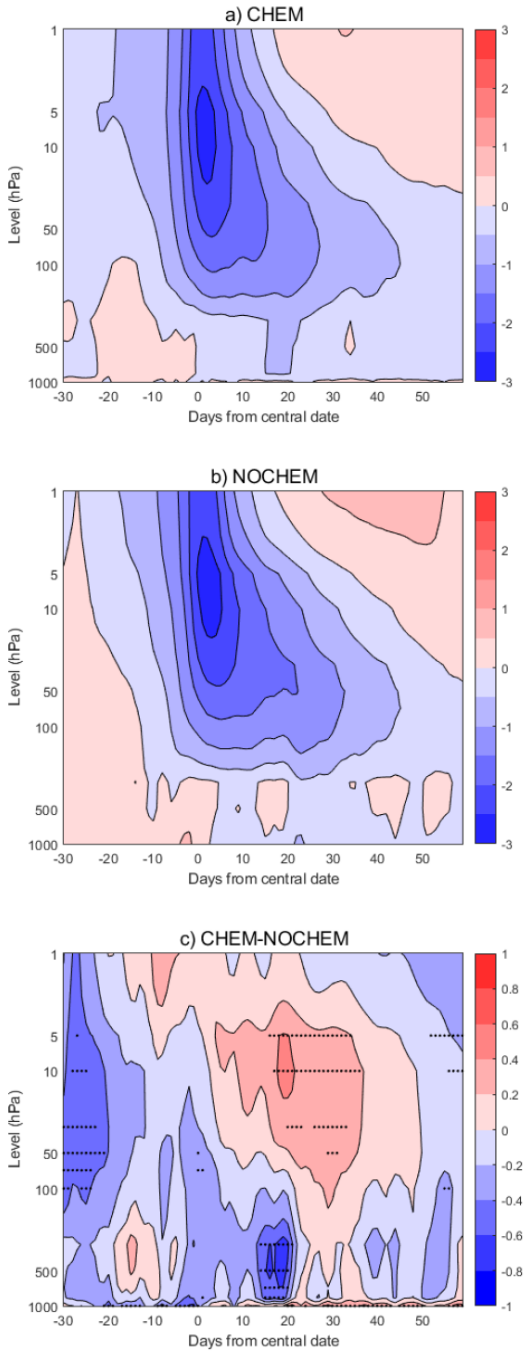

Figure S3.2: NAM anomaly composites around March SSW central dates in CHEM (a), NOCHEM (b), CHEM-NOCHEM (c). Stippling shows significance at the 95% level (with a Monte Carlo test for CHEM and NOCHEM and a two-tailed t-test for CHEM-NOCHEM). Contours are every 0.5 standard units for CHEM and NOCHEM and every 0.2 standard units for CHEM-NOCHEM.

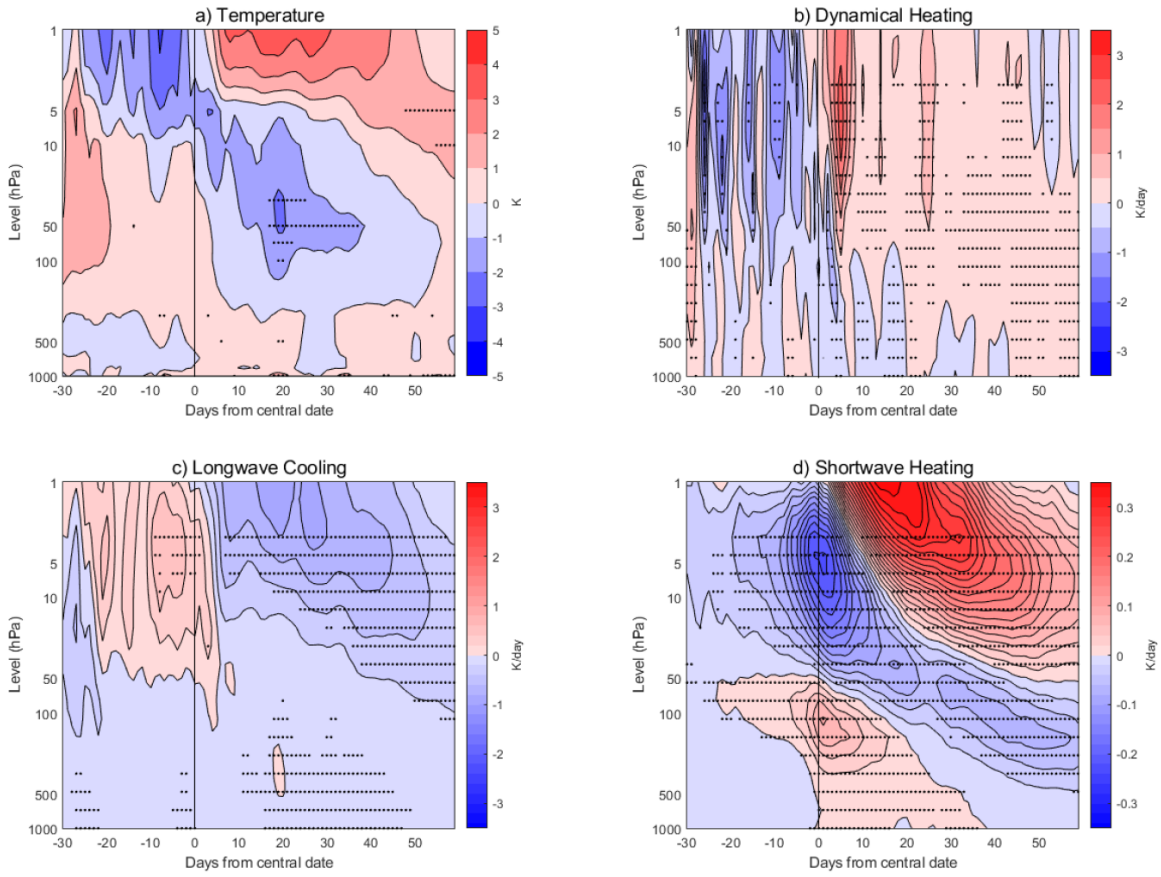

Figure S3.3: CHEM-NOCHEM differences in the temperature and heating anomalies over 60-90° N from -30 to +60 days around the SSW March central dates. (a): Temperature anomalies. Contours are every 1 K. (b): Dynamical heating anomalies. Contours are every 0.5 K/day. (c): Longwave heating anomalies. Contours are every 0.25 K/day. (d): Shortwave heating anomalies. Contours are every 0.02 K/day. Stippling shows significance at the 95% level under a two-tailed t-test.

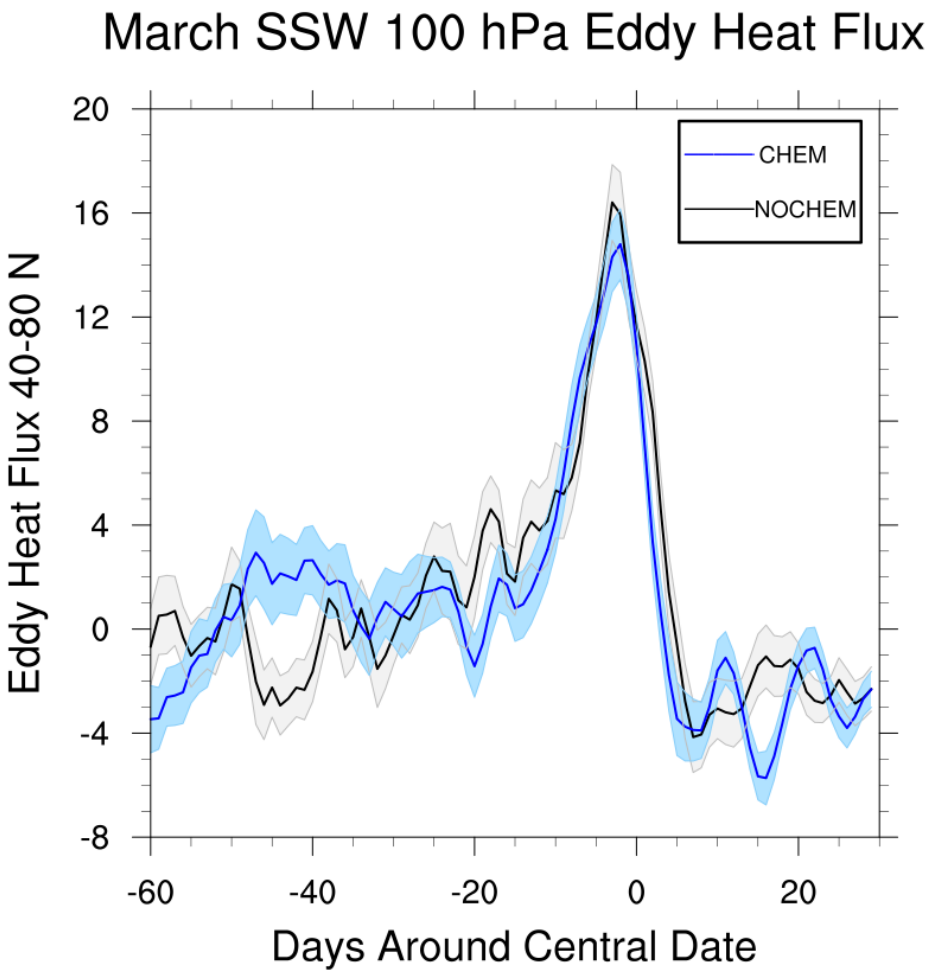

Figure S3.4: Eddy heat flux in mK/s over 40-80° N from -60 to +30 days around the SSW March central dates. The CHEM average is in blue, with confidence intervals shown in pale blue. The NOCHEM average is in black, with confidence intervals shown in gray.

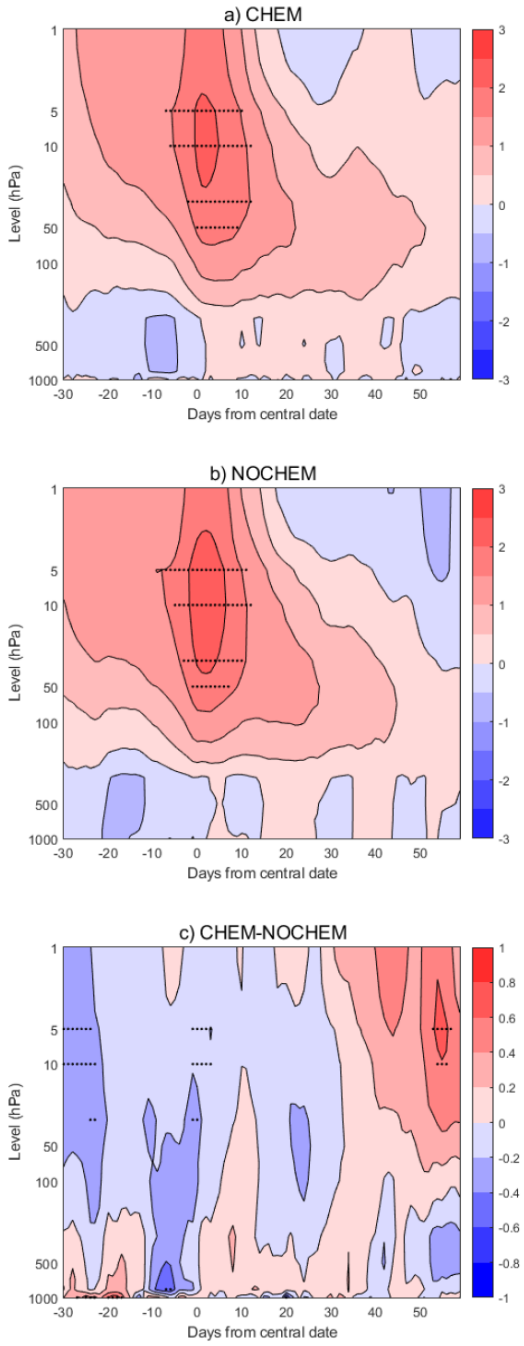

Figure S3.5: NAM anomaly composites around DJF SPV central dates in CHEM (a), NOCHEM (b), CHEM-NOCHEM (c). Stippling shows significance at the 95% level (with a Monte Carlo test for CHEM and NOCHEM and a two-tailed t-test for CHEM-NOCHEM). Contours are every 0.5 standard units for CHEM and NOCHEM and every 0.2 standard units for CHEM-NOCHEM.

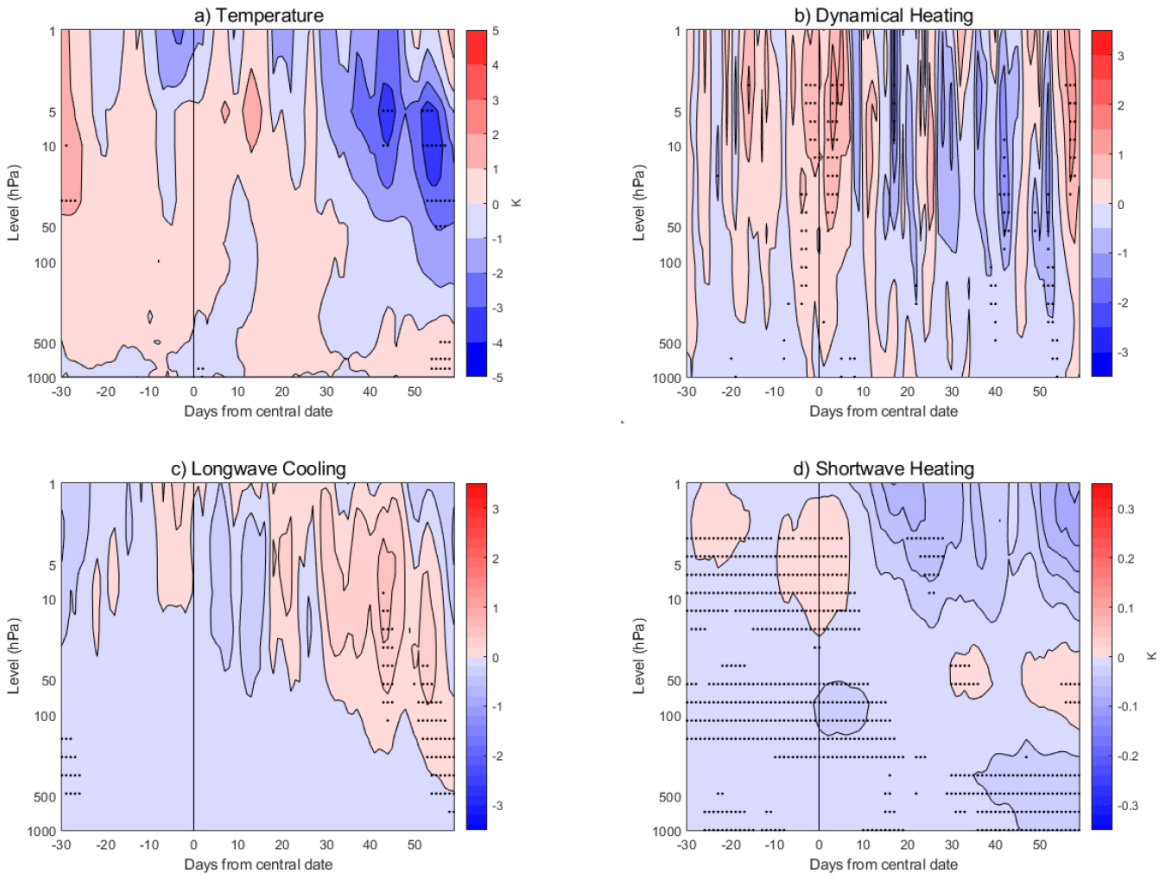

Figure S3.6: CHEM-NOCHEM differences in the temperature and heating anomalies over 60-90° N from -30 to +60 days around the SPV DJF central dates. (a): Temperature anomalies. Contours are every 1 K. (b): Dynamical heating anomalies. Contours are every 0.5 K/day. (c): Longwave heating anomalies. Contours are every 0.25 K/day. (d): Shortwave heating anomalies. Contours are every 0.02 K/day. Stippling shows significance at the 95% level under a two-tailed t-test.

Appendix C: Supplementary Material to "Characterizing the surface impact of sudden stratospheric warmings in the context of internal variability"

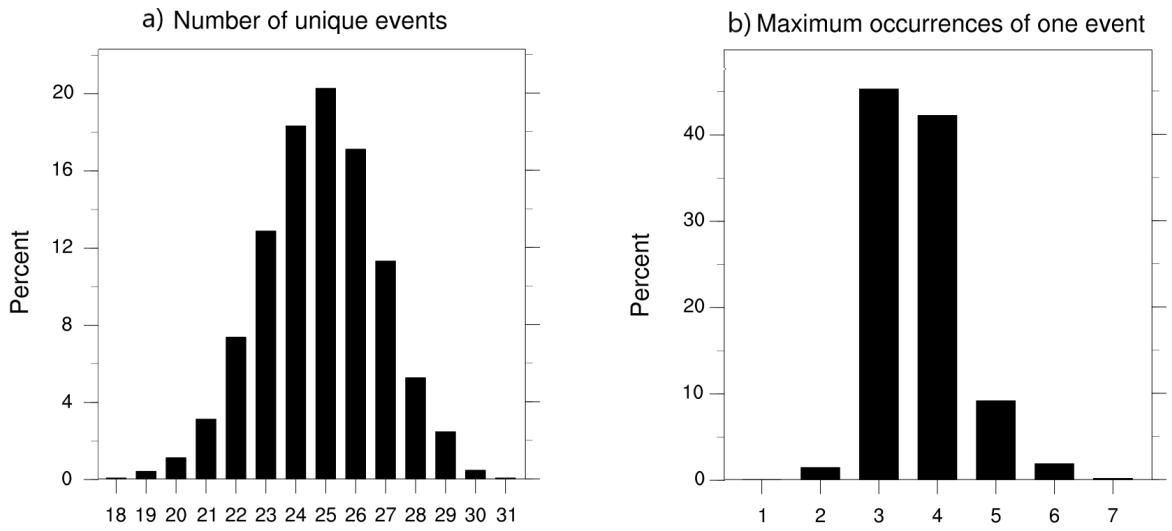

Figure S4.1: Distributions across all 2000 composites of a) the number of distinct events in each bootstrapped composite and b) the maximum number of occurrences of a single event in each composite.

Table C.1: The number of occurrences of each SSW events in the 10th and 90th percentile composites for the regions of interest.

Event	NAO 10th	NAO 90th	E. Canada 10th	E. Canada 90th
30 Jan 1958	1	0	1	1
17 Jan 1960	3	0	1	1
30 Jan 1963	1	0	3	2
18 Dec 1965	0	1	1	4
23 Feb 1966	2	1	0	2
7 Jan 1968	2	0	1	0
29 Nov 1968	2	1	1	1
2 Jan 1970	1	1	2	1
18 Jan 1971	2	0	2	0
20 Mar 1971	0	0	0	2
31 Jan 1973	0	1	2	0
9 Jan 1977	3	3	0	0
22 Feb 1979	0	0	0	1
29 Feb 1980	1	1	0	1
6 Feb 1981	0	2	1	3
4 Mar 1981	1	0	0	2
4 Dec 1981	1	1	0	0
24 Feb 1984	2	2	2	0
1 Jan 1985	2	0	2	0
23 Jan 1987	1	1	1	0
8 Dec 1987	0	1	0	2
14 Mar 1988	0	2	1	4
21 Feb 1989	1	0	1	1
15 Dec 1998	1	2	1	0
26 Feb 1999	2	1	2	1
20 Mar 2000	0	0	1	3
11 Feb 2001	1	1	1	0
31 Dec 2001	1	3	1	1
18 Jan 2003	1	0	2	1
5 Jan 2004	2	1	3	1
21 Jan 2006	0	0	0	2
24 Feb 2007	1	3	1	1
22 Feb 2008	0	1	1	0
24 Jan 2009	1	2	0	0
9 Feb 2010	0	2	1	1
24 Mar 2010	0	2	0	0
7 Jan 2013	3	1	1	0
12 Feb 2018	0	0	2	0
2 Jan 2019	0	2	0	0

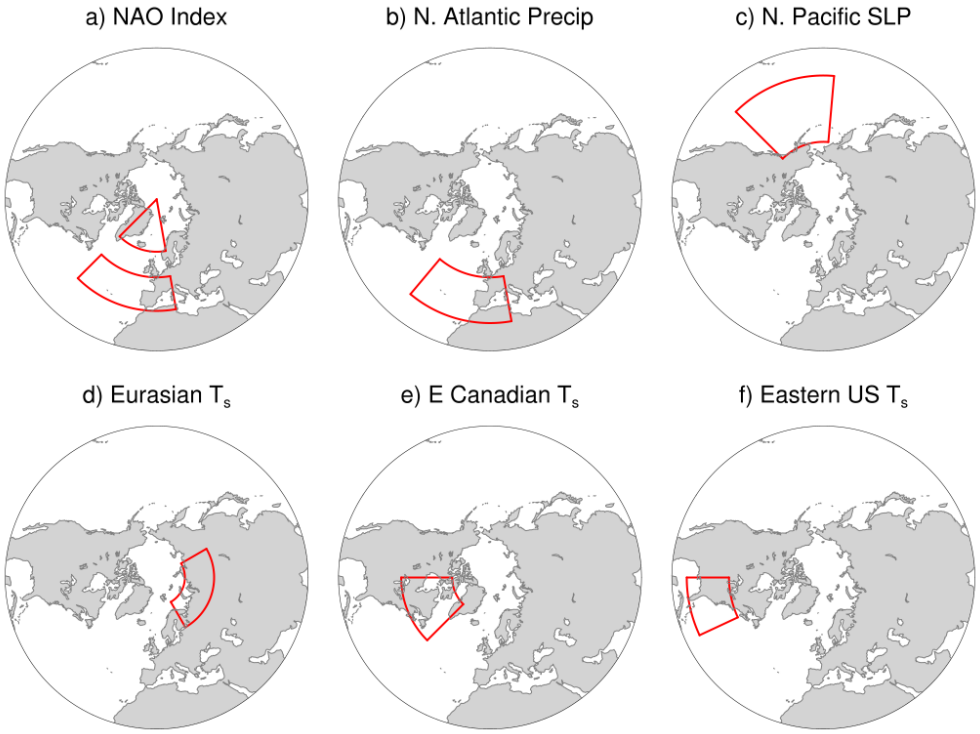

Figure S4.2: The regions for further analysis. (a) Regions for the centers of the NAO dipole: 62.5°-90° N, 45° W-10◦ E (northern center) and 35°-50° N, 45° W-10◦ E (southern center). (b) North Atlantic precipitation region: 30°-50° N, 40° W-10° E. (c) North Pacific sea level pressure region: 30°-60° N and 175° E-135° W. (d) Eurasian surface temperature region: 60°-75° N and 30°-120° E. (e) Eastern Canadian surface temperature region: 45°-70° N and 45°-90° W. (f) Eastern United States surface temperature region: 25°-42.5° N, 65°-90° W.

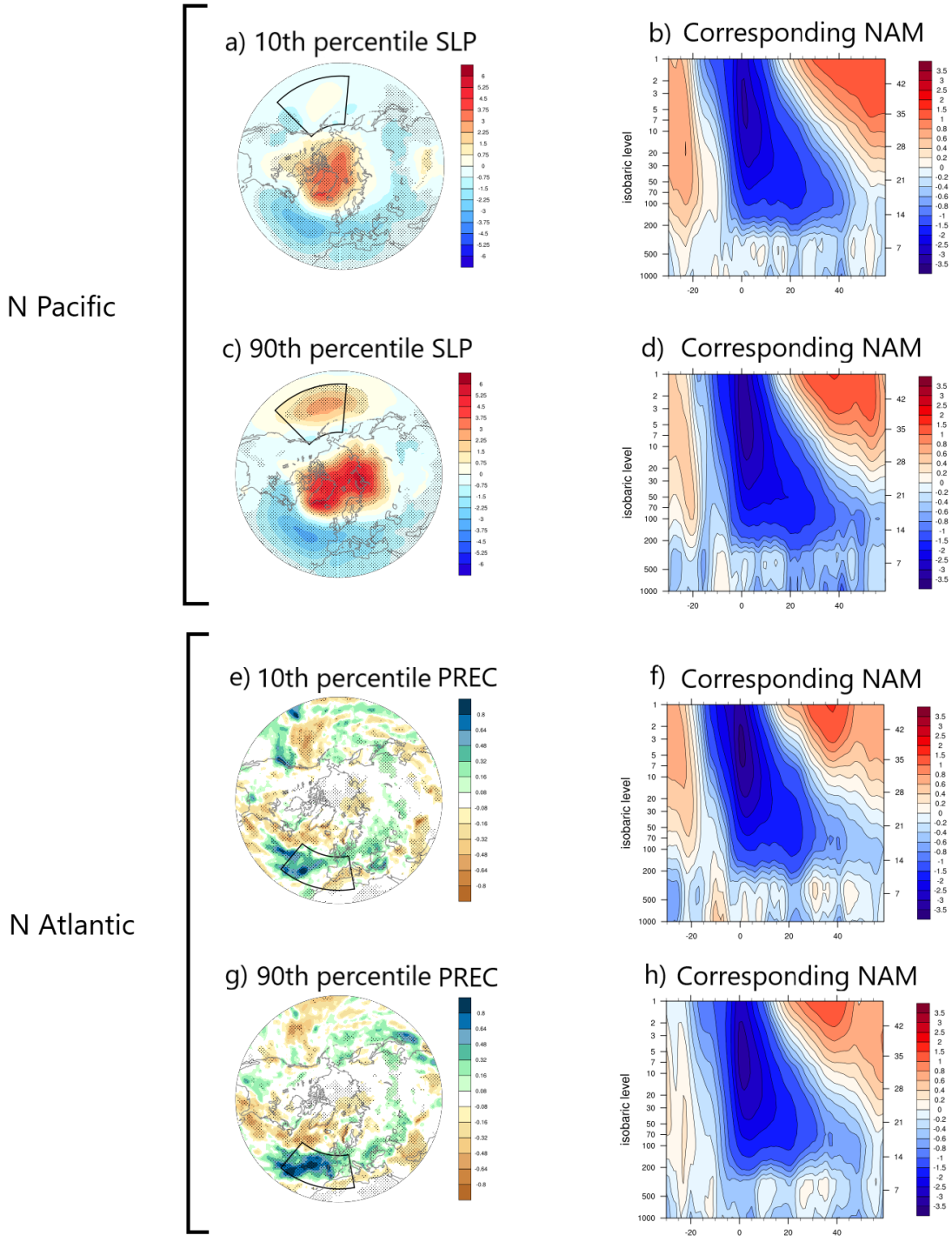

Figure S4.3: The 10th and 90th percentile composites of the North Pacific SLP and North Atlantic precipitation anomalies in days 0-60 following the SSW central date, along with the corresponding NAM responses.

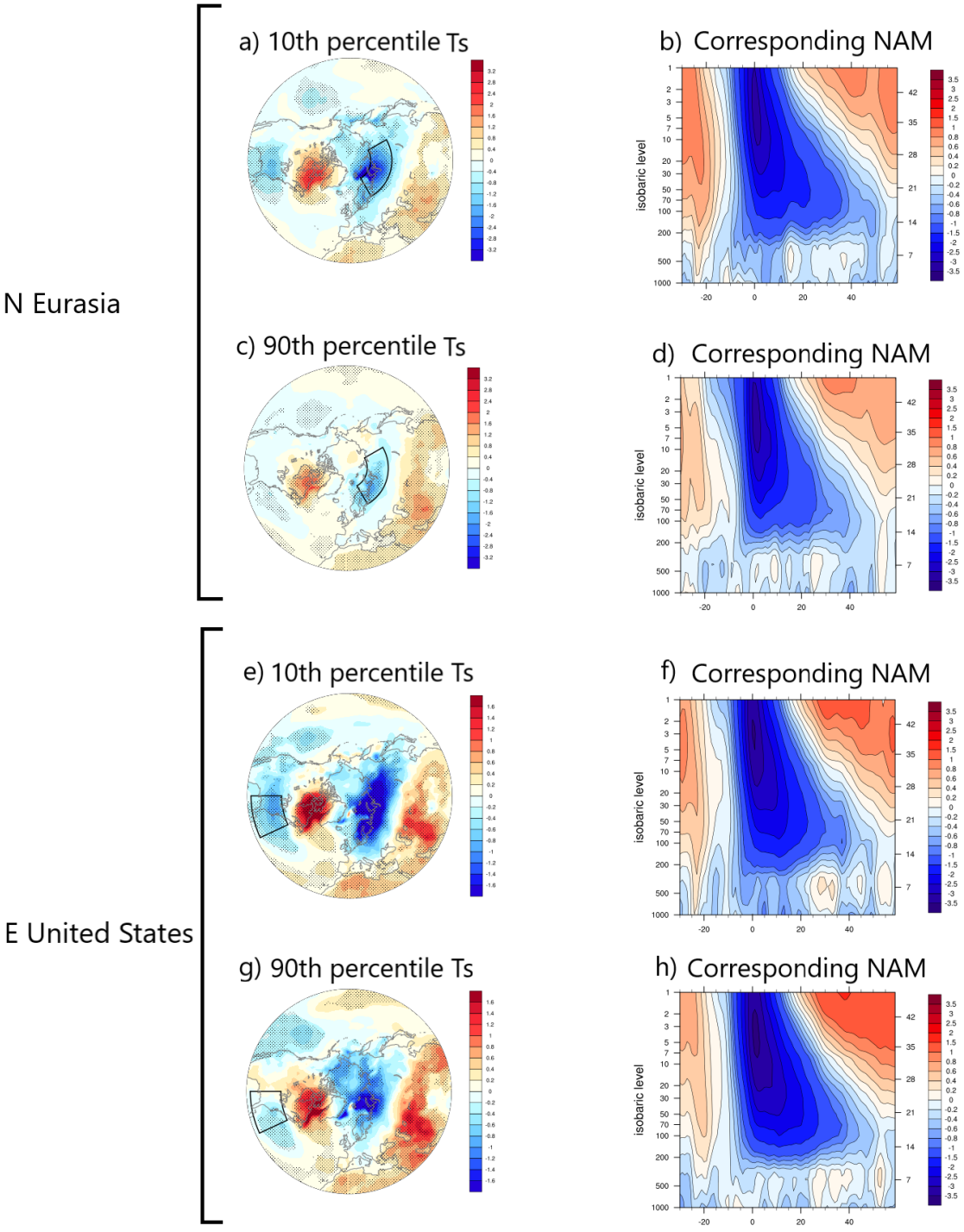

Figure S4.4: The 10th and 90th percentile composites of Northern Eurasian and Eastern United States temperature anomalies in days 0-60 following the SSW central date, along with the corresponding NAM responses.

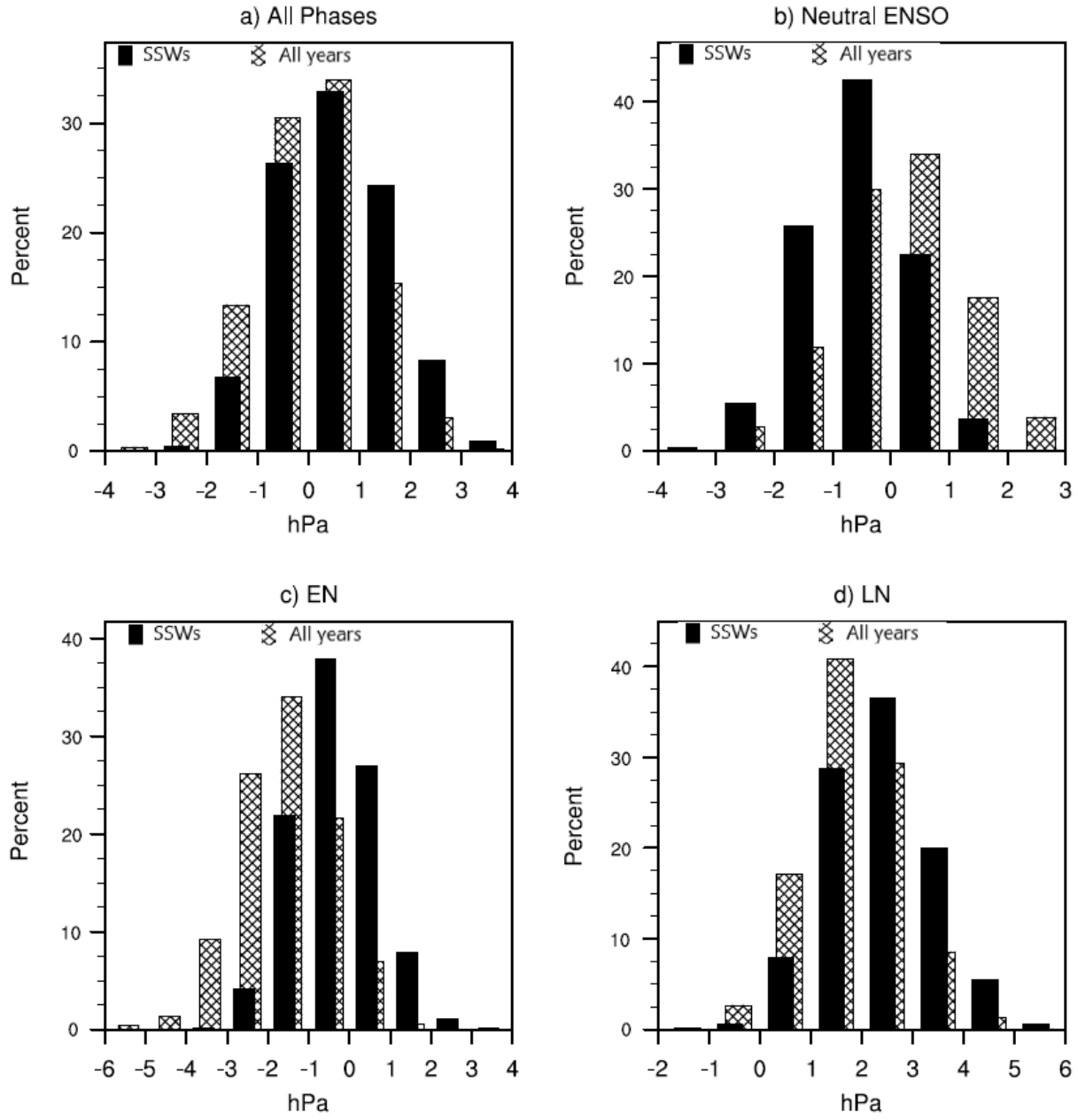

Figure S4.5: Histograms showing responses of North Pacific SLP anomalies in composites of the 0-60 days following 10 events by ENSO phase: (a) all phases, (b) neutral ENSO, (c) El Niño (EN), and (d) La Niña (LN). SLP anomalies after SSWs are shown in black; those after 0-60 day periods across all winters (of that phase where applicable) are hatched.

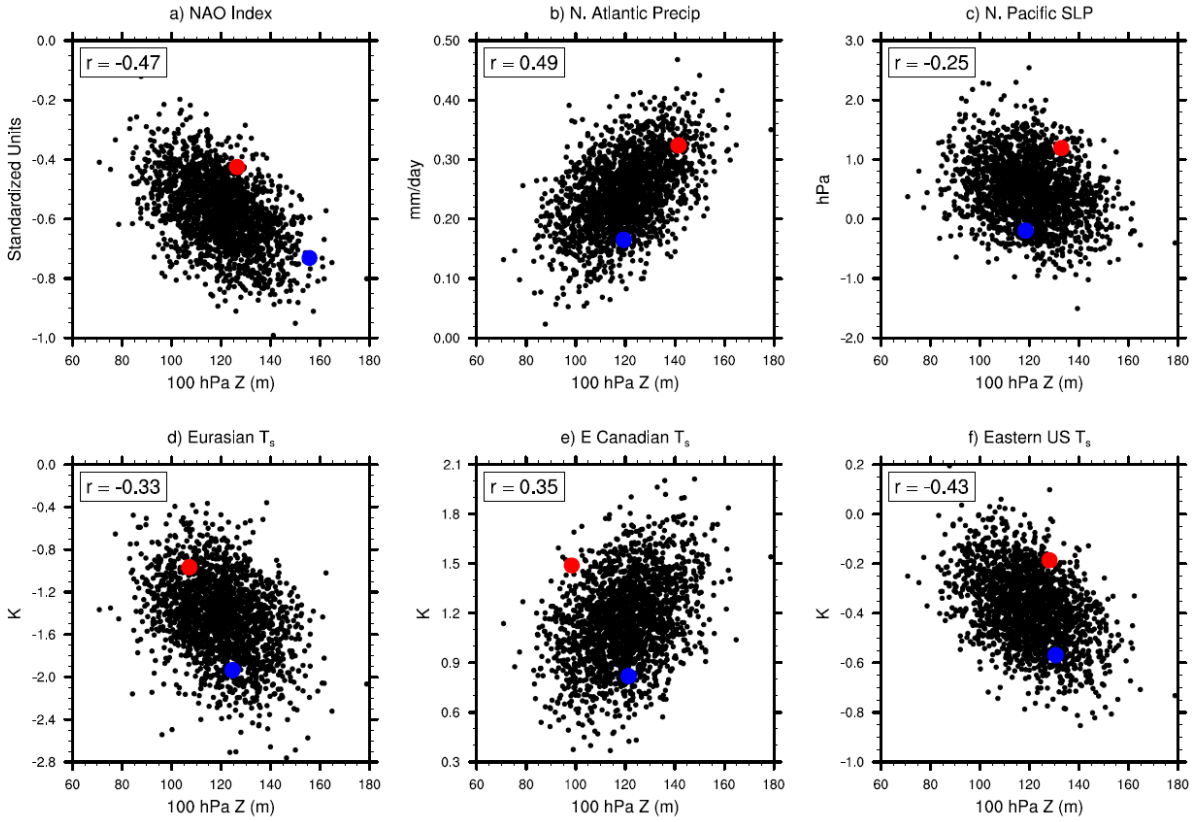

Figure S4.6: The responses of surface temperature in the 60 days following SSWs and relationships to the polar cap geopotential height anomalies in days 0-5 at 100 hPa. Blue and red dots denote the 10th and 90th percentile composites by surface index/anomaly respectively.

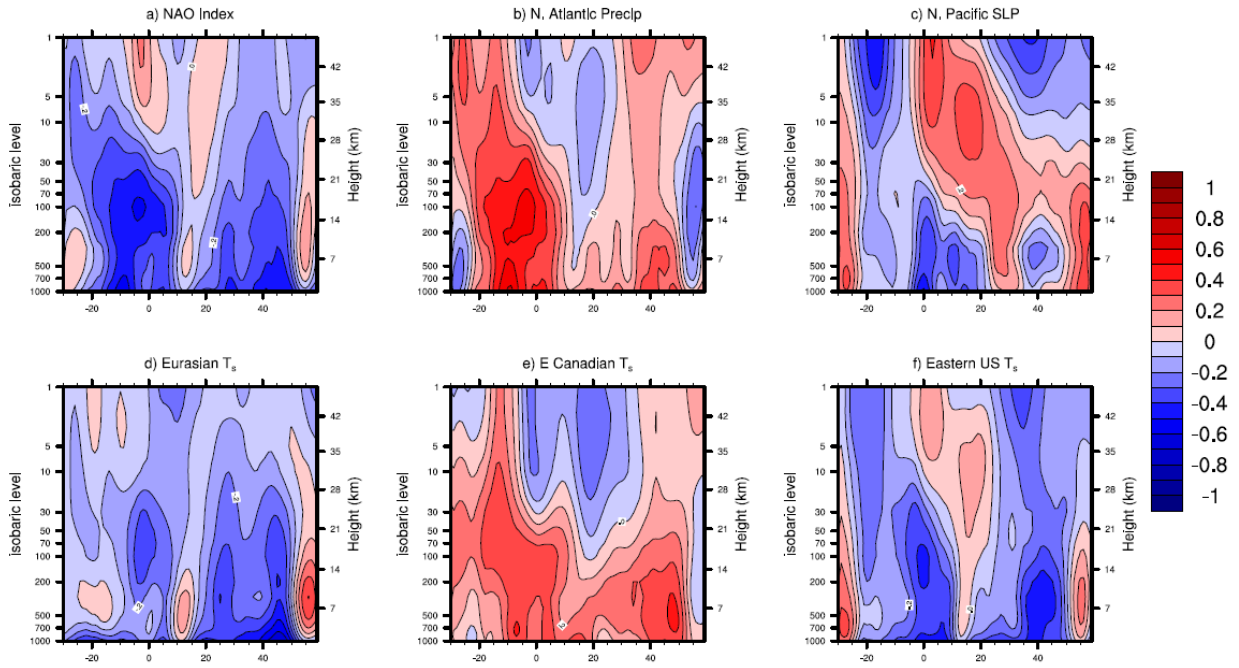

Figure S4.7: Correlations at each pressure and lag between a five-day geopotential height anomaly and the 0-60 day surface response.